DETERMINING THE FIRING CONDITION OF ANCIENT CHINESE PORCELAIN

BY

RUIFENG OUYANG

A THESIS
SUBMITTED TO THE FACULTY OF

ALFRED UNIVERSITY

IN PARTIAL FULFILLMENT OF THE REQUIREMENTS
FOR THE DEGREE OF

MASTER OF SCIENCE

IN

CERAMIC ENGINEERING

ALFRED, NEW YORK

AUGUST, 2015

DETERMINING THE FIRING CONDITION OF ANCIENT CHINESE PORCELAIN

BY

RUIFENG OUYANG

B. ENG. JINGDEZHEN CERAMIC INSTITUTE (2011)

SIGNATURE OF AUTHOR_____

APPROVED BY _____
WILLIAM M. CARTY, ADVISOR

_____
DOREEN D. EDWARDS, ADVISORY COMMITTEE

_____
S. K. SUNDARAM, ADVISORY COMMITTEE

_____
CHAIR, ORAL THESIS DEFENSE

ACCEPTED BY _____
DOREEN D. EDWARDS, DEAN
KAZUO INAMORI SCHOOL OF ENGINEERING

ACKNOWLEDGMENTS

First of all, I would like to thank Chinese Scholarship Council, New York Service Center for Chinese Study Fellows and all the teachers working there. Thank you for providing not only funding support, but kind care and understanding to me during two years at Alfred. The experience of my study abroad wouldn't be this comfortable without your countless help.

Many thanks to my advisor, Dr. William M. Carty for continuous help during this two years at Alfred. Thanks to your amazing teaching and guidance that really broadens my horizon again and again. Thanks to your patience for training me from a rookie to a beginning researcher step by step. Thank you for establishing model of a great researcher with your passion and personality. Thank you so much for being my boss, I really appreciate it. And I would like to also thank my committee, Dr. Doreen Edwards and Dr. S.K. Sundaram, for their interest and discussion in this work.

My thanks to Hyojin Lee for helping me in so many aspects in this research. Thanks to your patience and time for troubleshooting my problems always, even though I occasionally come at wrong time. Thanks to my fellow, Wirat Lerdprom for your encouragement and suggestions through this two years. I would never forget the scene that you first greet with me when I was awaiting outside of our office. Life is much harder for me without you being here!

Thanks to Aubrey Fry and Corine Pettit for reviewing my thesis. Thanks to Gerald Wynick, Swavek Zdzieszynski and Matt Katz for all their help with used instruments. Thanks to all my classmates at Alfred: David Tseng, Victor Colorado, Diksha Kini, Yan Yang, Wei Zhang, Wenxia Tan, Peng Gao, Yiyu Li, Yin Liu, Sureeporn Chothirawat and Kevin Keefe. Thanks to all my friends in this warm community at Alfred. A special thank to

Aodi Liang for providing accommodation and vehicle for me in the last two months, since I was so close to sleep in the lab.

Huge thanks to my parents, Xiaosheng Ouyang and Shuangyan Feng. It is your love and support that make me feel warm even in the long winter here. Thank you so much for raising me up and leading direction for me throughout my life.

Thanks a lot to Alfred for being a precious part of my memory. Thank you!

Ruifeng Ouyang (欧阳瑞丰)

Alfred, NY - August, 2015

TABLE of CONTENTS

LIST of TABLES

Page

LIST of FIGURES

Page

ABSTRACT

Firing conditions have consistently played a vital role in the research of ancient ceramics for archeologists. Eighteen ancient Chinese porcelain shards of between 900-1200 years ago, excavated from Jingdezhen were evaluated to determine their firing conditions using three proposed models. In addition, newly created specimens using only Chinese raw materials and typical Chinese commercial bodies were examined to assess the applicability of models. Model #1 in terms of body-glaze penetration appears to be unsuitable for shards because the original body-glaze interface could not be estimated. Model #2, incorporated mullite crystallite size in (110) direction, appears to be reasonably applicable because of an apparent variability in the ratio of primary : secondary mullite. The silica level in the glass phase constituting Model #3, was demonstrated to be dependent on initial silica level in the body as well as firing temperature and dwell time. Potential correction for this model is proposed based on the available silica level in body. And the validity of Models #2 and #3 is checked with specimens with known firing parameters. The firing temperature of collected shards were predicted with estimated dwell times of 72 and 96 hours based on historical records. This difference in dwell time only generates a firing temperature difference of 10 K.

I. INTRODUCTION

The production of ancient Chinese ceramics has quite a long history in terms of the number of designs, the broad range of raw materials from different regions, the various types of kilns used and regional manufacturing techniques. These critical factors contribute to the diversity of ceramic productions with respect to different firing conditions. Three proposed models established on the basis of body-glaze penetration depth, mullite crystallite size in (110) direction and silica level in the glass phase provided the potential to determine the firing conditions (firing temperature and dwell time) of ancient porcelains with better accuracy relative to existing approaches.

The primary goal of this work was to develop a more accurate and complete model to address the firing conditions of ancient Chinese porcelain by utilizing ancient shards from Jingdezhen City, China in the period of Five Dynasties to Song Dynasty, about one thousand years ago and to offer reliable guidance and potential convenience to archaeological fields and fabricators of different ancient porcelains by knowing approximate firing parameters. However, the measured data from ancient shards did not match the predicted results from previous models, so the validity of previous models is being challenged.

In order to evaluate the applicability of proposed models, newly created porcelain bodies made of only Chinese raw materials and Chinese modern commercial porcelain specimens were examined. Reasonable corrections are provided on the basis of measured results for further optimization.

From this work, the three proposed models for estimating firing conditions are unique and promising except for the proposed restrictions. The restrictions are the difficulty in determining the original body-glaze interface for Model #1, the different amount of

primary mullite tends to disproportionally contribute to the X-ray line broadening for Model #2, and distinct contribution from initial silica in body for Model #3. Therefore, the global applicability of the three models still requires further modification.

II. LITERATURE REVIEW

2.1 Porcelain

Porcelain is defined as a hard, translucent ware of triaxial composition, often bisque fired at a low temperature, and glost fired at a high temperature.[1] Different from earthenware with high porosity and stoneware with slight lower porosity, porcelain is highly dense with nearly zero porosity after fired under proper conditions, and translucent owing to the low porosity. The mixture of glass and crystalline phases initially have three resources: clay, feldspar and quartz. These transform to precipitated mullite, glass (saturated with alumina) and undissolved quartz. As one of the most complex ceramic materials, the firing process of porcelain can be divided into a number of steps as shown in Figure 1. For a typical clay-quartz-feldspar system, the basic reaction steps during firing are the dehydroxylation of clay at 550°C to form metakaolin, the α- to β-quartz inversion at 573°C, the transformation of metakaolin to a spinel-type structure and amorphous silica at 980°C, onset of a eutectic melt at 990°C (for potash feldspar), formation of mullite at about 1100°C, and aggressive dissolution of quartz commencing at 1200°C.[2, 3] The firing process, as the most critical step of porcelain production, has gained a lot of attention, but still requires further understanding in terms of raw material behavior as well as phase and microstructure evolution.

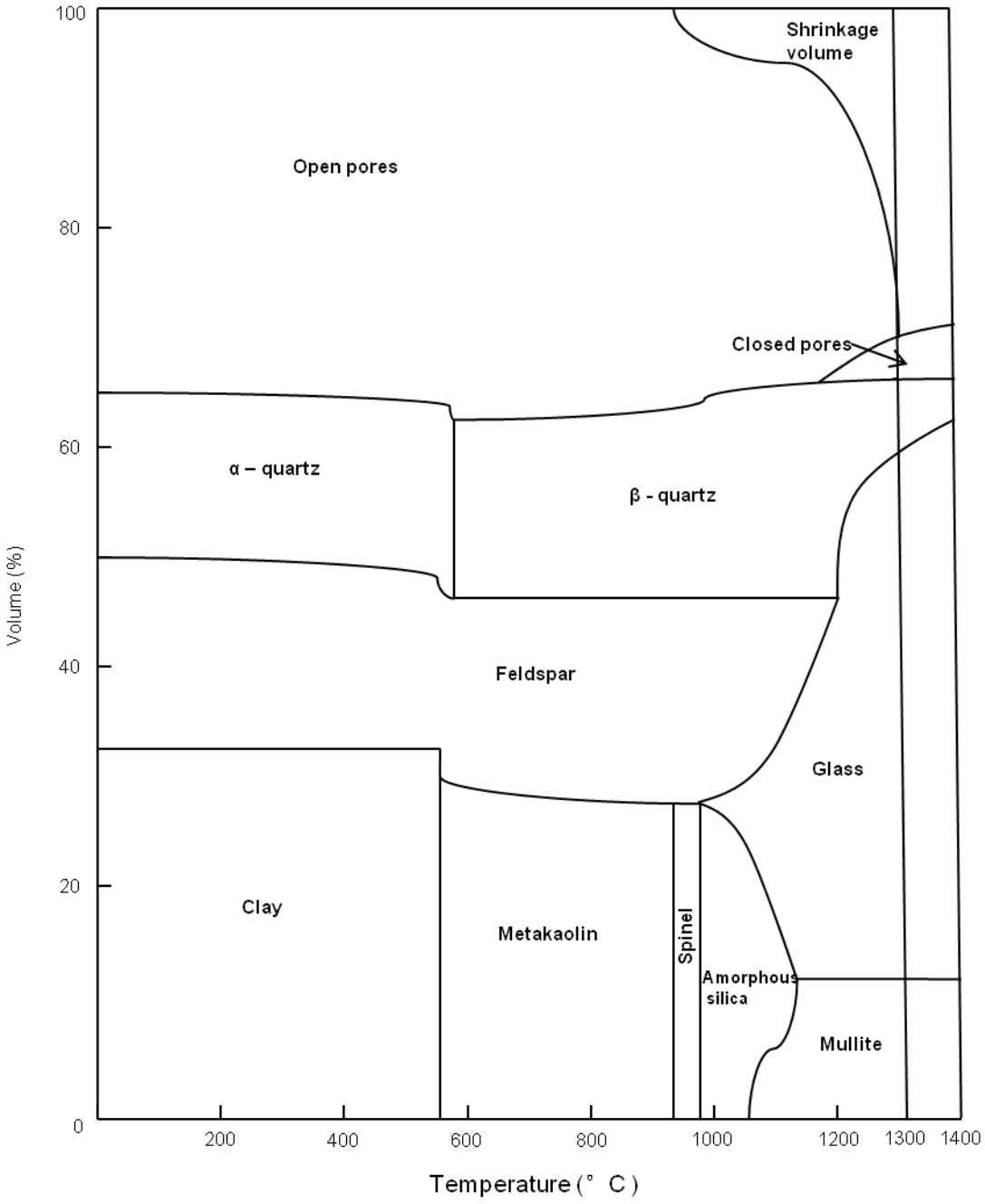

Figure 1. Reactions when firing a triaxial porcelain body.[1, 3]

2.2 Brief history of porcelain in China

Ceramic manufacturing has ancient roots which go back to prehistoric times when craftsmen discovered that clay can be hardened by firing.[1] China is famous for its ceramics especially in ancient times. The emergence and development of ceramics in

China contributed to the progress of civilization as well as the development of the ceramic industry. Archaeological discoveries of pottery have been associated with the development of manufacturing technology from early times, and thus the examination of these shards has been one of the chief tools for obtaining the historical knowledge. The Chinese chronology is presented in Figure 2.

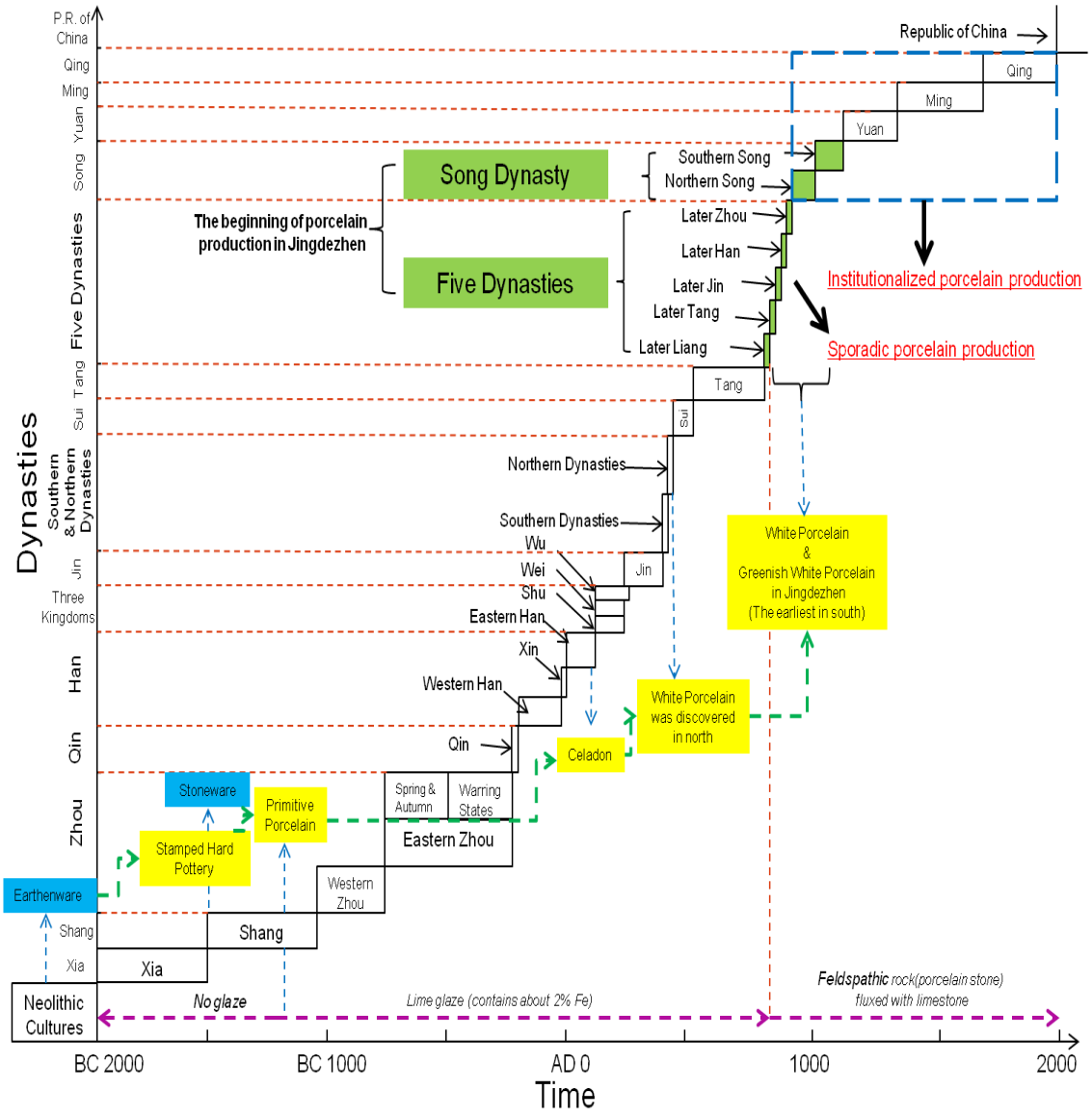

Figure 2. The Chinese chronology.[4, 5, 6]

Perhaps the most significant development throughout the history of ceramics was the production of true porcelain in China with a vitrified, translucent body. Porcelain did not evolve suddenly, but rather was a result of the gradual and necessary refinement of stoneware over several centuries due in part to the slow adaption of feldspathic glazes.[1]

In the history of Chinese ceramics, as early as the Neolithic Age about 8,000 years ago, Chinese ancestors began to make pottery, mainly earthenware, by basic forming and burning.(Craftsmen started to smelt bronze at higher temperatures during the Xia Dynasty (2000-1500 B.C.) The "Stamped Hard Pottery" which was slightly harder and denser appeared in the early time of the Shang Dynasty (1500-1000 B.C.), followed by "Primitive Porcelain" with partial glaze (typically CaO-based glaze). This prototype porcelain was still defined as stoneware because of its lower firing temperature and color. Originating from the "Primitive Porcelain", Chinese Celadon was successfully fired during the Eastern Han Dynasty (25-200 C.E.) as a result of rapid escalation in productivity. In spite of continuous debate about the origin of white porcelain, it was concluded by Chinese archeological experts that white porcelain was first produced in northern China during the Northern Qi (550-557 C.E.), (although this deduction is still questionable). White porcelain did lay a solid foundation for the development of various painted porcelains. The refinement of white porcelain seems to be the result of the patient efforts of northern potter testing whiter raw materials (lower iron content) at higher firing temperatures. During the Tang Dynasty (618-906 C.E.), the ceramic production in China was divided into two regions: north and south, each utilizing different local raw materials. Specifically, Celadon was primarily produced in southern China and white porcelain was mainly produced in northern China, which literally translated as "South Celadon, North Porcelain", hence the phrase "Nan Qing Bei Bai" was born.[4]

During the time of Five Dynasties (907-960 C.E.), Jingdezhen (written as "Ching-te-chen" in some references), the porcelain capital city in both China and the

world began to join the historical stage. The discovered kiln sites in Jingdezhen were considered to be the earliest kilns to produce white porcelain (written as "whiteware" in references) in southern China. The Song Dynasty (960-1279 C.E.) was a much more prosperous period of porcelain production, and is regarded as the beginning of institutionalized porcelain production in Chinese ceramic history. About 75% of unearthed kiln sites in China were dated to the Song Dynasty according to archaeological reports. The exquisite greenish white porcelain (as "Chhing pai ware" in references) from Jingdezhen and Celadon from Longquan area stood out extraordinarily having massive exports overseas during this period. In Yuan, Ming and Qing Dynasties (1279-1911 C.E.), Jingdezhen still maintained its dominating position in porcelain, relying on its continuous optimization and innovations for both body and glaze.[4]

2.3 Porcelain development in Jingdezhen from Five Dynasties to Song Dynasty

2.3.1 The geology advantages in Jingdezhen

Due to its pre-eminent achievements in the ceramic history, Jingdezhen has always been a valuable region for research on porcelain development. Jingdezhen is situated in Fouliang County in the northern part of Jiangxi Province, at the juncture of Jiangxi and Anhui Province as shown in Figure 3.[7]

Figure 3. The geological map of Chinese kiln sites.[8]

The whole region of Jingdezhen is on the transition belt between Mount Huang and the Poyang plateau. Favorable porcelain stones and kaolins for porcelain manufacturing can be found not far from Jingdezhen. The English term "kaolin" is the transliteration of "Gaoling" Village (about 50km northeast of Jingdezhen as shown in Figure 4) where the famous clay was originally found. The diversity of porcelain stones, ascribing to variable deposits of raw materials rightly and necessarily led to the changing firing conditions of ceramic production throughout history.

In addition, the rivers (Chang River and Nanhe River principally on Figure 4) pass through Jingdezhen, delivered an abundance of water which is an indispensable aspect of traditional ceramic manufacturing. The water sources ensured that the needs of ceramic processing, such as elutriation and crushing of raw materials for bodies and glazes were met. The critical transportation of porcelains by cargo ships was far more

adequate than horse and cart in ancient times because of the fragility of porcelains and road conditions.

Jingdezhen has favorable natural conditions with a subtropical climate. The average annual temperature is around 17°C and the average frost-free period is approximately 285 days annually. The abundant rainfall and sunlight in Jingdezhen are appropriate for the growth of trees like pine, fir and bamboo.[7] Furthermore, plentiful pine wood around Jingdezhen area is not only ideal as a fuel for firing due to its long flame and low price, but also is suitable for obtaining reduction atmosphere for targeted glaze color.

Hence, Jingdezhen developed on the strength of rich deposits of porcelain stone and kaolin, broad cover of forests and several rivers which flowed into two major river systems. This coincidence of raw materials, fuel, water and cheap transport put Jingdezhen in a position to satisfy a large scale development of porcelain manufacturing. [9, 10]

Figure 4. The map of kiln sites in Jingdezhen together with the photos of Xianghu (top) and Nanshijie (bottom) kiln site.[11]

2.3.2 White porcelain in Five Dynasties and greenish white porcelain in Song Dynasty

The distinctive white porcelain which led to Jingdezhen's eminence in the porcelain history was first developed during the Five Dynasties period. Although craftsmen in Jingdezhen started imitating stoneware with bluish grey-green glazes far earlier than Five Dynasties, the true porcelain manufacturing of Jingdezhen had not been initiated prior to Five Dynasties.[12, 13] Different from stoneware, the white porcelain in Jingdezhen with a remarkably white and translucent appearance was favored by most people at that time. Employing local porcelain stone with much lower iron and titania content is the main breakthrough which led its success. According to the excavation report of Jingdezhen kiln sites from Five Dynasties, the shards were in the form of white porcelain and the coexistence of Celadon and white porcelain, the deeper depth of the coexistence indicates that the white porcelain gradually became the prime product of this period, while the Celadon declined slowly.[14, 15, 16, 17]

Wares in Song Dynasty were so renowned for their diversity, unique elegance and beauty, that this dynasty has been regarded as a classical period of Chinese ceramics. Greenish white porcelain from Jingdezhen is one of the most outstanding porcelain specimens from the Northern Song Dynasty. Compared with the Five Dynasties, the Song Dynasty used a higher amount of Fe and thicker glaze application, which are considered to be the main reasons for the special greenish white glaze color.[10, 13, 18, 19]

It is believed that the luxuriant growth and development of porcelain during the Song Dynasty gave special meaning to Jingdezhen, because the name of "Jingde" actually originates from the title of an emperor ("Zhenzong Song" in 1004 C.E.). In addition, the bottoms of all produced wares in Jingdezhen were marked with the emperor's title, which addressed to the prohibition of illegal sales among ordinary people.

In order to comprehensively understand porcelain development in Jingdezhen and to

obtain inspiration from traditional porcelain technology from its beginning, it is worthwhile to research porcelain production from the start period (Five Dynasties) and the subsequent prosperous period (Song Dynasty) in Jingdezhen.

2.3.3 Firing technology from Five Dynasties to Song Dynasty in Jingdezhen

2.3.3.1 Porcelain stone

The white, pure porcelain stone is a rock consisting of quartz, feldspar, smectite and a small amount of kaolinite; it can be used to make porcelain without other added raw materials, and so is called "single formula". Principally, porcelain stone itself is low in clay and therefore low in plasticity. The shortfall of low plasticity is partially resolved by the presence of smectite with its flat plate-shaped crystals, allowing particles to slide smoothly over each other.[5, 6]

In its raw state, the porcelain stone needs thorough preparation to improve its plasticity. Historically, large lumps of porcelain rock were successively crushed by hand-hammers and water-powered trip hammers (Figure 5). The raw material was refined by skimming off the floating sediment in water and then dehydrated into fine mass.[6] Since the water-powered hammer normally relies on the volume of mountain stream to operate, spring was recorded to be the optimum season for processing raw materials.[20]

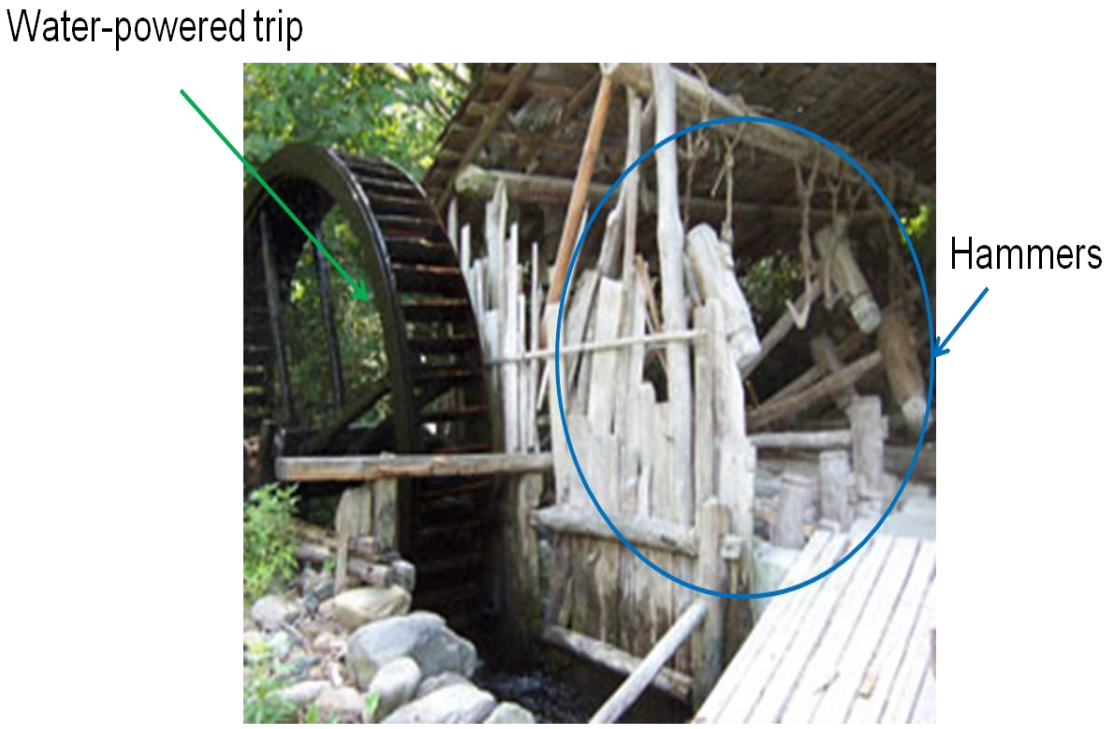

Figure 5. Water-powered trip hammers in Jingdezhen.[21]

In the later Song Dynasty, continuous high demand of porcelain led to excessive mining, resulting in a temporary shortage of superior porcelain stone. Not long after this resource crisis, potters in Jingdezhen started to employ a classical binary formula (porcelain stone & kaolin) to prepare porcelain rather than using only residual porcelain stone with inferior quality.[10, 22, 23] Moreover, the introduction of kaolin contributes to the increase of plasticity and fired qualities of its vast porcelain yield in Jingdezhen area. The typical binary formula flourished in Yuan, Ming and Qing Dynasty, and is even still used considerably in modern porcelain manufacturing in Jingdezhen.

2.3.3.2 Kiln evolution

Jingdezhen used more kiln types than any other site in China, including dragon kilns, man-thou kilns, "gourd-shaped" and "egg-shaped" kilns, as well as some enamel kilns in small-scale. The dragon kiln dominated porcelain firing in Jingdezhen from Five

Dynasties to Song Dynasty according to excavation reports.[24, 25]

The dragon kiln is a definitive southern type because of the mountainous topography in southern China, which is essentially a narrow tunnel built up a low slope as shown in Figure 6. From the schematic diagram in Figure 7, the dragon kiln must lean on the elevated ground and the top end of the kiln serves as the chimney. Wood was burned at the bottom end of the kiln (firebox) and the stacked wares received heat treatment from both the firebox and side-stoking (a further refinement developed in Western Han Dynasty). Even though the side-stoking refinement has helped significantly in equalizing temperature along the length of the chamber, the given dynamic tendency of hot gas and difficulty in setting wares in high stacks, a considerable fall-off of heat (reported to be 1250-1000°C on average) still remains from the firebox to chimney and from the roof to floor respectively.[6]

Figure 6. The scale of residual dragon kiln in Jingdezhen.[26]

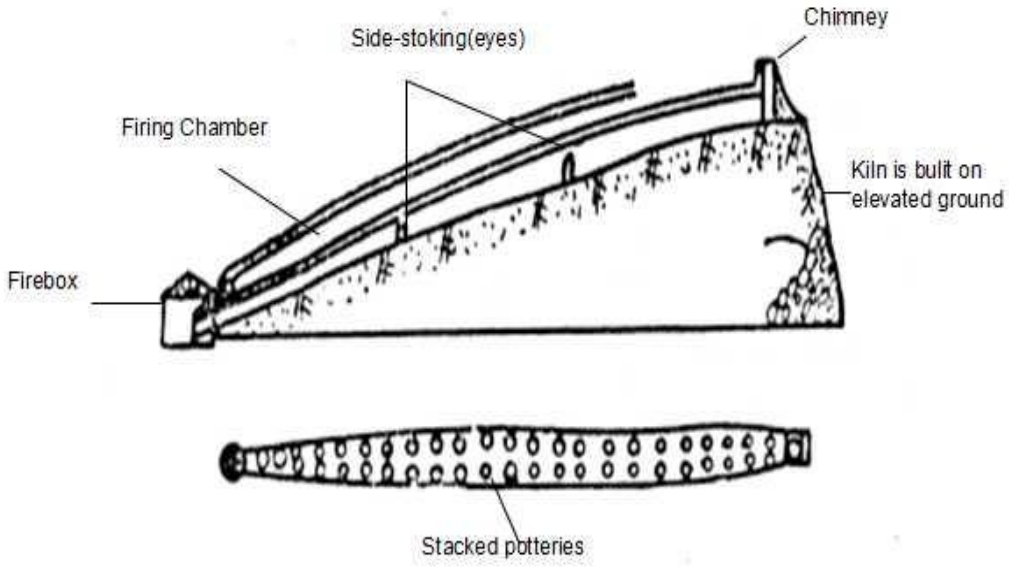

Figure 7. The schematic map of a typical dragon kiln in Jingdezhen.

2.3.3.3 Firing furniture evolution

In general, the firing furniture for porcelain manufacturing in Jingdezhen has gone through dramatic changes from the Five Dynasties to Song Dynasty. On the basis of excavation reports and dating research, dots of fine quartz-grit and thrown columns were used as support pins and setting-wads respectively to support feasible stacks of wares. However, glaze defects like attaching ashes and other impurities by direct fire exposure and potential explosions of wares did substantially affect the yield. Thus, saggers (fired clay box, usually cylindrical) were developed to pack different shapes and sizes of biscuit wares in the kiln later in the Song Dynasty, which encouraged an increasing number of decent wares without defects. In addition, the introduction of "Yang-shao" (firing right-way up) and "Fu-shao" (firing upside-down) techniques also improved the efficiency of porcelain production. This technical breakthrough was concluded to be the first improvement on firing technology in Jingdezhen.[12, 19] The evolution of firing furniture in Jingdezhen together with the residual marks on ancient porcelain specimens are shown in Figure 8.

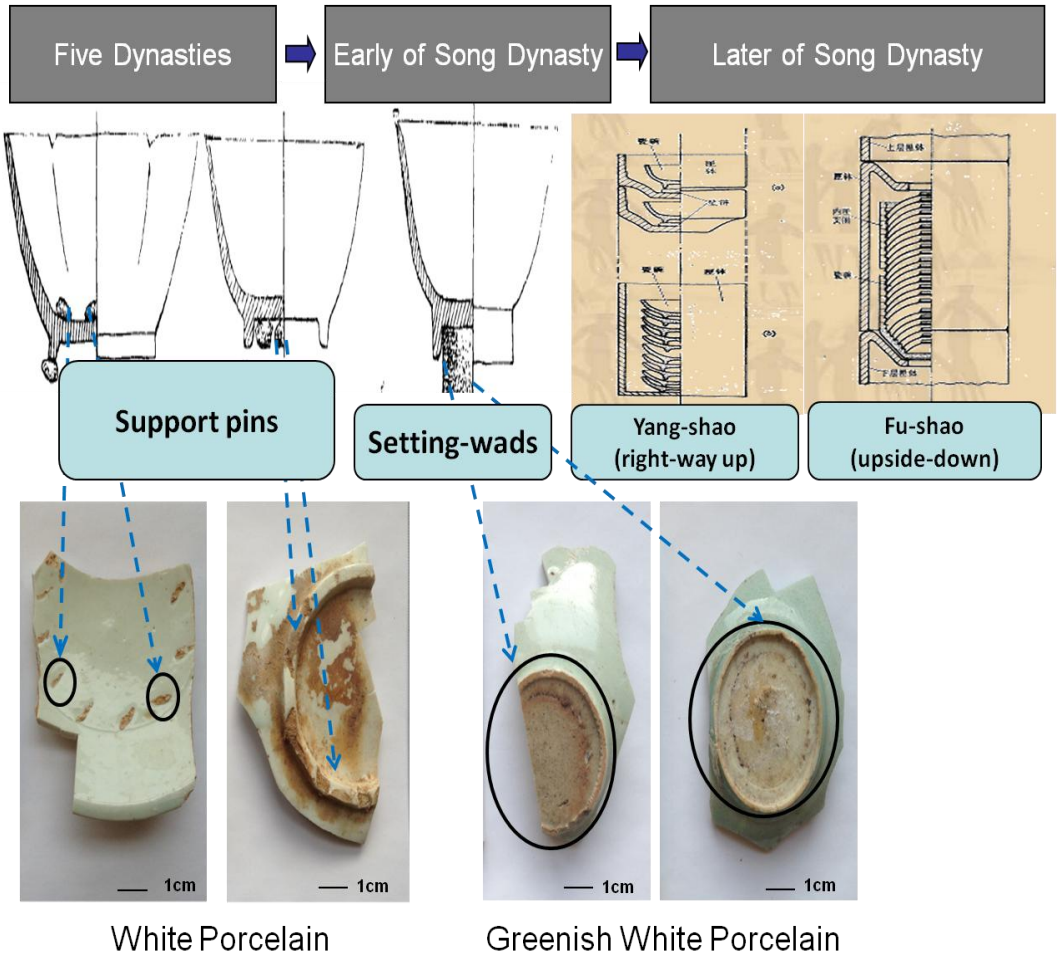

Figure 8. The evolution of firing furniture from Five Dynasties to Song Dynasty in Jingdezhen.[12, 27]

2.3.3.4 Firing conditions

Jingdezhen was assigned to operate the imperial kiln of China given its remarkably high and stable yield following the Song Dynasty. During the early period from the Five Dynasties to Song Dynasty in Jingdezhen, only a few kilns supported the Court and were supervised by government officials directly. Thus, most active kilns were run by an individual family or several families. Since the capacity of the kiln is dependent on kiln size and the kiln size was related to the amount of taxation, common people could not afford a long dragon kiln normally. The weather also affected porcelain production. For example,

the colder outdoor temperature in winter led to lower firing efficiency; as did the long rainy season in summer; comparatively, the processing of porcelain stone in spring was much efficient than the rest of seasons. By taking these into account, archaeologists believe that the porcelain output was not very high from the Five Dynasties to Song Dynasty in Jingdezhen and folk kilns tended to just fire once or twice a year.[6, 18]

In ancient China, specific craftsmen, so-called "fire eyes", were responsible for controlling the firing process. When the saggers were totally white and the atmosphere was clear during firing, the "fire eyes" spit saliva into the kiln through the observing hole. Decisions to terminate the firing was made judging by the vaporization of saliva.[6]

Firing temperature and dwell time which are the most critical integral to firing, have been discussed in excavation reports, researching papers and historical records. Table I lists some typical numbers in terms of firing parameters from the Five Dynasties to Song Dynasty in Jingdezhen. However all these numbers cannot be regarded with great accuracy, because neither uniform kilns, nor reliable measurements could be applied to porcelain production in ancient times.

Table I. Some Typical Firing Parameters from Five Dynasties to Song Dynasty in Jingdezhen

	Dragon Kilns
Firing Temperature (°C)	1230-1260 [28] 1220-1270 [6] 1230-1250 [6] 1150-1200 [19, 29]
Firing Time (hours)	36-48 [30] Short one (30m in length): 24-48 [6, 31] Long one (42m in length): 36-72 [6] The one with a lot of successive chambers: 66 [32]
Capacity (once)	20,000 pieces for 50-60m in length[6]
Fuel	Once: typical kilns required 120 loads* of wood[20] One year: 600,000 loads of wood in AD 1074 in southern [33]

* 120 loads is about six tones[34]

2.4 Current methods for determining the firing conditions of porcelain

The firing temperature of archaeological ceramics are estimated by a number of different methods. For instance, observation of the thermal expansion of regularly shaped samples: the specimen was sliced into a cuboid and its surface was polished to remove the glaze layer or any external contamination, then it is tested in a dilatometer and the specific temperature is measured as its firing temperature once the thermal expansion peak was observed.[35, 36] Moreover, Support Vector Regression (SVR) was proposed to support the dilatometer data with the prediction of the specific behavior of porcelain based on density, shrinkage and applied stress during sintering.[37] Another method, which relied on measuring the magnetic susceptibility of a step-wise refired sample, had shown its validity in the range from 400 to 1000°C.[35] Thermoluminescence (TL), Optically

Stimulated Luminescence (OSL) and Electron Paramagnetic Resonance (EPR) usually measure the accumulated dose of quartz grain for dating purposes.[38, 39, 40] Some researchers also depend on Scanning Electron Microscope (SEM) to estimate firing temperatures by checking the morphology of pores.[41] Environmental Scanning Electron Microscopy (ESEM) can be set to compare the vitrification stages achieved by refiring sample.[42] And Infrared Microscopy (IR) was suitable for estimating low firing temperatures of stoneware according to the assignment of IR peaks.[43, 44] Other methods had been invoked, such as the X-ray Diffraction (XRD) measurement of the layer spacing in the clay mineral illite, monitoring the intensity of Mossbauer lines and the use of color coordinates.[35]

However, limited accuracy and applicability over a limited temperature range is the obvious drawback for most methods in terms of firing temperature. What's more, there seems to be no available technique for estimating the dwell time for ancient porcelains. Therefore, any scientific techniques for predicting both firing temperature and dwell time with measureable reliability is going to improve archaeological ceramic dating and the understanding of manufacturing technology in ancient times.

2.5 Proposed models to determine the firing conditions

Three models were developed to determine the firing conditions. Theoretically, combining any two of the three models is able to obtain firing temperature and firing time respectively.

2.5.1 Model #1: Glaze penetration versus firing time

2.5.1.1 Body-glaze interaction

Generally, the level of R_2O is nearly constant in the typical body and glaze, but RO is much higher in the glaze compared to the body. That’s because calcium carbonate

(Whiting) is predominately added to common glaze as the flux. As the firing process goes on, after the glass phase is saturated with alumina and silica, the excessive alumina and silica in the body move to the glaze, while the RO component (calcium) from glaze penetrate into the body.[45] This process is termed as body-glaze interaction or glaze penetration to body.

2.5.1.2 WDS

Wavelength Dispersive Spectroscopy (WDS) is employed to examine the penetration depth from glaze to body. In Figure 9, the average border of Ca was used to determine the final body-glaze interface and the stationary zircon was added into body as a marker for the original body-glaze interface, as described in detail elsewhere.[46] The Ca-migrated distance correlated with the penetration depth and followed a log-log dependence with time at certain temperatures, as shown in Figure 10.

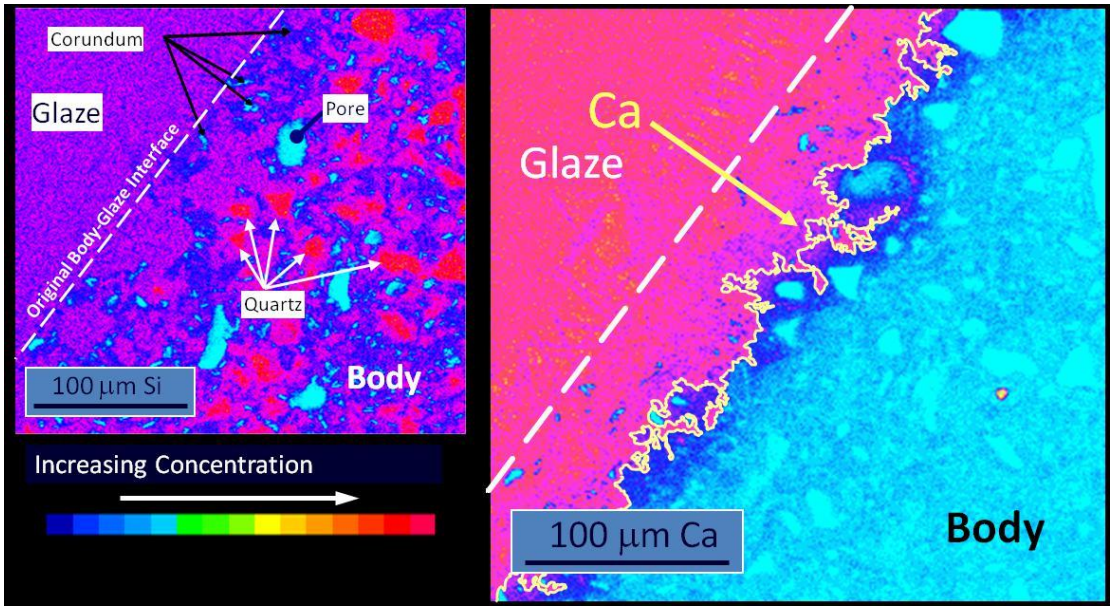

Figure 9. WDS maps of chemistry at body-glaze interface, Si (left) and Ca (right).[47]

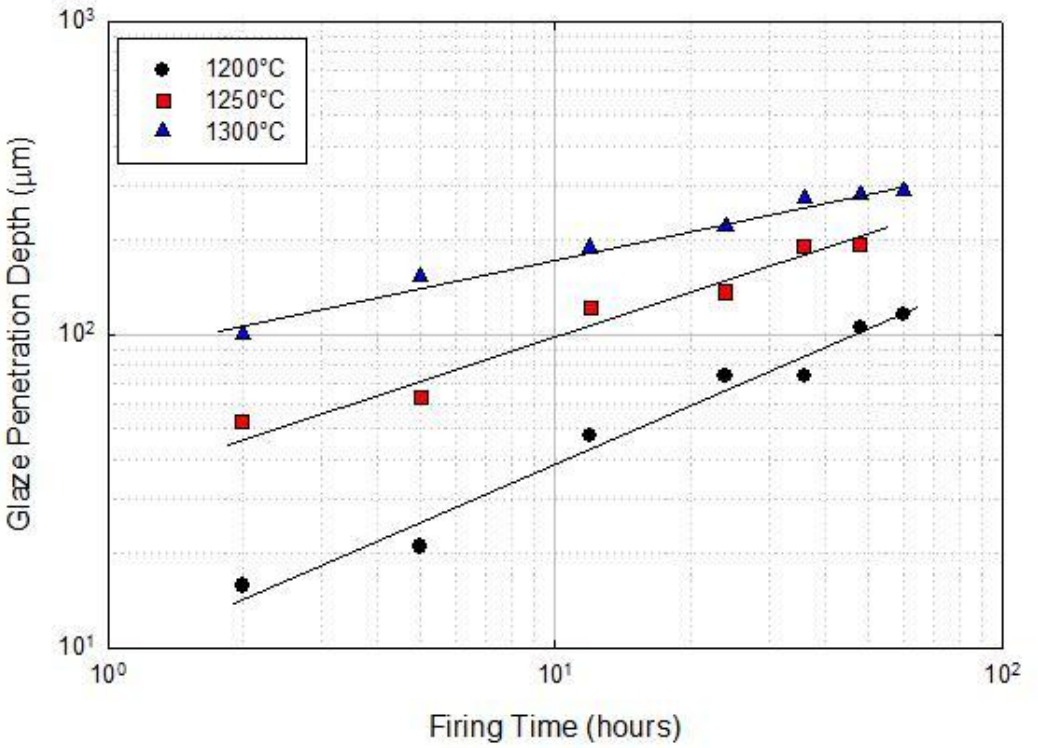

Figure 10. Body-glaze penetration depth as a function of time for three different temperature (1200, 1250 and 1300°C).[47]

2.5.1.3 Determining the firing conditions of ancient Korean shards

Previous work about determining the firing conditions of ancient Korean Celadons had demonstrated the feasibility of this method. Different from the modern samples with added zircon as indicator, this time, the original body-glaze interface was determined by the position of mullite appearing in the glaze layer as shown in Figure 11. Since mullite precipitation in glaze is impossible, the presence of mullite in the glaze was proposed to originate from the recycled body, which marks the original body-glaze interface. Then the firing conditions for ancient Korean Celadons were estimated by combining the body-glaze penetration and glass chemistry through iteration method.[47]

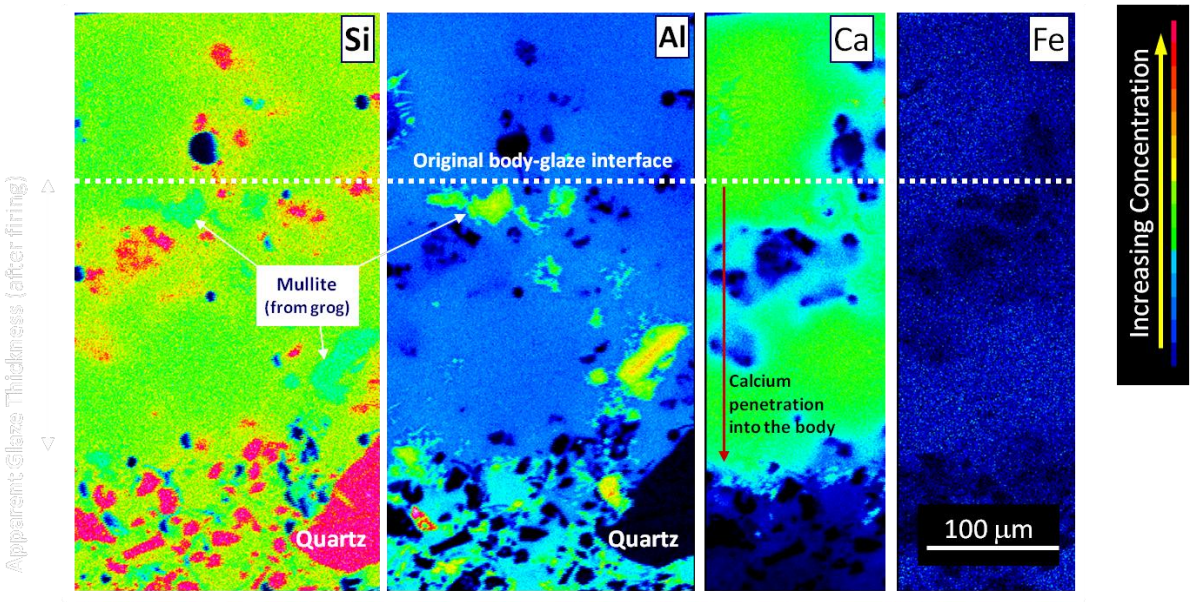

Figure 11. WDS chemical maps of ancient Korean Celadon.[47]

2.5.2 Model#2: mullite crystalline size in (110) direction versus firing conditions

2.5.2.1 Mullite formation

Mullite forms in vitreous porcelain bodies as a result of interplay among raw materials during the firing process. It seems of great interest to research on the crystallization and evolution of mullite during the firing .

It was reported that primary mullite formed above 990°C.[48, 49] This temperature which is around the eutectic point of the typical porcelain system, can be regarded as the point at which aluminosilicate spinel forms. As alkalis diffuse out from feldspar with increasing temperature, secondary mullite forms at about 1275°C.[50, 51] Previous works in terms of QXRD analysis showed that mullite crystallizes between 1100-1150°C. Moreover, the mullite amount kept constant above 1150°C for different dwell time.[52] Alumina UMF (alumina to alkali molar ratio) in glass phase remains constant in the temperature range of 1200-1400°C.[53] It was observed that mullite begins to dissolve at 1400°C as indicated by SEM.[54]

Several factors that affect mullite formation were proposed in references. For

instance, evidences have been found that Fe contributes to the growth of mullite crystals during mullite nucleation from iron-containing kaolinite fired at 900-1250°C.[55] Other variables are still questionable, like type of flux and level of alkalis influenced mullite formation by affecting the composition and viscosity of the liquid in which it grew. In addition, mullite formation tended to enhance by increasing heating rate happening below 1100°C.[56]

2.5.2.2 Primary mullite versus secondary mullite

Universally accepted, the precipitated crystalline mullite is distinguished as primary mullite and secondary mullite. Primary mullite (type-I) derived from pure clay relict is demonstrated to form at lower temperature, as the primary mullite forms from the breakdown of metakaolin earlier. Secondary mullite (granular type-II and elongated type-III) derived from feldspar relicts, is considered to form at higher temperature, because the precipitation of secondary mullite requires alkalis to diffuse out of feldspar later. Hence, the mullite that appears later is termed as "secondary".[3]

Primary mullites are mostly in the form of scaly crystals with small size (<0.5μm), whereas secondary mullites are mostly in the form of needle shaped crystals with relatively larger crystal size (>1μm). Large mullite crystal size from mixed clay-feldspar matrix than that from the pure clay relic was attributed to the higher feldspar content which makes the liquid more fluid, facilitating the mass transport and enhancing crystal growth. In contrast, the small mullite crystal is precipitated from clay relics with highly viscous matrix.[54, 57, 58] It was reported that the fluidity of local liquid was dependent on temperature and composition owing to the content of surrounding feldspar.[59]

Most likely, mullite does not crystallize as a single composition, but as a range of compositions, from $2Al_2O_3 \cdot SiO_2$ (2:1) to $3Al_2O_3 \cdot 2SiO_2$ (3:2).[3, 52] It was reported that the stoichiometry of mullite acts as a complex function of the starting materials and

processing route and tended to depend on the local situation, for example the liquid composition or the availability of solid particles.[60] Since the mullite crystals are embedded in an aluminosilicate glass matrix, the stoichiometry of the mullite formed is difficult to determine. The results of Energy Dispersive Spectroscopy (EDS) indicated that the ratio of Al_2O_3: SiO_2 of primary mullite was close to 2:1, while it was close to 3:2 for secondary mullite. And that was presumed to be dependent with the varying Al_2O_3 content in clay and feldspar relics.[60, 61] Proposed explanation is that primary mullite forms from the breakdown of pure clay to metakaolin, thus is near to 2:1 mullite (Al_2O_3-rich). Secondary mullite comes from the reaction of feldspar and primary mullite. Therefore, it is likely to form an alumina deficient mullite, thus is near 3:2.[58]

2.5.2.3 X-ray line broadening

Based on the X-ray diffraction, the mullite crystallite size has been systematically researched. It was reported the initial width of the mullite peak is very broad and then decreases between 1150 and 1250°C, indicating the transformation from primary to secondary mullite.[48]

The difference in mullite crystallite size had been deduced to be caused by the different crystalline of the involved kaolinite.[50] Previous results have shown that the coarsening of mullite occurs with increasing temperature.[1, 52, 62] It was observed that the mullite grain size in (110) direction coarsened as a function of firing temperature and dwell time owing to Oswald Ripening type effect.[63] A more obvious crystal growth oriented in the (001) plane, rather than (110) direction, was witnessed in another study.[64] A recent study showed that the heating rate did affect the mullite crystallite size in (110) direction, but only plays a minor role if compared to firing temperature and dwell time.[65]

2.5.2.4 A broad range of firing conditions in terms of mullite crystallite size in (110) direction

Average mullite crystallite size in the (110) direction was evaluated by collecting Full Width Half Maximum (FWHM) via Debye-Scherrer's Equation. The equation can be written as:

$$\tau = \frac{\mathrm{K}\lambda}{\beta cos\theta} \quad (1)$$

Where τ is the average size of crystallite domain, β represents Full Width Half Maximum (FWHM), θ is the Bragg angle, K is dimensionless shape factor and λ is the X-ray wavelength.

A potential assumption here is that the mullite crystallite size is no larger than 100nm.[63] Regardless of heating rate, a model for predicting the firing conditions (firing temperature:1200~1300°C and dwell time:0.1~100h) of typical porcelain bodies was generated, shown as a contour map in Figure 12. The relationship of mullite crystallite size ($L_{(110)}$) as a function of temperature, *T (°C*) and time, *t (hours*) was expressed by the given equation:[65]

$$L_{(110)} = \{7.71 * LOG(t)\} + \{((0.1168 * T) - 106.54)\} \quad (2)$$

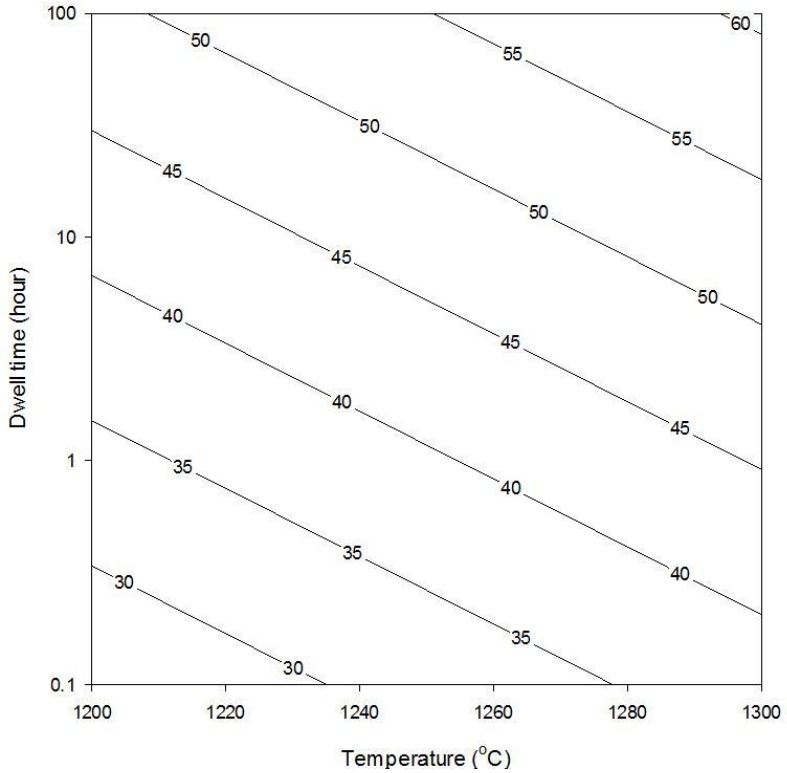

Figure 12. A contour map of mullite crystallite size as a function of firing temperature and dwell time.[65]

2.5.3 Model #3 silica UMF level in the glass phase versus firing conditions

2.5.3.1 The concept of Unity Molecular Formula

Unity Molecular Formula (UMF), also called the Seger formula, was invented by a German ceramist, Herman August Seger back in the 19th century.[45] Initially, the typical formula was made to normalize the chemical composition of glazes. To be specific, the constituent oxides from the glaze recipe were separated into three categories: fluxes (RO & R_2O), amphoteric oxides, also called network modifiers or stabilizer (R_2O_3) and glass former (RO_2),[1, 3] in the form as shown:

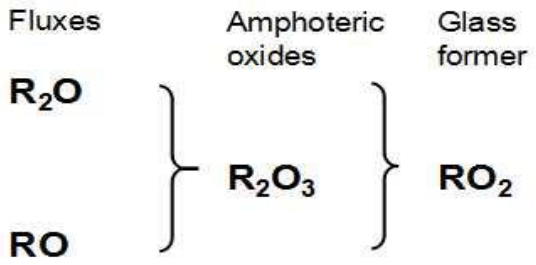

This unique approach provides a direct comparison between various glazes. For example, in the industrial or art development of glaze, the ratio of silica to alumina of the fluxes derived from this form is widely used to predict the surface texture, melting behavior and glaze defects like crazing. The famous Stull Curve (Figure 13) successfully addressed the behavior of glazes based on the concept of UMF. Briefly, the calculation of UMF starts with summing oxides on the weight basis, then converts to the mole basis. Dividing each oxide by flux summation gives the UMF level. The detailed procedures of calculation are described elsewhere.[45]

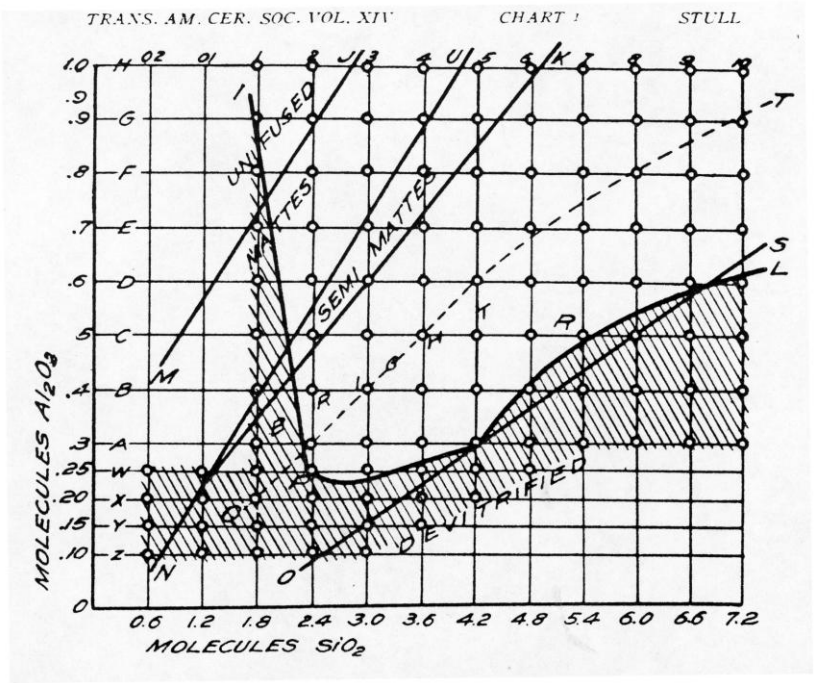

Figure 13. The Stull Curve (K_2O UMF ~ 0.3, CaO UMF ~ 0.7, Cone 11).[66]

2.5.3.2 Quartz dissolution in porcelain

Quartz, as the most widely used filler in porcelain, forms a skeletal network to support the body and provides silica for the glass phase. The increasing viscosity as a result of quartz dissolution decreases the tendency of pyroplastic deformation.[3, 65] The densification process of porcelain can be regarded as a gradual permeation of the glassy matrix involving crystalline phases (mullite and undissolved quartz). As the dissolution of quartz goes on, the increasing amount of glass keeps filling the void fractions in the body, which contributes to the further densification in the way of increasing bulk density.

Carty proposed the quartz dissolution starts sluggishly at about 1100°C, then becomes aggressive at 1200°C, this is consistent with a fast firing research.[65] The transformation of β-Quartz to tridymite at 867°C via Si-O bond breaking and rearrangement actually assists the quartz dissolution, which makes quartz an ideal raw material for porcelain.

Several models describing quartz dissolution were generated based on the assumption that quartz size contributes to the dissolution rate.[67, 68] However, previous works from quantitative XRD (QXRD) measurement and microstructure analysis had demonstrated that the quartz dissolution level in porcelain glass phase was independent of quartz particle size, because the dissolution of quartz in the glass phase is limited by the ability to diffuse the silica from quartz dissolution region into the glass matrix.[3, 53, 65] Moreover, quartz dissolution is independent of the heating rate, but acts as a function of firing temperature and log dwell time.[65]

2.5.3.3 A broad range of firing conditions in terms of silica UMF level in the glass phase

The silica UMF level in the glass phase was calculated by incorporating chemical analysis results with QXRD data. In detail, the wt.% of silica in porcelain glass phase was

obtained by using the total amount to subtract the silica amount in both mullite and undissolved quartz. After converting to a molar basis, dividing the flux amount by grouping alkali and alkaline earth oxides together, gave the silica UMF level in the glass phase. The assumption here is that only 3:2 mullite ($3Al_2O_3 \cdot 2SiO_2$) was formed. Since the silica UMF level in the glass phase acts as a function of firing temperature and log dwell time, a model for predicting the firing conditions (firing temperature: 1200~1300°C and dwell time: 0.1~100h) of typically porcelain bodies was generated, shown as a contour map in Figure 14. The relationship of silica level in the glass phase ($SiO_{2(G)}$) as a function of temperature, *T (°C*) and time, *t (hours*) was expressed by the given equation:[65]

$$SiO_{2\,(G)} = \{((-0.00063 * T) + 1.22) * LOG(t)\} + \{((0.021 * T) - 11.83)\} \quad (3)$$

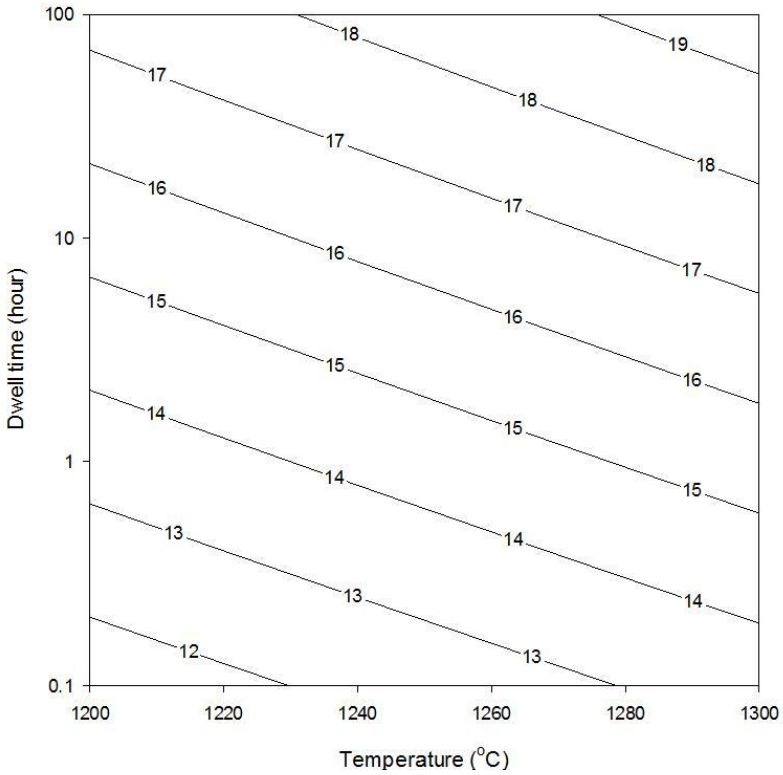

Figure 14. A contour map of silica level in glass phase as a function of firing temperature and dwell time.[65]

2.5.4 Combination of two models to determine firing conditions

The goal of these models is to determine the specific firing temperature and dwell time of porcelain specimens, especially for the unknown specimens from ancient times. By combining Model #2 with Model #3 as an example, the silica level in the glass phase and mullite crystallite size in (110) direction were obtained respectively via XRD diffraction analysis incorporated with chemical composition. It is possible to locate the intersection on the overlapping contour maps of Model #2 and Model #3 as shown in Figure 15. The firing temperature and dwell time are achieved by extrapolating point to the x-axis and y-axis respectively.

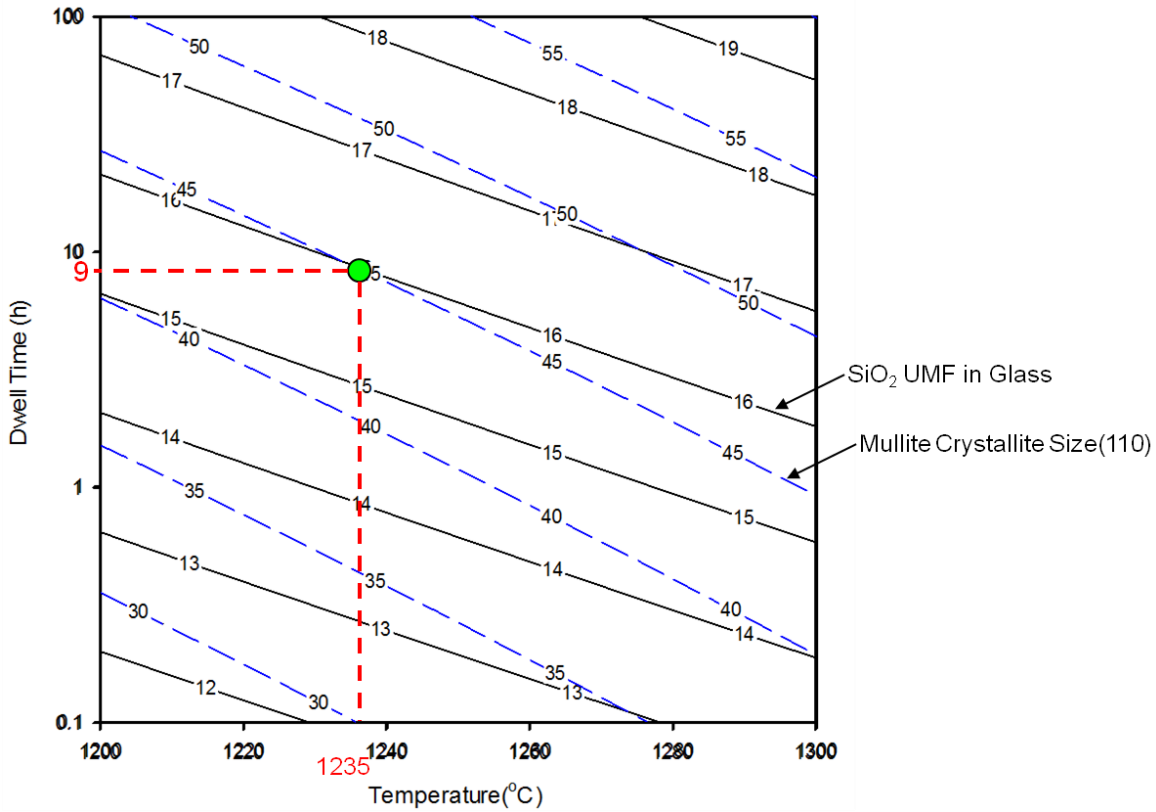

Figure 15. Determination of firing conditions via intersection of combined Models #2 and #3.

III. EXPERIMENTAL PROCEDURE

3.1 Chinese ancient shards

3.1.1 Dating of shards

The 18 ancient Chinese porcelain shards provided by Jingdezhen Ceramic Institute and the Jingdezhen Institute of Archaeological Ceramic were excavated from Jingdezhen City, Jiangxi Province, China. The excavated kiln sites of white porcelain and greenish white porcelain are Xianghu and Nanshijie kiln sites respectively, and the location of kiln sites are shown in Figure 4.

The shards were classified into two groups, white porcelain (WP) and greenish white porcelain (GWP), judging by their appearance: WP represents the specimens that are translucent with glossy white glaze. GWP stands for the translucent appearance with slightly bluish grey-green glaze. Photographs of these shards were taken from several orientations (front, back, cross section and side). Typical photographs of WP and GWP shards are shown in Figure 16. All photographs are provided in appendix.

The traces of support pins and setting-wads are shown up on the bottom of porcelain shards, which is consistent with the evolution process of firing furniture from the Five Dynasties to Song Dynasty, as described in Section 2.3.3.3. Based on this, the WP group could be dated back to the Five Dynasties with the presence of support pins, while the GWP is likely to originate from the subsequent Song Dynasty with a firing furniture transition from support pins to setting-wads.

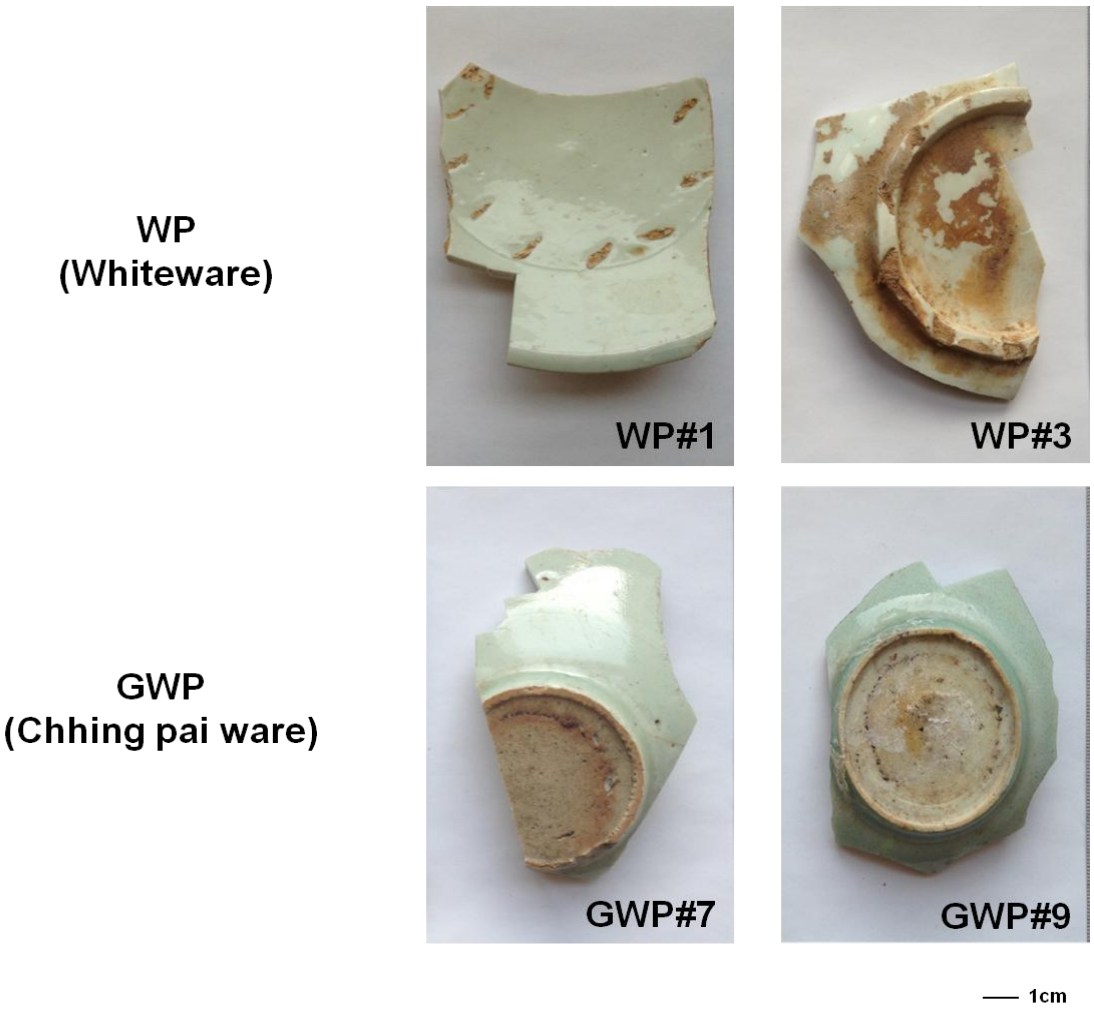

Figure 16. Typical photographs of white porcelain (WP #1 & #3) and greenish white porcelain (GWP #7 & #9).

3.1.2 Characterization of shards

Upon cleaning stain and dirt of shards on the surface, apparent open porosity, water absorption and bulk density of ancient shards were measured by using the standard test method of boiling water.[69]

Shards were cut down to small pieces by diamond saw (Isomet low speed saw, Buehler, Lake Bluff, IL, USA) and mounted in epoxy, then polished with diamond compound. Followed by ultrasonic clean, specimens were etched by 20% HF at room temperature for 10 seconds and dried overnight. A wavelength dispersive X-ray

spectrometer (WDS) was used to perform elemental concentration mapping for Si, K, Ca, Al and Fe respectively.

3.1.3 Chemical composition of shards

The body chemical composition of those 18 shards were measured by Inductively Coupled Plasma-Emission Spectroscopy (ICP-ES, ACME Laboratories Ltd., Vancouver, B.C.) after getting rid of glaze. The averaged results of body chemistry for both WP and GWP groups are listed in Tables II and III, together with the cited chemical compositions from references. The similarity between the measured chemistry and the cited ones seems to be another clue to support that the collected WP and GWP samples stem from the Five Dynasties and Song Dynasty respectively.

Table II. Body Chemical Comparison Between Typical Jingdezhen WP from Five Dynasties and Collected WP Samples

Chemical Composition (Wt.%)		**SiO_2**	**Al_2O_3**	**TiO_2**	**Fe_2O_3**	**CaO**	**MgO**	**K_2O**	**Na_2O**	**MnO**	**P_2O_5**
Cited[70]	**Five Dynasties**	77.50	16.90	0.00	0.80	0.80	0.50	2.60	0.35	0.14	0.00
Measured	***Ave. of WP**	77.22	17.31	0.04	0.64	0.21	0.19	3.03	0.25	0.10	0.03
	Stan. Dev.	1.01	0.51	0.04	0.07	0.09	0.03	0.36	0.13	0.03	0.01

* Ave: the averaged result of seven WP specimens. Raw data is provided in appendix.

Table III. Body Chemistry Comparison Between Typical Jingdezhen GWP from Song Dynasty and Collected GWP Samples

Chemical Composition (Wt.%)		**SiO_2**	**Al_2O_3**	**TiO_2**	**Fe_2O_3**	**CaO**	**MgO**	**K_2O**	**Na_2O**	**MnO**	**P_2O_5**
Cited[71]	**Song Dynasty**	77.90	16.20	0.07	0.60	0.80	0.40	3.20	0.85	0.00	0.00
Measured	***Ave. of GWP**	75.89	17.39	0.05	0.89	0.56	0.18	2.78	1.49	0.07	0.02
	Stan. Dev.	1.08	1.07	0.01	0.10	0.31	0.04	0.22	0.64	0.02	0.01

* Ave: the averaged result of eleven GWP specimens. Raw data is provided in appendix.

Rather than ICP analysis, EDXRF as a nondestructive analysis method, is preferable for precious ancient porcelain samples because the measurement is able to carry out without consuming samples. In this work, the glaze chemical composition is obtained from EDXRF acknowledged to Jingdezhen Ceramic Institute. The results are listed in Table IV.

Table IV. The Glaze Chemical Composition of Collected WP and GWP Specimens by EDXRF Measurement

Glaze Chemical Composition		**SiO_2**	**Al_2O_3**	**TiO_2**	**Fe_2O_3**	**CaO**	**MgO**	**K_2O**	**Na_2O**	**MnO**	**P_2O_5**
White Porcelain	***Ave.**	69.21	14.55	0.03	0.69	10.60	0.98	2.74	0.10	0.17	0.17
	Stan. Dev.	3.06	0.96	0.01	0.03	3.08	0.23	0.58	0.09	0.05	0.07
	UMF	5.01	0.62	-	-	0.866		0.134		-	-
Greenish White Porcelain	**Ave.**	67.63	13.10	0.03	0.87	13.28	0.41	2.16	1.52	-	-
	Stan. Dev.	1.40	0.73	0.01	0.31	1.03	0.18	0.36	0.68	-	-
	UMF	3.84	0.44	-	-	0.839		0.161		-	-

* Ave: the averaged result of total 18 specimens. Raw data is provided in appendix.

The ratios of SiO_2 to Al_2O_3 on UMF basis of both WP and GWP groups are around 8 that falls well within the glossy area in Stull's map,[45, 66] which is consistent with the glaze texture. The most common way to color ceramic is by adding transition metals, such as Fe.[72] Historically, the level of iron oxide in glaze recipe played a vital role for the color of porcelain in ancient China. And wood was the typical fuel for firing in south of China that provided an ideal reduction atmosphere. The shifting color from white to light green is due to the presence of Fe^{2+} ions. Thus, the slight change of Fe level (from 0.69% in WP to 0.87% in GWP) from Table XIII is proposed to contribute to the glaze color transition.

3.2 Newly created bodies by using Chinese raw materials

3.2.1 Raw materials

Four typical porcelain stones and one identical Chinese kaolin from commercial porcelain industry of Jingdezhen were used for following experiments. The chemical composition of each raw material was measured by ICP and results are listed in Table V. True density of each raw material was measured by using a pycnometer (AccuPyc 1330, Helium Pycnometer, Micromeritics Instrument Corp., Norcross, GA, USA), together with the X-ray diffraction (Bruker D2 Phaser, Madison, WI, USA).

Table V. The Chemical Composition of Chinese Raw Materials by ICP

	SiO_2	Al_2O_3	Fe_2O_3	MgO	CaO	Na_2O	K_2O	TiO_2	P_2O_5	MnO
***Chin. kaolin**	49.44	33.51	1.75	0.20	0.03	0.06	1.71	0.14	0.03	0.02
Sanbao **P. S.	73.58	14.81	0.68	0.12	0.67	5.04	2.83	0.03	0.11	0.08
Nangang P. S.	75.90	14.45	0.83	0.28	0.65	0.80	2.90	0.05	0.05	0.13
Qimen P. S.	74.40	15.04	0.74	0.20	0.49	3.54	2.80	0.04	0.10	0.05
Yugan P. S.	73.92	14.80	1.02	0.23	0.61	1.82	3.92	0.10	0.04	0.05

* Chin. stands for Chinese.

** P.S. is abbreviated for "porcelain stone".

3.2.2 Green samples preparation

The processing of all prepared bodies started with weighing (70% solid loading & 30% water fraction), then ball-milling for 1 hour, followed by slip-casting. After demolding, samples were stored in a drier until heat treatment.

The experiment "Spot Check" (SC) was designed to check the validity of models by randomly creating body. Green bodies were formulated in either single different porcelain stone or binary formula (80% porcelain stone + 20% kaolin).[73] The "Comparative Experiment" (CE) was implemented by mimicking previous formulas including Lerdprom's (C-WL)[65] and Colorado's (C-VC)[2] by only using Chinese raw materials, together with three typical Chinese commercial green bodies(CC #1, #2 and #3) acknowledged to Shuguang porcelain factory, Jingdezhen City, Jiangxi Province, China. The formulas of "SC" and "CE" experiments are provided in Tables VI and VII.

Table VI. The Formulations of "Spot Check" group.

Spot Check	
1	100% Sanbao porcelain stone (wt.%)
2	100% Nangang porcelain stone
3	100% Qimen porcelain stone
4	100% Yugan porcelain stone
5	80% Sanbao porcelain stone & 20% Xingzi kaolin
6	80% Nangang porcelain stone & 20% Xingzi kaolin
7	80% Qimen porcelain stone & 20% Xingzi kaolin
8	80% Yugan porcelain stone & 20% Xingzi kaolin

Table VII. The Formulations of "Comparative Experiment" Group

Comparative Experiment	
Chinese -> Lerdprom's (C-WL)	50% Nangang porcelain stone & 50% Xingzi kaolin (wt.%)
Chinese -> Colorado's (C-VC)	44% Yugan porcelain stone & 44% Xingzi kaolin & 12% Nepheline Syenite
Chinese Commercial #1 (CC #1)	#1 Body from Shuguang porcelain factory
Chinese Commercial #2 (CC #2)	#2 Body from Shuguang porcelain factory
Chinese Commercial #3 (CC #3)	#3 Body from Shuguang porcelain factory

3.2.3 Firing apparatus

A bottom loading electric furnace was used to achieve targeted firing schedules. Firing temperatures were verified by using pyrometric cones (Edward Orton Jr. Ceramic Foundation, Westerville, OH, USA).

Specimens were placed on an alumina substrate and fired at different schedules, as listed in Table VIII. Previous work had demonstrated that both silica UMF level in the glass phase and mullite crystallite size are independent of heating rate, thus a fixed heating rate (2.5 K/min) is used for all firing conditions.

Table VIII. Experimental Heat Treatment Parameters

	Firing Temperature (°C)	**Dwell Time (hours)**
Spot Check	1150 1250	3.2 32
Comparative Experiment	1250 1300	3.2 32

3.2.4 Characterization of the fired specimens

Fired specimens were crushed and ground to particle size which is smaller than 10μm approximately. Each specimen was ground for 20 minutes in a motorized mortar pestle (RM100 Mortar Grinder, Retsch GmbH & Co.KG, Germany). True density of crushed powder was measured by using a pyconometer (AccuPyc 1330, Helium Pycnometer, Micromeritics Instrument Corp., Norcross, GA, USA), followed by Quantitative XRD analysis (QXRD).

QXRD analysis was performed using CaF_2 as an internal standard and analyzed by Jade (Version 9, Materials Data Inc., Livermore, CA, USA), as described in detail elsewhere.[2, 65] Peak areas of three non-overlapping peaks were selected for these three mineral phases: mullite, quartz and calcium fluorite, as specifically listed in Table IX. Besides, mullite crystallite size in (110) direction was calculated by utilizing Full Width Half Maximum (FWHM) from X-ray diffraction patterns, as described elsewhere.[63, 65]

Table IX. The Position of Selected Peaks for Quantitative X-ray Analysis

	Diffraction Peak (hkl)	**2-Theta Interval (°)**	**Averaged 2-Theta (°)**	**Reliability* (wt.%)**
Mullite	(001) (220) (121)	30-32 32-34 40-42	30.927 33.187 40.799	±2%
Quartz	(110) (111) (112)	19-22 38.2-41.5 49-51	20.809 40.255 50.095	±3%
CaF_2	(111) (220) (331)	27-29.5 46-48 51-59	28.225 46.953 55.728	

*The reliability is relative to the measured value, not absolute.

IV. RESULTS AND DISCUSSION

4.1 General observation of ancient Chinese shards

Wavelength Dispersive Spectroscopy (WDS) was used to obtain cross-section chemical maps of the 18 shards.

A previous work demonstrated that Ca penetration depth is a reliable indicator of the final glaze thickness. According to the Ca WDS maps of body-glaze interface as shown in Figure 17, the final glaze thickness of a typical WP specimen (about 200μm) is roughly as half that of a typical GWP specimen (500μm approximately).

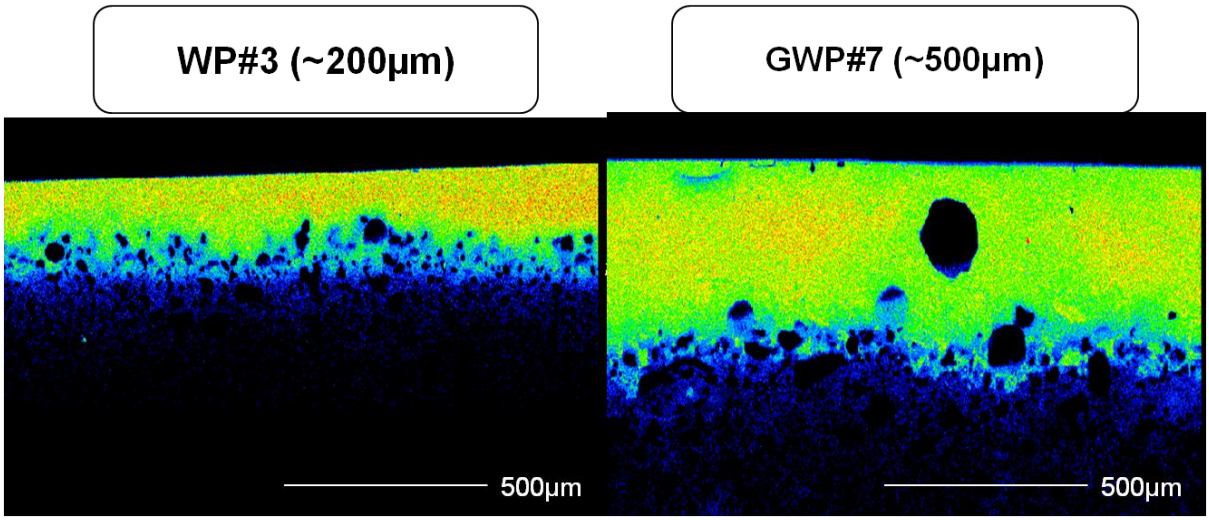

Figure 17. Ca WDS maps of typical white porcelain and greenish white porcelain from Jingdezhen in the period of Five Dynasties to Song Dynasty.

In Figure 18, a large quartz cluster was observed in the glaze layer which is not uncommon in ancient Chinese porcelain specimens. The presence of quartz particle is observed for about half of the 18 shards. In modern porcelain production, however undissolved quartz is rarely observed in the glaze layer after heat treatment. Hence, the observation of large quartz clusters suggests that the mixing process for the porcelain manufacturing in Jingdezhen during the period of Five Dynasties to Song Dynasty was probably insufficient. In addition, the presence of cristobalite in 3 of overall 7 WP

specimens also supports the deduction of poor mixing at early times, as shown in Figure 19. Because insufficient mixing tends to result in the isolation of quartz without contacting from the glass (formed during firing), promoting cristobalite formation.[63] This is consistent with historical records as stated in Section 2.3.3.1, since porcelain stone was the single component to produce body in Jingdezhen from Five Dynasties to early of Song Dynasty. Therefore, there were no additional mixing procedures involved in the preparation of raw materials, resulting in the presence of larger quartz cluster in glaze layer.

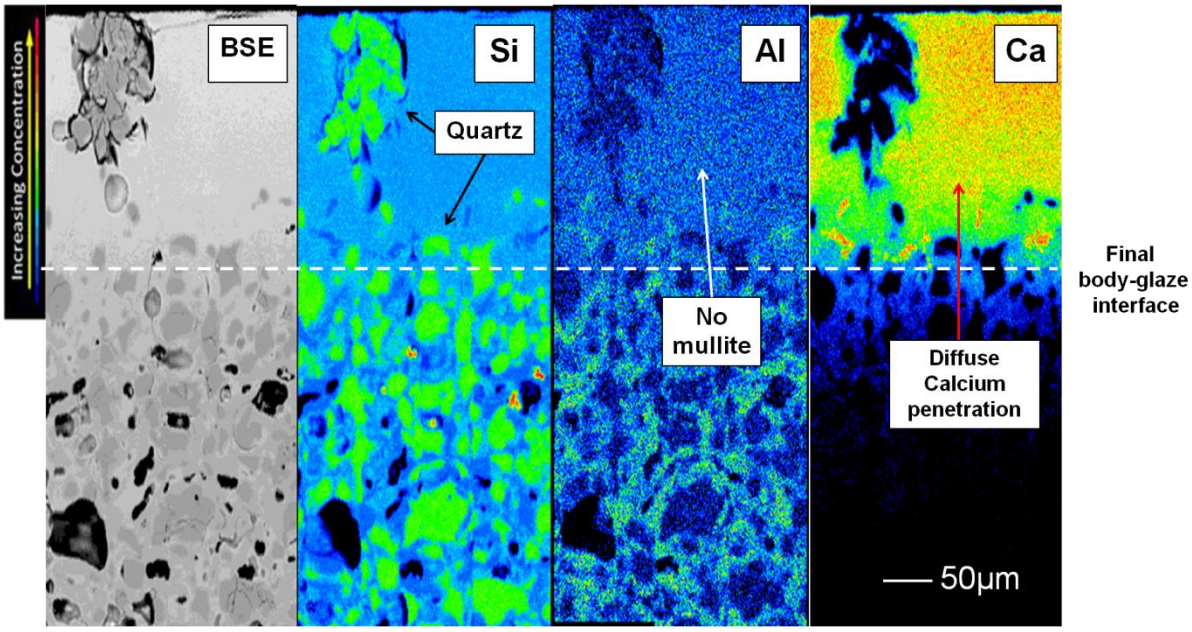

Figure 18. WDS mapping (Si, Al and Ca) and backscatter image of WP#4.

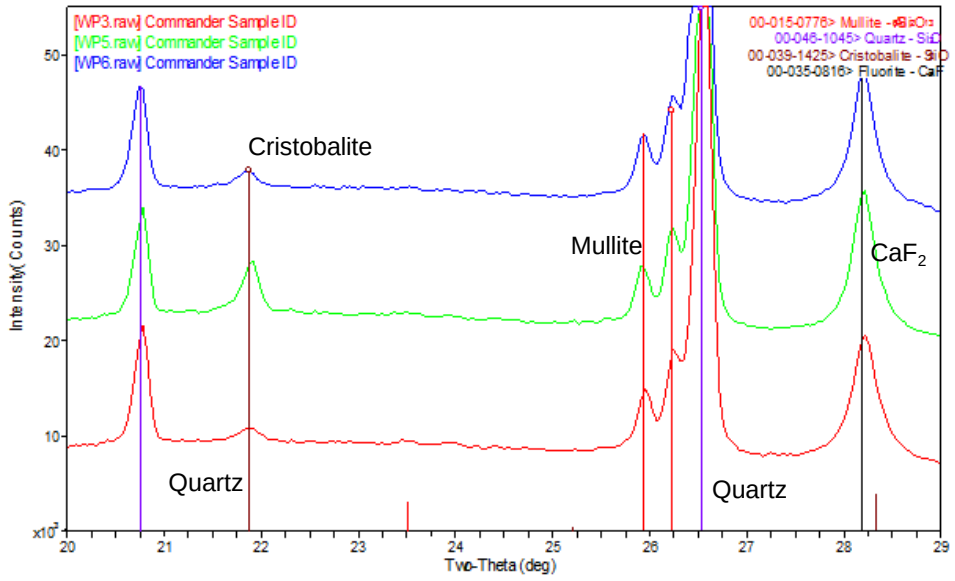

Figure 19. X-ray diffraction pattern for ancient Jingdezhen porcelain specimens showing the evidence of cristobalite (WP#3, WP#5, WP#6).

4.2 Approximate estimation of firing time

In 1074 C.E., an inspection accounted for the use of the annual quota of approximately 600,000 loads of wood in south China, where there were located 11 main ceramic manufacturing areas including Jingdezhen.[74] And there were 36 kilns in operation in Jingdezhen area during the period of Five Dynasties to Song Dynasty.[74] The typical firing for a dragon kiln with averaged length consumed about 120 loads of wood per firing.[20]

In general, winter is not suitable for firing due to poor heating efficiency. Spring is optimal for preparation of superior raw materials with high flow volume of mountain streams to drive the water wheel. In spite of high ambient temperatures, summer in Jingdezhen also is the rainy season with intermittent heavy rain occasionally, making firing impractical. Therefore autumn tends to be the most ideal period to fire the kiln. In addition, it is recorded that as both to utilize the residual heat for initial drying and to save

the amount of fuel for heating the kiln structure, the kiln was set again right after the last firing.[6] Because of all of these constraints, there were only about 90 days per year that were suitable for continuous kiln operation.

Under the assumption that total wood was distributed evenly to 11 main manufacturing areas and the kilns in Jingdezhen were of similar size. It is possible to roughly estimate the approximate firing cycle of Jingdezhen kilns in this time period. The results of calculations are presented in Table X.

Table X. Estimation of Firing Cycles by Rough Calculation

Overall Used Wood in Southern China (loads)	**Wood Used in Jingdezhen (loads)**	**Wood Used Per Kiln (loads)**	**Firing Time per kiln**	**Firing Cycles**
Total of southern	Total /11 (areas)	54545 / 36 (kilns)	1515 / 120 (loads for each firing)	90 (days) / 12.62
600,000 per year	54,545 per area	1515 per kiln	12.62 per kiln	7.1 days per firing

The estimated firing cycle of individual kiln in Jingdezhen area during the Five Dynasties to Song Dynasty is about 7 days which including loading, heating, dwell at peak temperature, cooling and unloading. The reasonable dwell time would be estimated to be between 2 to 4 days if these procedures except dwelling required one day each. These estimations are consistent with historically recorded dwell time listed in Table I.

4.3 Three proposed models to determine the firing conditions of Chinese ancient shards

Model #1 was developed from a series of studies on body-glaze interaction. In the study of ancient Korean Celadons, WDS mapping was proposed to be viable for determining the glaze penetration depth by locating the original and final body-glaze interfaces. The original body-glaze interface was identified based on the presence of mullite in the glaze layer, proposed to be an artifact of recycling fired body as grog.[47] However, the lack of recycled body in ancient Chinese porcelain specimens renders Model #1 unsuitable for this case.

Figure 20 is a comparison of Models #2, #3 and experimental results obtained from the ancient shards. The measured results of WP and GWP specimens do not match the model predictions. And this challenges the validity of the proposed models.

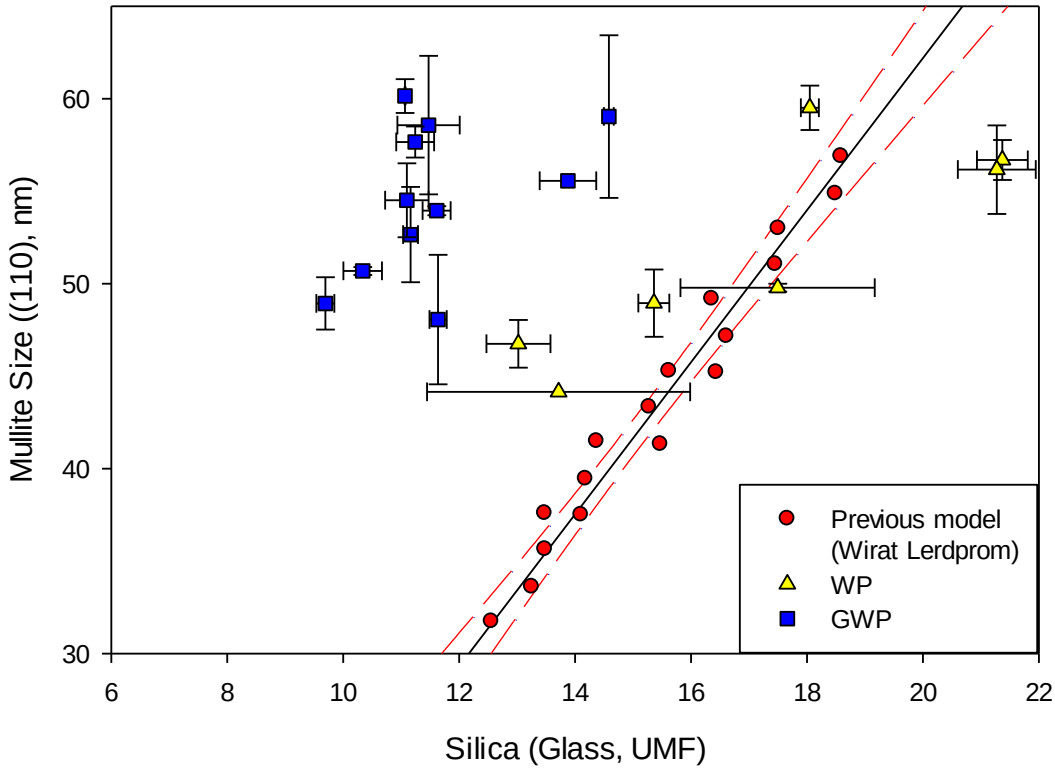

Figure 20. Comparison of ancient Chinese shards and previous models in terms of silica UMF level in glass phase and mullite crystallite size in (110) direction.

4.4 Evaluation of three proposed models

In order to explore the applicability of those three models, evaluations combined with further experimental results are provided.

4.4.1 Model #1: glaze penetration depth versus firing time

4.4.1.1 Three potential conditions

In the study of ancient Korean Celadons, three potential conditions were necessary for applying Model#1:

1) The presence of mullite in the glaze layer. (Identifying the original body-glaze interface)
2) Well defined Ca penetration depths into the body.

3) Limit undissolved quartz remains in body-glaze interface.

1) The location of observed mullite from WDS gave the marker of original body-glaze interface for Korean Celadon. The presence of mullite in glaze layer indicated that recycling body was used for porcelain manufacturing in ancient Korea.[47] There is no evidence of mullite precipitated in the glaze layer of ancient Chinese porcelain samples eliminating the opportunity to determine the original body-glaze interface. This is consistent with Chinese manufacturers process only virgin raw materials, due to abundant raw material reserves locally and a exercised tradition of destroying imperfect products.

2) Ca penetration depth is the critical aspect of Model #1. The end of Ca penetration depth from glaze to body marks the final body-glaze interface. In Figure 21, different from the homogeneous distribution shown as uniform for the Korean Celadon specimen, the distribution of Ca within glaze layer appears to be diffuse for many of Chinese ancient porcelain specimens. Thus, the deduction is made that the kinetic diffusion of Ca^{2+} for some of those collected ancient Chinese porcelains with Ca gradient tends to be more sluggish (for reasons that are unclear) than that of ancient Korean Celadon.

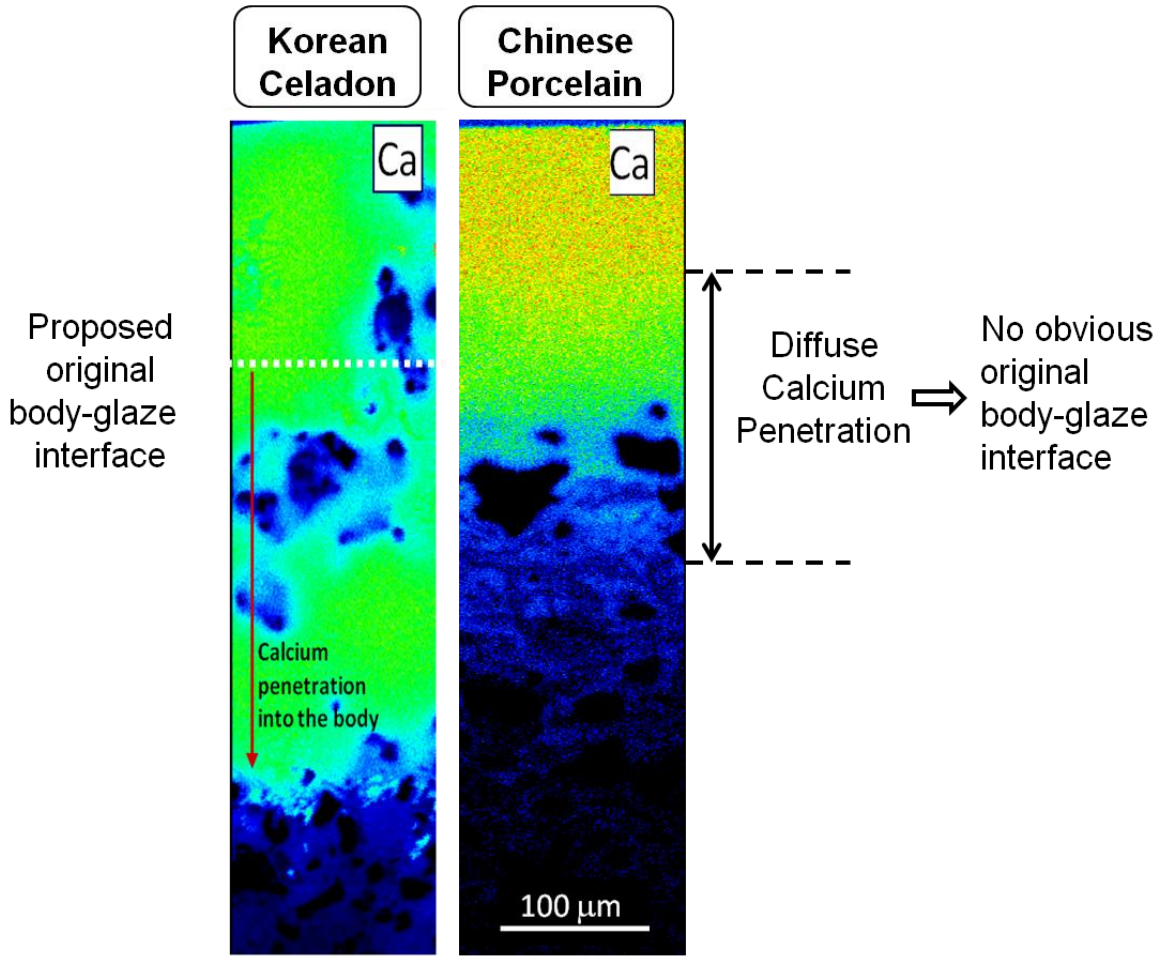

Figure 21. A comparison of ancient Korean Celadon (left) and ancient Chinese porcelain (right) in Jingdezhen.

3) Figure 18 is a set of WDS maps of the typical ancient Chinese porcelain in terms of Si, Al and Ca. The dashed line in Ca map represents the approximate ending place of a penetration from glaze to body, which is regarded as the final body-glaze interface. From the Si WDS map, a considerable number of undissolved quartz particles (yellow ones) still remain within the body-glaze interface, whereas undissolved quartz particles within the body-glaze interface for both ancient Korean Celadon and modern porcelains are rare. Since the aggressive dissolution of quartz was demonstrated to occur at 1200°C by previous work,[2, 65] which suggests that the collected specimens from Jingdezhen were

likely fired at temperatures lower than 1200°C, which is outside of the 1200 - 1300°C range of Model #1.

4.4.1.2 Low firing temperature

It was reported that the feldspar dissolution is complete by 1200°C and feldspar requires longer time to completely melt at temperatures lower than 1200°C.[65] In addition, incomplete melting of feldspar reduces the amount of available flux in glass phase, which is supposed to decrease alumina UMF level in the glass phase on the basis of the concept of glass formation boundary. Based on this, WP#4 was employed as an example to examine the presence of residual feldspar as it has the lowest alumina level (0.89) in the glass. The WDS maps in Figure 22 show a non-uniform K gradient in the feldspar relics, which suggests incomplete feldspar dissolution. For comparison, a standard specimen consisting of large feldspar grain was fired at 1150°C for 3hrs and then mapped by WDS. Different from WP#4, a more obvious K gradient together with sharper edge of quartz was observed in Figure 23. Hence, the low firing temperature hypothesis does not seem to fit the WDS data for the low firing temperature specimen. This is consistent with most firing temperatures from historical records and researching results, as listed in Table I.

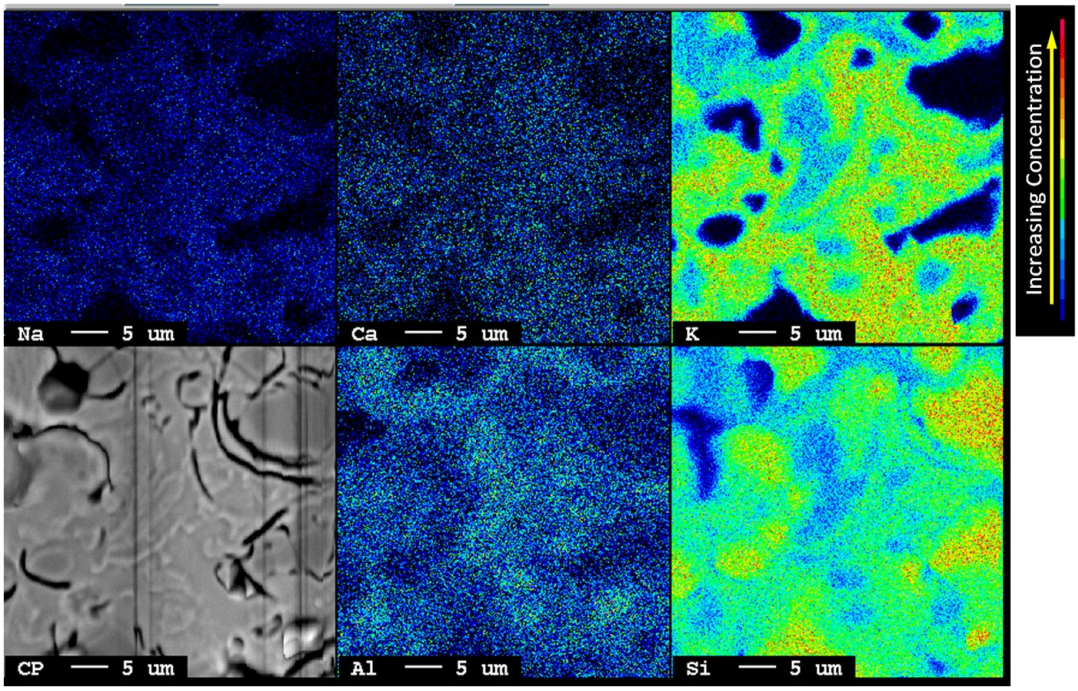

Figure 22. WDS maps (Na, Ca, K, Al and Si) of body of WP#4.

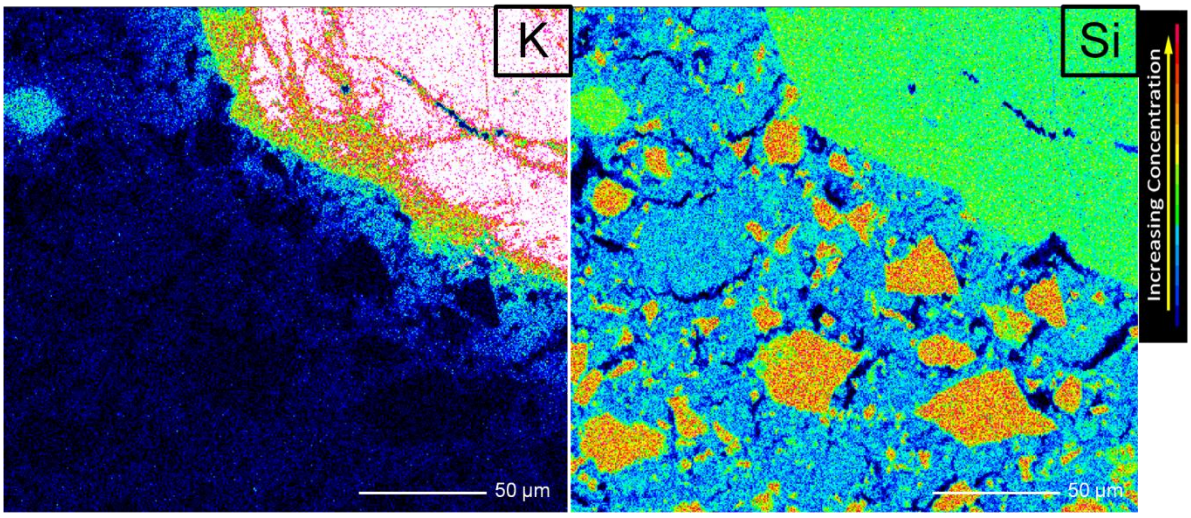

Figure 23. WDS maps (K and Si) of standard consisting of feldspar clusters fired at 1150°C.

4.4.2 Assumptions for Model #2 and Model #3

The two models are based on five conditions:

1) Iron level is unimportant.
2) Specimen fired only once (no recycled body incorporated).
3) Alkali levels stay constant and do not change with time.
4) Mullite crystallite size is only a function of firing temperature and dwell time, not the mullite source.
5) The glass chemistry is only related to overall raw material chemistry, not raw material mineralogy. And it scales linearly with temperature and the log of dwell time.

1) It was found that the presence of iron can significantly alter the glass phase chemistry when the iron level cannot be ignored (>3%). The SiO_2 level in the glass phase would be greater, because Fe^{2+} ions would function as extra flux component and Fe^{3+} can substitute for Al^{3+} to form additional mullite.[47] In this work, the Fe_2O_3 levels (wt.%) of ancient Chinese porcelain specimens are less than 1% according to chemical analysis, thus iron level does not contribute a considerable error to the estimation of firing condition. Therefore, the condition #1 of "iron is unimportant" is acceptable.

2) If recycled body was used for producing new body, the measured mullite wt.% by QXRD could be greater if the recycled body had a higher mullite content. This would lead to overestimation for the consumed SiO_2 amount in mullite formation. Then, the calculated SiO_2 level in glass phase tends to be underestimated. Moreover, the mullite contained in recycled body would be coarser than mullite obtained from virgin materials. Since no evidence of precipitated mullite was found in the glaze after firing process basing on Al and Si WDS maps, thus these shards do not appear to contain recycled body. This is consistent with historical tradition for ceramic manufacturing in China.

3) In ancient China, the porcelain shards were thrown away and piled up not far from kiln sites as shown in Figure 4. The shards were expected to stay at near-surface position with alternately wet and dry for a great time, providing the potential for weathering. Inevitably, the shards would experience greater loss of R_2O compared to other oxides. Since all chemistry calculation are normalized to sum of flux (R_2O+RO), loss of R_2O would increase the relative levels of Al_2O_3 and SiO_2 in the glass phase, but this does not match with the SiO_2 level as shown in Figure 20. In addition, the WDS results do not support the loss of R_2O due to no depleting from glaze surface. Therefore, the condition #3 is apparently valid.

4) Model #2 was developed based on the assumption that raw materials do not contribute to the mullite crystallite size in (110) direction. However, the measurements of bodies using Chinese raw materials do not match previous results for mullite crystallite size. To evaluate this discrepancy, it was proposed that the amount of primary mullite disproportionally contributes to X-ray line broadening. The proportion of primary mullite (clay) has the potential to affect the measured mullite crystallite size in (110) direction, resulting in deviation from Model #2, which means the condition #4 is invalid. This will be addressed in detail later.

5) Initially, it was also assumed that the characteristics of raw materials including chemistry, particle size and particle size distribution, do not contribute to glass chemistry. However, four regression lines in Figure 24 show the correlations between silica level in glass phase and the initial silica level in the body under the firing conditions (1250°C or 1300°C for 3.2 or 32h). The similar trends indicate that the silica UMF level in the glass phase appears to also be dependent on the initial silica amount, as well as firing temperature and dwell time, which means condition #5 is invalid too. This also needs to be evaluated later.

Since raw materials appear to potentially affect the mullite crystallite size in (110) direction and contribute to glass chemistry with respect to SiO_2 level, the global applicability of both Model #2 and Model #3 appears to be limited and challenges the models' applicability.

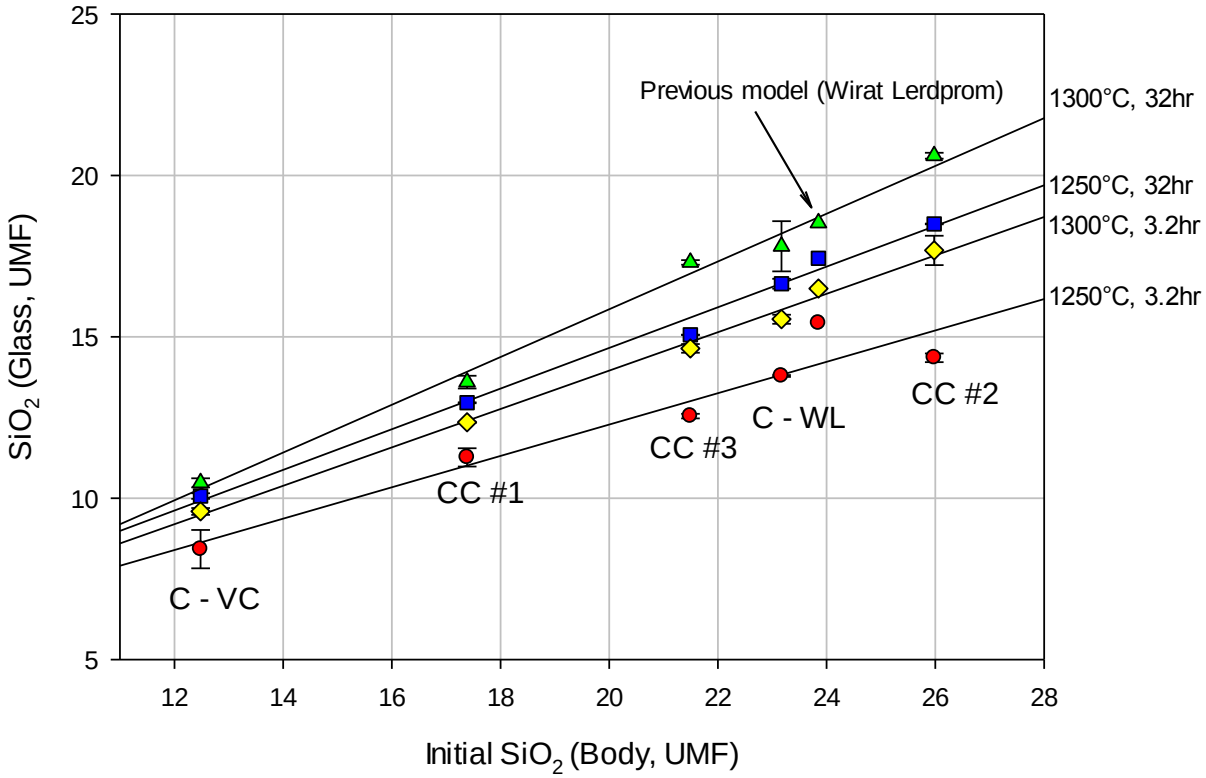

Figure 24. The relationship between initial SiO_2 UMF in the body and SiO_2 UMF in the glass phase under different firing conditions with their regression lines.

4.4.3 Validation of glass formation boundary

The glass formation boundary theorizes that over the firing temperature range of 1200-1400°C, the mullite level is dictated by the solubility of Al_2O_3 in the glass phase. Previous work has demonstrated that the precipitated mullite amount is independent of firing temperature and dwell time. The dissolved alumina level in the glass phase was calculated by using overall chemistry to subtract the Al_2O_3 content in mullite via QXRD.

As shown in Figure 25, a mean value of Al_2O_3 UMF in glass phase was determined to be 1.15 (±0.1) using only Chinese raw materials and Chinese commercial bodies under different firing conditions, which is in excellent agreement with previous work (Table XI). This confirms that the glass formation boundary concept is not dependent on raw material selection and eliminates raw material contributions.

Table XI. Comparison of Al_2O_3 UMF in Glass Phase from Different Studies

Carty, 2002[62]	**Lerdprom, 2014[65]**	**Colorado, 2014[2]**	**Current Work, 2015**
1.19 (±0.1)	1.24 (±0.06)	1.16 (±0.06)	1.15 (±0.1)

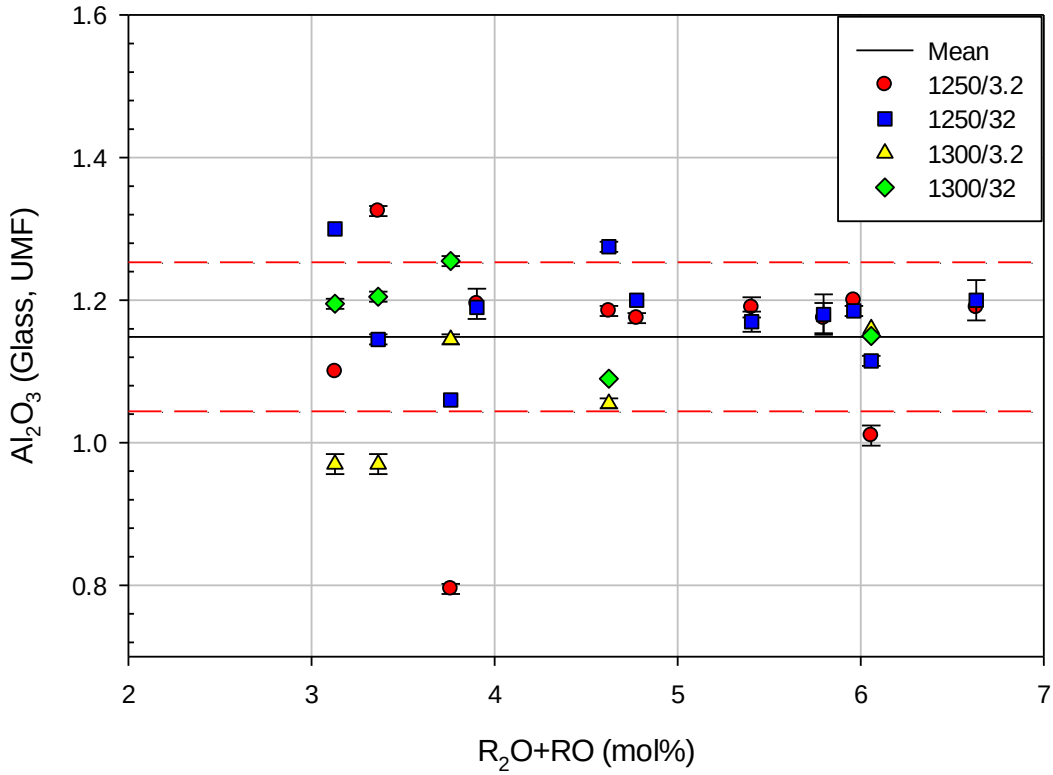

Figure 25. Relationship between Al_2O_3 UMF in the glass phase and the mole% of flux in body under different firing conditions. The solid line represents the mean value of Al_2O_3 UMF in the glass phase and the dashed lines represent the standard deviation.

4.4.4 Contribution of fine particles to X-ray line broadening

Primary mullite which is precipitated in clay relics is limited by the small clay particles, while the secondary mullite that originates from feldspar relics basically is appeared to be coarser by having more room for needles to grow after the diffusion of alkali ions from feldspar. Therefore, the size of primary mullite is typically finer than secondary mullite. Consequently, the measured mullite crystallite size is proposed to be reduced with higher proportion of primary mullite.

With the assumption that primary mullite forms from clay components and secondary mullite only precipitates within feldspar relics. An experiment was conducted to evaluate the ratio of clay to feldspar.

The proportion of primary mullite was calculated from the chemical composition obtained by ICP. Specifically, the summation of Al_2O_3 levels in different feldspars are obtained first and the Al_2O_3 amount from clay is calculated by the subtraction of Al_2O_3 levels in feldspar from overall Al_2O_3 content in the body. Dividing the overall Al_2O_3 content gives the proportion of clay, namely "primary mullite %" in this work.

In Figures 26 and 27, experimental results of mullite crystallite size in (110) direction are plotted on the graph with the individual value of primary mullite% of each body. With previous model as x-axis and measured results as y-axis, the solid line represents the previous model.

In Figure 26, the measured results of "SC" samples do not align with the model, but improve with a increase in primary mullite. Comparatively, Figure 27 presents a much closer relationship between the measured results of "CE" samples and the previous model. In general, specimens with a primary mullite% higher than 65% match reasonably well with the model predictions.

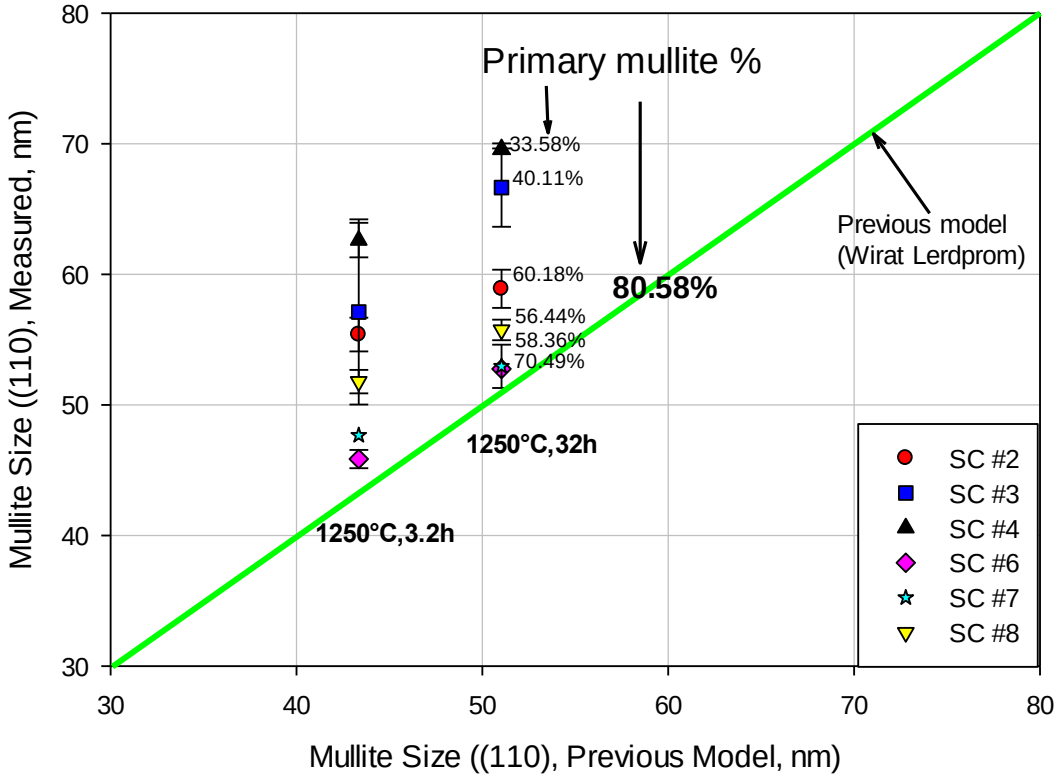

Figure 26. The mullite crystallite size in (110) direction - comparison of previous model and experimental data of "Spot check" (SC) group in terms of primary mullite%.

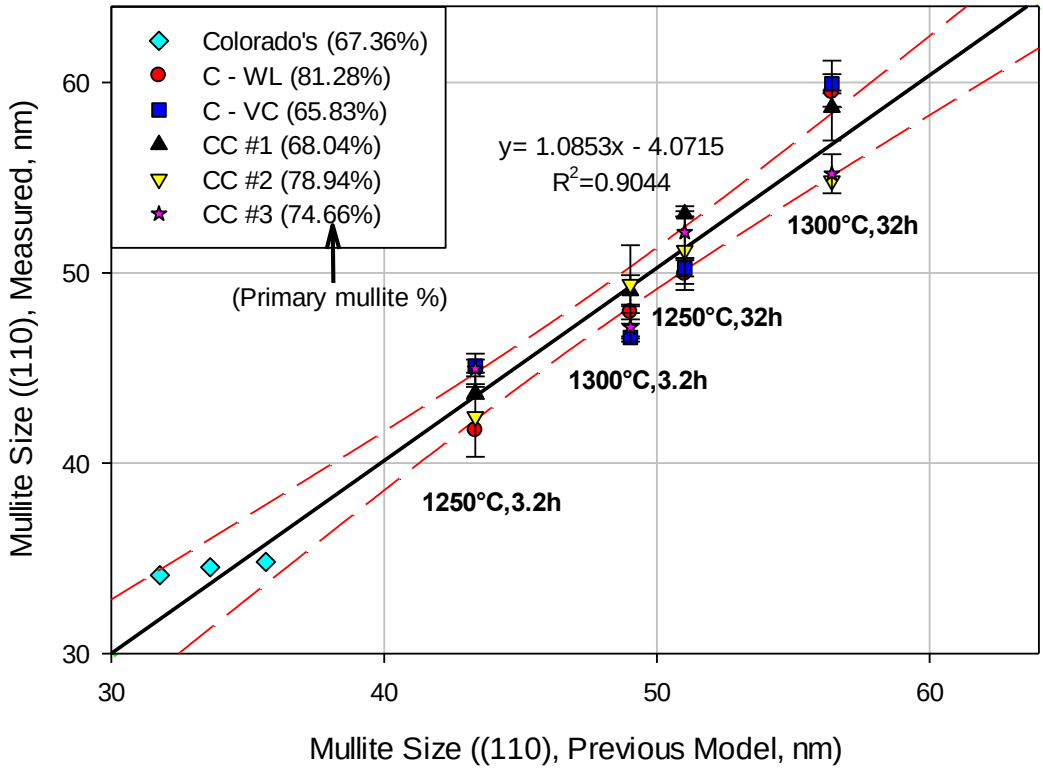

Figure 27. Comparison of measured versus predicted mullite crystallite size in (110) direction for "Comparative Experiment" (CE). The solid line is the regression line and the dashed lines represent 99% confidence.

By combining the results together, two regression lines show the relationship between the mullite crystallite size and the primary mullite% for two different firing conditions (1250°C, 3.2h and 1250°C, 32h) in Figure 28. It appears that the mullite crystallite size decreases as the primary mullite ratio increases for same firing conditions, which is consistent with the proposed argument that primary mullite contributes disproportionally to X-ray line broadening. In addition, the correlated slopes is decreasing when the primary mullite% exceeds 65%, which means the contribution from fine particle to Model #2 becomes much weaker. In other words, Model #2 is able to reasonably predict the firing conditions with a relatively high amount of primary mullite content. Therefore, the validity of Model #2 is dictated by the amount of primary mullite.

Subsequent work was conducted based on this idea and firing temperatures of the Chinese shards were also predicted from Model #2, as described in detail in the "Addendum".

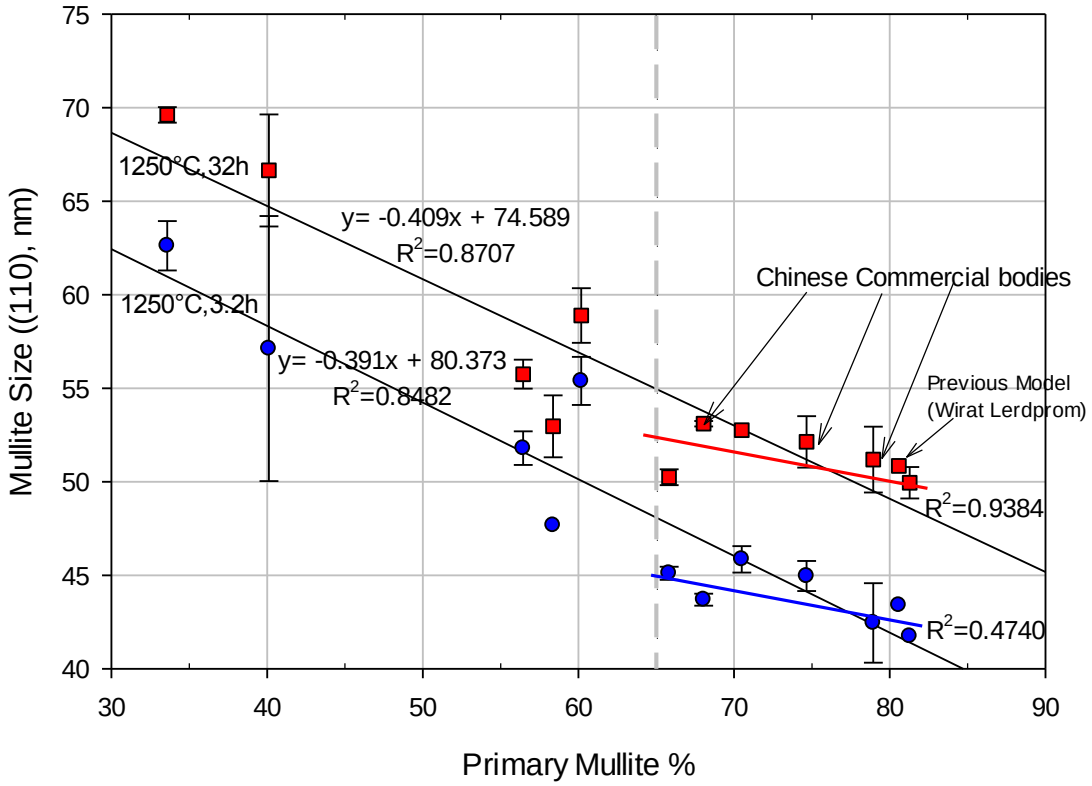

Figure 28. The relationship between the primary mullite% and the mullite crystallite size in (110) direction.

4.4.5 Potential correction for Model #3 silica UMF level in glass phase versus firing conditions

Previous studies demonstrated that the quartz dissolution thickness is independent of particle size and identical under specific firing conditions.[65] If the size of the quartz particle is similar, the number of quartz particles at a higher initial quartz content would be larger. On the basis of constant dissolution rim for individual quartz particle, increasing the number of quartz particles results in more dissolved SiO_2 in the glass phase.

The relationship between different quartz contents and dissolved quartz amount was calculated and is presented in Figure 29. Assuming a quartz dissolution rim thickness of 0.5μm[65] and that the shape of a quartz particle is monodispersed and spherical. The dissolved volume of individual quartz particle can be obtained using a simple spherical shell model. As expected, the results indicate that the amount of dissolved quartz increases with the level of quartz in batch for same quartz particle size, and increases with decreasing particle size at the same addition level. The result proposed to explain the relationship between initial SiO_2 level in body and dissolved SiO_2 in the glass phase, shown in Figure 24.

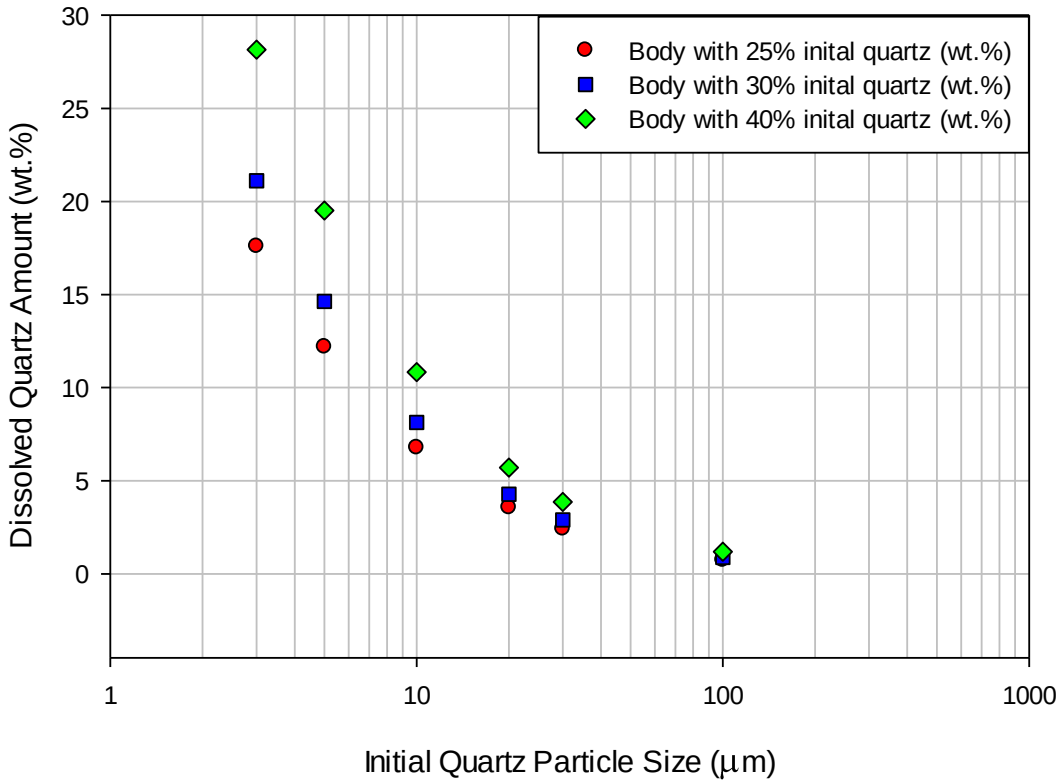

Figure 29. The correlation between quartz particle size and according dissolved quartz amount (wt.%) by calculation on the basis of 0.5μm dissolution rim.

The silica level in glass phase for both "SC" and "CE" samples are plotted in Figures 30 and 31, with measured versus predicted results. Similar trends are observed for two figures: as initial SiO_2 in body approaches that of the model, the prediction improves.

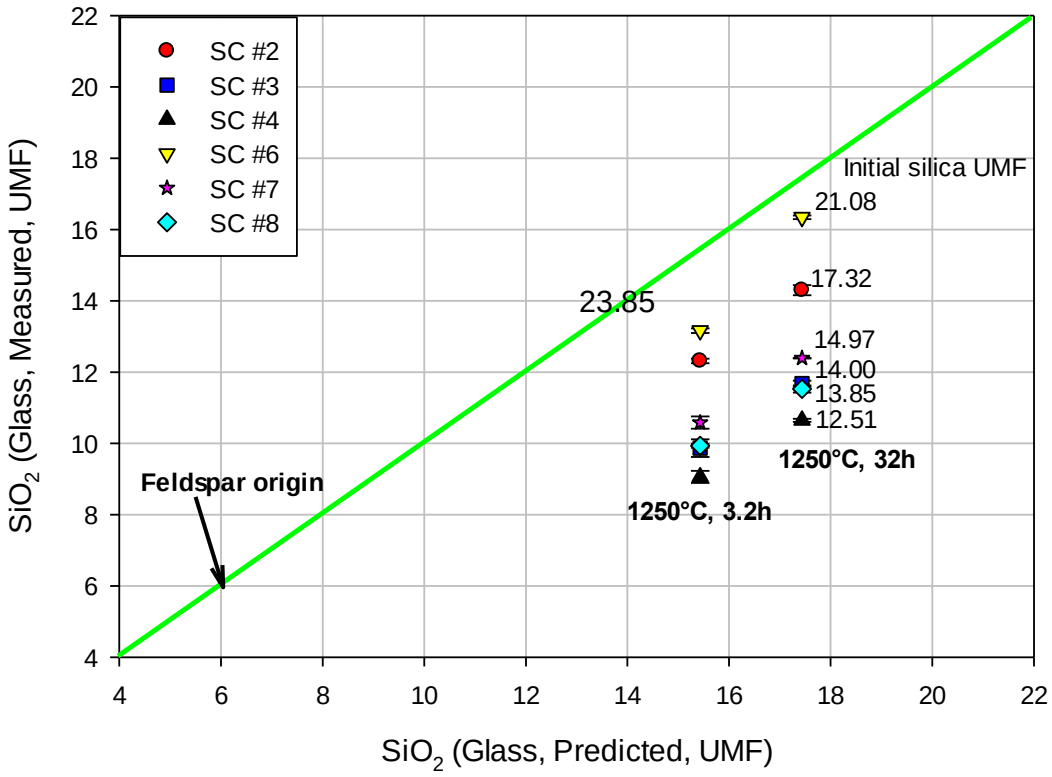

Figure 30. The silica UMF level in the glass phase - comparison of previous model and experimental data of "SC" group, with initial SiO_2 UMF. The line represents the previous model.

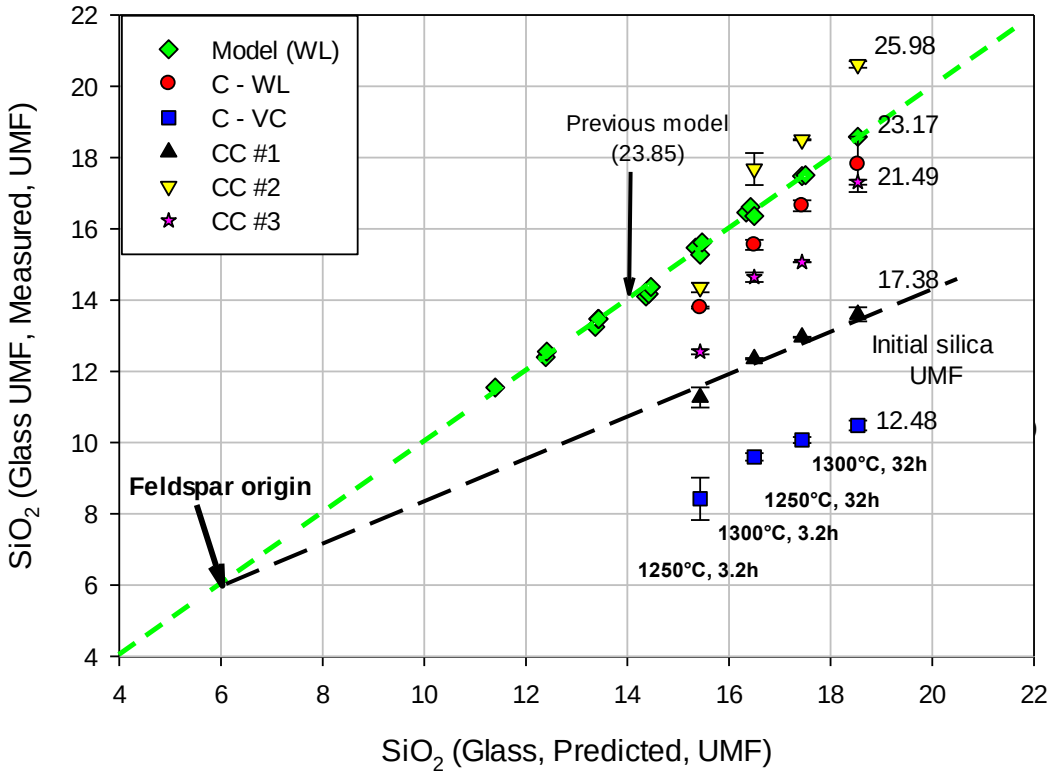

Figure 31. The silica UMF level in the glass phase - comparison of previous model and experimental data of "CE" group, with initial SiO_2 UMF.

The "feldspar origin" represents the threshold value of six moles of silica per mole of flux, which is equivalent to the amount of silica provided solely from feldspar ($R_2O.Al_2O_3.6SiO_2$). This is the minimum silica level possible in a glass derived from feldspar. As stated previously, at 1200°C, the feldspar melting is complete and aggressive dissolution of quartz begins, thus the predicted SiO_2 level in the glass originates at the "Feldspar origin". Regression analysis of measured silica in the glass phase versus predicted silica level for different bodies are shown in Figure 31. It is found that the value of slope (incorporating with feldspar origin) increases as the increasing of initial silica UMF in body, as shown in Table XII. Besides, this appears to indicate that "Chinese raw materials" are not unique and the raw material source does not appear to be important.

Table XII. The Regression Analysis of Measured Silica in the Glass Phase Versus Predicted Silica Level (compared to "WL" model)

Body	Initial Silica (UMF)	Slope	Intercept	R^2
C-VC	12.48	0.350	3.8304	0.984
CC #1	17.38	0.607	2.2436	0.990
CC #3	21.49	0.843	0.6737	0.969
C-WL	23.17	0.972	-0.0672	0.979
Model (WL）	23.85	1.000	-0.0036	0.997
CC #2	25.98	1.116	-1.0887	0.968

Table XIII. The Correction for the Consumed Silica Level in Mullite Formation

Body	Initial Silica UMF	Initial Alumina UMF	Formed Mullite	Consumed Silica in Mullite	Available Silica Level
C-VC	12.48	2.93	0.580	1.160	11.32
CC #1	17.38	3.13	0.647	1.293	16.09
CC #3	21.49	3.95	0.920	1.840	19.65
C-WL	23.17	5.34	1.383	2.767	20.40
Model (WL)	23.85	5.15	1.320	2.640	21.21
CC #2	25.98	4.75	1.187	2.373	23.61

In Table XIII, the initial silica level in body is corrected for the silica consumed in mullite formation, which gives the total available silica level in the body. Figure 24 is then replotted with the available silica level in the body as Figure 32.

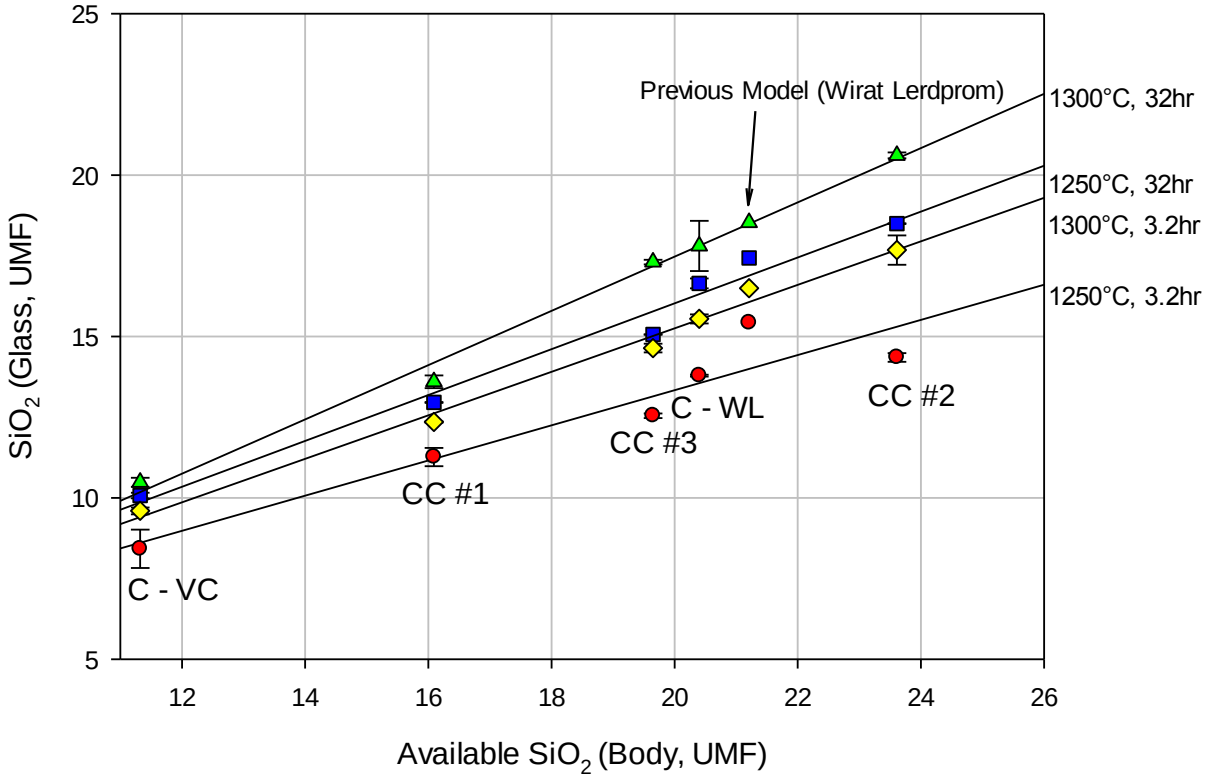

Figure 32. The relationship between available SiO_2 level in the body (corrected for mullite formation) and SiO_2 level in the glass phase under different firing conditions with their regression lines.

After the correction for mullite formation, the relationship of the corrected silica level in the body, $SiO_{2(B,C)}$ (on a UMF basis) and the slope of (measured silica in the glass versus predicted silica in the glass) (k) in Figure 33:

$$k = -0.4026 + 0.065 * SiO_{2(B,C)} \quad (4)$$

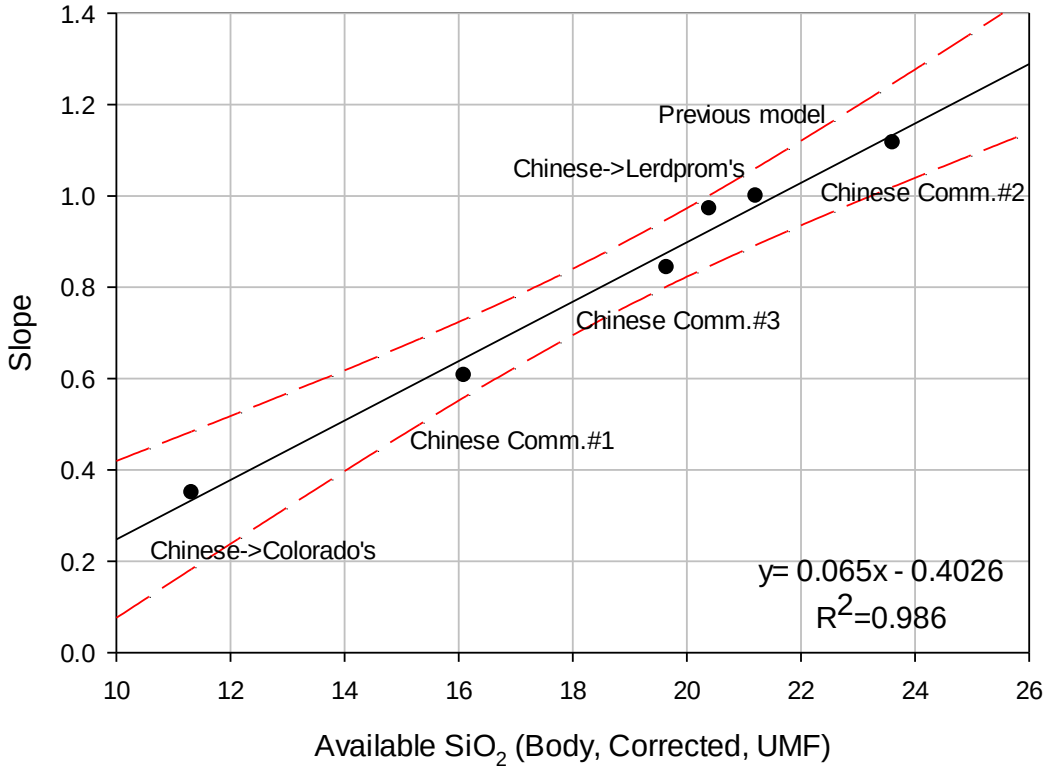

Figure 33. The correlation between the available silica UMF for glass in body and the slope of measured silica UMF in glass divided by predicted silica UMF in glass. The solid line is the regression line and the dashed lines represent 99% confidence.

As shown in Figure 31, if feldspar is the only flux source which is a reasonable assumption, the regression lines for different bodies must converge to the feldspar origin. Therefore, the relationship of corrected silica level in the glass phase ($SiO_{2(G,C)}$) as a function of measured silica level in the glass phase ($SiO_{2(G,M)}$) and the corrected silica level in the body ($SiO_{2(B,C)}$) can be expressed by the given equation:

$$SiO_{2(G,C)} = \left[\frac{(SiO_{2(G,M)} - 6)}{0.065 * SiO_{2(B,C)} - 0.4026}\right] + 6 \qquad (5)$$

This correlation corrects the silica level in the glass phase based on available silica amount in body. Eventually, the firing temperatures, *T (°C)* can then be predicted by

combining the corrected silica level in the glass phase ($SiO_{2(G,C)}$) and dwell time, *t (hours*) via Equation (6):

$$T = \frac{(SiO_{2(G,C)} + 11.83 - 1.22 * LOG(t))}{(0.00063 * LOG(t) + 0.021)} \quad (6)$$

In addition, the examination of this correction is conducted by using bodies with known firing parameters. The results of predicted temperatures via the corrected model are listed in Table XIV and plotted in Figure 34. The predicted temperature differences of 10 times dwell time are about 60 and 24 K for firing temperatures of 1250 and 1300°C, respectively.

Table XIV. The Checking of Corrected Model with Known Firing Parameters

Body	**Available Silica Level (UMF)**	**Slope**	**Predicted Temperature for (1250°C,3.2h) (°C)**	**Predicted Temperature for (1250°C,32h) (°C)**	**10*Δt (K)**	**Predicted Temperature for (1300°C,3.2h) (°C)**	**Predicted Temperature for (1300°C,32h) (°C)**	**10*Δt (K)**
C-VC	11.32	0.350	1190	1270	80	1300	1300	0
CC #1	16.09	0.607	1200	1250	50	1300	1310	10
CC #3	19.65	0.843	1180	1220	40	1290	1340	50
C-WL	20.40	0.972	1180	1230	50	1310	1330	20
CC #2	23.61	1.116	1160	1240	80	1290	1330	40
Average			1180	1240	60	1300	1320	24
Standard Deviation			15	19	19	8	16	21

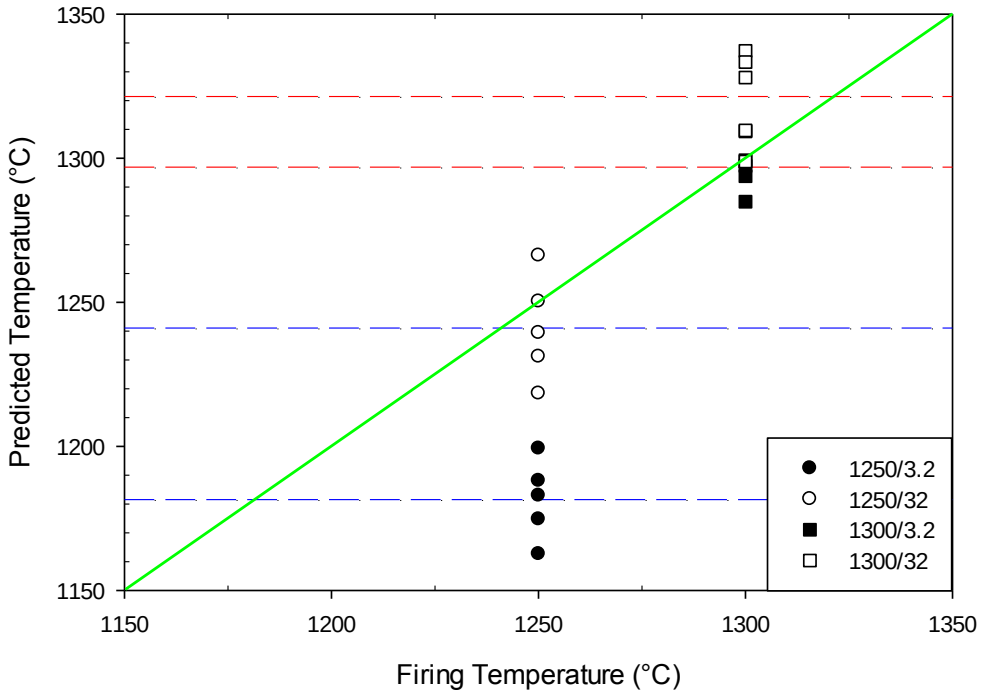

Figure 34. The examination of the corrected model with known firing conditions. The dashed lines are mean values of each predicted firing temperatures.

The predicted temperatures for the eighteen shards are calculated based on the corrected model with a selected dwell time of 72 and 96 hours (estimated in Section 4.2), as listed in Table XV. The predicted temperatures (dwell time:72h) appear to be roughly reasonable with the results of water absorption, as shown in Figure 35. Due to the limited size of these shards, the measurement of water absorption was only carried out once, which is likely to contribute to the inconsistent relationship for the shards whose predicted temperatures are higher than 1100°C.

The predicted temperature difference between the two firing times is 10 K. However, the apparent quartz dissolution rim thickness (about 1.7μm) as shown in Figure 36, suggests that the predicted temperatures (lower than 1100°C especially) are unlikely to be reasonable for the shards. The proposed reason is that the particle size of quartz used in the shards is likely to be larger than the previous model. Because the difference of

dissolved silica in the glass phase decreases with increasing quartz particle size for a same initial quartz content, as shown in Figure 29. And the proposed correction for Model #3 is based on an underlying assumption that the quartz size of specimen is similar to that of previous model. Therefore, this silica level in the glass phase model still needs further correction by taking different sizes of quartz particle into account, which was addressed in detail in the "Future Work".

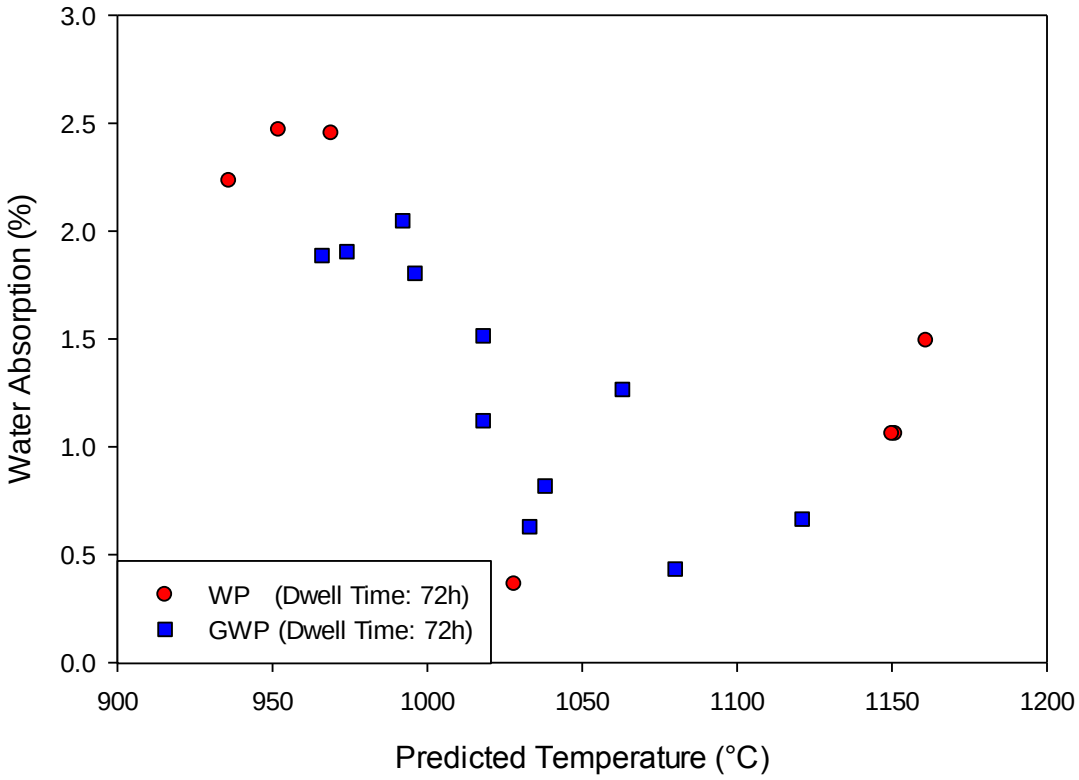

Figure 35. The relationship between the predicted temperature (72h) of the shards and the water absorption.

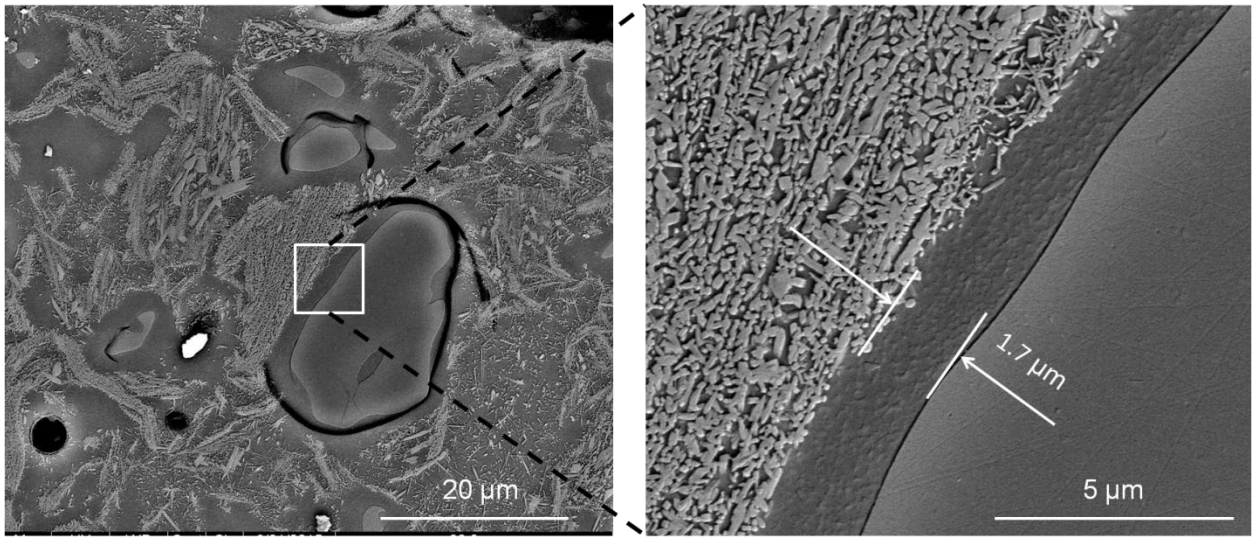

Figure 36. SEM micrographs for quartz dissolution rim (GWP #8).

Table XV. Predicted Firing Temperatures for Collected Shards (with Water Absorption)

Body	Corrected Silica in Body (UMF)	Slope	Measured Silica in the Glass (UMF)	Corrected Silica in the Glass (UMF)	Predicted Temp. for 72 hrs (°C)	Predicted Temp. for 96 hrs (°C)	ΔT of (72 and 96 hrs) (K)	Water Absorption (%)
WP#1	26.5	1.32	15.17	12.95	1020	1010	10	0.36
WP#2	34.8	1.86	18.68	12.82	1010	1000	10	2.47
WP#3	24.7	1.20	18.16	16.13	1160	1150	10	1.06
WP#4	24.3	1.18	15.32	13.90	1060	1050	10	2.23
WP#5	29.0	1.48	21.68	16.59	1180	1170	10	1.49
WP#6	29.0	1.49	21.75	16.57	1180	1170	10	1.06
WP#7	23.4	1.12	13.41	12.62	1000	990	10	2.45
GWP#1	19.5	0.87	11.85	12.72	1010	1000	10	1.89
GWP#2	18.3	0.79	11.47	12.92	1010	1000	10	2.05
GWP#3	16.9	0.69	11.25	13.61	1050	1040	10	0.63
GWP#4	15.9	0.63	10.57	13.25	1030	1020	10	1.81
GWP#5	15.9	0.63	9.58	11.68	960	950	10	1.90
GWP#6	18.3	0.79	11.74	13.27	1030	1020	10	1.52
GWP#7	16.8	0.69	11.36	13.77	1050	1040	10	1.12
GWP#8	16.6	0.68	11.06	13.44	1040	1030	10	0.82
GWP#9	16.3	0.65	11.78	14.89	1100	1090	10	0.43
GWP#10	20.7	0.94	14.22	14.74	1100	1090	10	1.27
GWP#11	20.5	0.93	14.52	15.16	1120	1100	10	0.66

V. SUMMARY AND CONCLUSIONS

Eighteen ancient Chinese shards from Jingdezhen between 900 - 1200 years ago were analyzed to determine the firing conditions. Three proposed models in terms of body-glaze penetration depth, mullite crystallite size in (110) direction and silica UMF level in the glass phase were employed to obtain the firing temperature and dwell time.

Due to the difficulty in obtaining the original body-glaze interface, Model #1 is not suitable for these ancient Chinese shards. The mean value of Al_2O_3 UMF in glass is 1.15 (±0.1) from this work, which confirms that the glass formation boundary is independent of raw material selection. Since the amount of primary mullite has the potential to contribute to X-ray line broadening in (110) direction and the contribution appears to be weaker with higher primary mullite amount, therefore the validity of Model #2 is dictated by the amount of primary mullite. Other than firing temperature and dwell time, silica level in the glass phase of Model #3 is demonstrated to be also dependent of initial silica level in the body. Potential correction is provided basing on the correlation between available silica level in body (corrected for mullite formation) and the slope of measured silica divided by predicted silica level in the glass phase. The validity of this correction is checked with the known specimens.

Based on the corrected silica level in the glass phase model, the firing temperature of shards were estimated by assuming dwell times of 72 and 96 hours according to historical records and approximate calculation. The averaged difference of predicted temperatures is 10 K. The predicted temperatures are roughly consistent with the results of water absorption. However, some predicted temperatures are not reasonable, which is proposed to due to larger different quartz particle size used. The exact firing conditions of those collected shards could not be determined.

VI. FUTURE WORK

The proposed correction for the silica level in the glass phase Model #3 provides the potential to correct the predicted temperature based on the available silica in the body. However, this correction is established with a underlying assumption that the size of quartz particle is similar to that of previous model, and experimental results indicate that different quartz particle sizes also need to take into account. Proposed approaching method is to determine the different contribution of different quartz particle sizes to the dissolved silica level in the glass via microstructural analysis and QXRD. It is possible to generate a broad correction for quartz particle by starting with a number of initial sizes. Integrating the corrections for both silica level in the body and quartz particle size together is likely to give a more comprehensive Model #3.

Besides, further experiments can be focused on that whether the thickness of quartz dissolution rim is independent of raw material selection. Based on this work, the quartz dissolution rim thickness appears to be dependent with only firing temperature and dwell time.

REFERENCES

1. F. H. Norton, *Fine ceramics: Technology and applications.* Robert E. Krieger Publishing Company, INC., Florida, 1978.

2. V. Colorado, "Fast firing of pocelain"; M.S. Thesis. Alfred University, Alfred, NY 2014.

3. W. M. Carty and U. Senapati, "Porcelain—Raw Materials, Processing, Phase Evolution, and Mechanical Behavior," *J. Am. Ceram. Soc.,* **81**[1] 3-20 (1998).

4. X. Feng, *History of Chinese ceramic*. The press of cultural relics: Beijing, 1982.

   冯先铭，*中国陶瓷史*，文物出版社：北京，1982.

5. Z. Li and C. Wen, *Chinese pottery and porcelain.* Foreign languages press: Beijing, 1984.

6. N. Joseph, *Science and Civilization in China.* Vol. 5. Cambridge university press: Cambridge, United Kingdom, 2004.

7. M. Bai, *The traditional crafts of porcelain making in Jingdezhen.* Jiangxi fine arts publishing house, 2002.

   白明，*景德镇传统陶瓷工艺*，江西艺术出版社，2002.

8. E. C. U. o. A. Design, "Maps of Chinese, Japanese and SE Asia Kiln sites." in., 2009. Accessed on: October 2009, Available at < http://ahis335.blogspot.com/2009/10/maps-of-chinese-japanese-and-se-asia.html >

9. L. Zhong, "Studies on Jingdezhen Greenish White Porcelain of Song Dynasty"; M.S. Thesis. Chongqing Normal University, 2010.

钟立英，“宋代景德镇青白瓷之研究”，理学硕士论文，重庆师范大学，2010.

10. R. Ouyang, "Comparative study on the evolution from white porcelain in Five Dynasties to greenish white porcelain in Song Dynasty in Jingdezhen"; M.S. Thesis. Jingdezhen Ceramic Institute, 2014.

欧阳瑞丰，“景德镇五代白瓷至宋代青白瓷的演变对比分析”，理学硕士论文，景德镇陶瓷学院，2014.

11. S. Sten, "Jingdezhen, "The porcelain centre of the world."A short description of the history, developments, transport and production of ancient Chinese porcelain.." in. Nanhai Marine Archaeology Sdn. Bhd., 2007. Available at < http://www.thewanlishipwreck.com/Jingdezhen.html>

12. X. Luo, "A brief invesitgation of the transition from White Porcelain to Greenish White Porcelain in Jingdezhen," *Chinese Ceramic Industry,* **6** 27-33 (1986).

罗学正，“景德镇早期白瓷向青白瓷过渡考略”，中国陶瓷工业，**6** 27-33（1986).

13. J. Cao, "The preliminary study of the rise of Jingdezhen White Porcelain from Five Dynasties," *Jingdezhen Ceramic,* **8**[3] 37-40 (1998).

曹建文，“景德镇五代白瓷兴起原因初探”，景德镇陶瓷，**8**[3] 37-40 (1998).

14. C. Xiong, Z. Rao, C. e. Cao, N. Zheng, J. Wu, J. Cao, X. Lu, and F. Yu, "Discuss of the origin and development of Greenish White Porcelain in Jingdezhen," *China Ceramic,* **43**[11] 80-82 (2007).

熊春华，“景德镇青白瓷起源与发展的探讨”，中国陶瓷，**43**[11] 80-82 (2007).

15. L. Qiu, "The excavation report of Xianghu kiln site from Five Dynasties in Jingdezhen," *Literature and Art* **20** (2012).

邱莉，“景德镇湘湖五代窑址调查简报”，大众文艺 **20** (2012).

16. L. Zeng, "The excavation report of Xianghu kiln site near Jingdezhen Ceramic Institute," *Chinese Ceramic Industry,* **03** (2012).

曾令宜，“景德镇陶瓷学院旁湘湖窑挖掘报告”，中国陶瓷工业，**03** (2012).

17. C. Cheng, "The research of Jingdezhen White Porcelain in Five Dynasties"; MFA Thesis. Jingdezhen Ceramic Institute, Jingdezhen, 2012.

程彩虹，“景德镇五代白瓷研究”，文学硕士论文，景德镇陶瓷学院，景德镇，2012.

18. J. Cao, Jingdezhen Ceramic Institute, Jingdezhen, China, 2015, Private Communication.

19. Y. Song, "The innovation and influence of Jingdezhen kiln during Five Dynasties," *Chinese Ceramic Industry,* **47**[8] 73-76 (2011).

宋燕辉，“五代时期景德镇窑的创新与影响”，中国陶瓷工业，**47**[8] 73-76 (2011).

20. P. Lan, *Jingdezhen (Ching-Te-Chen) Tao-Lu,* 1815.

蓝浦，*景德镇陶录*，1815.

21. V. Carol, "Traditional Dunzi Production in Yaolin, China." in., 2004. Accessed on: 2004, Available at < http://www.carolventura.com/Yaoli.htm>

22. Y. Guo, "The body and glaze in ancient Jingdezhen," *China Ceramic,* **1** 52-60 (1993).

郭演仪，“古代景德镇瓷器胎釉”，中国陶瓷，**1** 52-60 (1993).

23. X. Liu, " The historical investigation of porcelain stone and kaolin in Jingdezhen from 10th to 19th century," *Chinese Ceramic Industry,* **7** 145-46 (1982).

刘新园，“高岭土史考：兼论瓷石，高岭与景德镇十至十九世纪制瓷业”，中国陶瓷工业，**7** 145-146 (1982).

24. X. Liu, "A study of Yung-Le and Hsuan-Te imperial porcelains excavated from the ancient site of the Ming Dynasty imperial factory at Ching-te-chen." in. Urban Council, Hong Kong, 1989.

刘新园，“景德镇明御厂故址出土永乐，宣德官窑瓷器之研究”，香港，1989.

25. X. Liu, "The excavation report of Imperial kiln site of the Ming and Qing Dynasty in Jingdezhen," *Cultural Relics,* **5** (2007).

刘新园，“江西景德镇明清御窑遗址发掘简报”，文物，**5** (2007).

26. "Dragon-kiln,″ in 24th Annual North Carolina Potters Conference, Available at <http://ceramicartdaily.org/2011-north-carolina-potters-conference/>

27. "The firing furniture." in., Chinese Ceramic Information Source, 2004. Accessed on: October 2014, Available at <http://www.ccisn.com.cn/tcys/reads-id-117.html>

28. X. Liu, "The kiln sites of Jingdezhen and their place in the history of Chinese ceramics," *Ceramic Finds from Jingdezhen Kilns (10th - 17th Century)* 32-54 (1992).

29. Y. Sheng, "Several problems about the manufacture of porcelain of ancient dragon kiln," *Cultural Relics,* **9** (2009).

沈岳明，“龙窑生产中的几个问题”，文物，**9** (2009).

30. Q. Jiang, *Thao Chi,* 1896.

蒋祈，*陶记*，1896.

31. Anon, *China Industrial Handbooks.* pp. 805: Jiangsu, 1933.

32. L. A. Cort, in Kodansha International conference. Shigaraki, Pottery's Valley, 1979.

33. S. Xu, *Edited draft of documents pertaining to matters of state in the Song Dynasty.* in., Taipei Repr., 1978.

徐松，*宋会要辑稿*，台北，1978.

34. Y. Hu, *Building and firing technique of Jingdezhen ancient wood kiln,* pp. 286-90 in Science and Technology of Ancient Ceramics Edited by J. Guo.

35. K. L. Rasmussen, G. A. De La Fuente, A. D. Bond, K. K. Mathiesen, and S. D. Vera, "Pottery firing temperatures: a new method for determining the firing temperature of ceramics and burnt clay," *J. Archaeol. Sci.,* **39**[6] 1705-16 (2012).

36. C. Ming, Y. Yang, J. Zhu, L. Guan, C. Fan, C. Xu, Z. Yao, J. M. Kenoyer, G. Song, and C. Wang, "Archaeometric investigation of the relationship between ancient egg-white glazed porcelain (Luanbai) and bluish white glazed porcelain (Qingbai) from Hutian Kiln, Jingdezhen, China," *J. Archaeol. Sci.,* **47** 78-84 (2014).

37. P. Blanchart, A. Azzou, P. Blanchart, and W. Lee, "Predicting the Sintering Curve of Porcelain by Support Vector Regression," *J. Am. Ceram. Soc.,* **94**[11] 3768-73 (2011).

38. G. S. Polymeris, A. Sakalis, D. Papadopoulou, G. Dallas, G. Kitis, and N. C. Tsirliganis, "Firing temperature of pottery using TL and OSL techniques," *Nuclear Instruments and Methods in Physics Research Section A: Accelerators, Spectrometers, Detectors and Associated Equipment,* **580**[1] 747-50 (2007).

39. N. F. Cano, C. S. Munita, S. Watanabe, R. F. Barbosa, J. F. D. Chubaci, S. H. Tatumi, and E. G. Neves, "OSL and EPR dating of pottery from the archaeological sites in Amazon Valley, Brazil," *Quaternary International,* **352** 176-80 (2014).

40. N. F. Cano, R. B. Ribeiro, C. S. Munita, S. Watanabe, E. G. Neves, and E. K. Tamanaha, "Dating and determination of firing temperature of ancient potteries from São Paulo II archaeological site, Brazil by TL and EPR techniques," *Journal of Cultural Heritage,* **16**[3] 361-64 (2015).

41. A. M. Musthafa, K. Janaki, and G. Velraj, "Microscopy, porosimetry and chemical analysis to estimate the firing temperature of some archaeological pottery shreds from India," *Microchem. J.,* **95**[2] 311-14 (2010).

42. M. Chatfield, "Tracing firing technology through clay properties in Cuzco, Peru," *J. Archaeol. Sci.,* **37**[4] 727-36 (2010).

43. S. Akyuz, T. Akyuz, S. Basaran, C. Bolcal, and A. Gulec, "Analysis of ancient potteries using FT-IR, micro-Raman and EDXRF spectrometry," *Vib. Spectrosc.,* **48**[2] 276-80 (2008).

44. G. Velraj, R. Ramya, and R. Hemamalini, "FT-IR spectroscopy, scanning electron microscopy and porosity measurements to determine the firing temperature of ancient megalithic period potteries excavated at Adichanallur in Tamilnadu, South India," *J. Mol. Struct.,* **1028** 16-21 (2012).

45. Q. Brian, "The unity molecular formula approach to glaze development"; M.S. Thesis. Alfred University, Alfred, NY, 2002.

46. T. E. Rein, "Body-glaze interactions as a function of sintering time"; B.S. Thesis. Alfred University, Alfred, NY, 2010.

47. W. M. Carty and H. Lee, "Determining the firing conditions of ancient Korean Celadons (correcting for iron level)." in 8th Asian Ceramic Ware Technology Symposium. Korea, 2013.

48. C. Dannert, B. Durschang, and F. Raether, "Optimization if sintering processes for porcelain using in-situ measuring methods," *Glass Sci. Technol. (Offenbach, Ger.),* **76** 71-77 (2003).

49. M. Romero, J. Martín-Márquez, and J. M. Rincón, "Kinetic of mullite formation from a porcelain stoneware body for tiles production," *J. Eur. Ceram. Soc.,* **26**[9] 1647-52 (2006).

50. F. J. Serrano, J. Bastida, J. M. Amigó, and A. Sanz, "XRD Line Broadening Studies on Mullite," *Cryst. Res. Technol.,* **31**[8] 1085-93 (1996).

51. M. A. Sainz, F. J. Serrano, J. M. Amigo, J. Bastida, and A. Caballero, "XRD microstructural analysis of mullites obtained from kaolinite–alumina mixtures," *J. Eur. Ceram. Soc.,* **20**[4] 403-12 (2000).

52. D. I. Seymour, "Phase evolution in electrical porcelains during firing"; M.S. Thesis. Alfred University, Alfred, NY, 2000.

53. A. Shah, "The glass phase formation boundary in porcelains"; M.S. Thesis. Alfred University, Alfred, NY, 2007.

54. Y. Iqbal and W. E. Lee, "Microstructural Evolution in Triaxial Porcelain," *J. Am. Ceram. Soc.,* **83**[12] 3127-27 (2000).

55. C. McConville, W. E. Lee, and J. H. Sharp, "Comparison of microstructural evolution in kaolinite powders and dense clay bodies," *Br. Ceram. Proc.,* **58** 75-92 (1998).

56. O. Castelein, B. Soulestin, J. P. Bonnet, and P. Blanchart, "The influence of heating rate on the thermal behaviour and mullite formation from a kaolin raw material," *Ceram. Int.,* **27**[5] 517-22 (2001).

57. S. T. Lundin, "Electron microscopy of whiteware bodies"; pp. 383-90 in Transactions of the 4th International Ceramics Congress.

58. K. H. Schuller, "Reactions between mullite and glassy phase in porcelains," *Trans. Br. Ceram. Soc.,* **63**[2] 103-07 (1964).

59. W. E. Lee and Y. Iqbal, "Influence of mixing on mullite formation in porcelain," *J. Eur. Ceram. Soc.,* **21**[14] 2583-86 (2001).

60. W. E. Lee, G. P. Souza, C. J. McConville, T. Tarvornpanich, and Y. Iqbal, "Mullite formation in clays and clay-derived vitreous ceramics," *J. Eur. Ceram. Soc.,* **28**[2] 465-71 (2008).

61. Y. Iqbal and W. E. Lee, "Fired porcelain microstructure revisited," *J. Am. Ceram. Soc.,* **82**[12] 3584-90 (1999).

62. W. M. Carty, "Observations on the Glass Phase Composition in Porcelains," *Ceramic Engineering & Science Proceedings.,* **23**[2] 79-94 (2002).

63. J. Juthapakdeeprasert, "The translucency of porcelain"; M.S. Thesis. Alfred University, Alfred, NY, 2011.

64. J. M. Amigó, F. J. Serrano, M. A. Kojdecki, J. Bastida, V. Esteve, M. M. Reventós, and F. Martí, "X-ray diffraction microstructure analysis of mullite, quartz and corundum in porcelain insulators," *J. Eur. Ceram. Soc.,* **25**[9] 1479-86 (2005).

65. W. Lerdprom, "Firing of porcelain"; M.S. Thesis. Alfred University, Alfred, NY, 2014.

66. W. M. Carty, "The unity molecular formula approach to glaze development," *J. Am. Ceram. Soc.,* **21**[2] 95-107 (2000).

67. M. Jackson and B. Mills, "Dissolution of Quartz in Vitrified Ceramic Materials," *J. Mater. Sci.,* **32**[20] 5295-304 (1997).

68. A. Monshi, "A Kinetic Equation for Diffusion-Controlled Dissolution of Quartz Spherical Particles in Glassy Matrix of Whitewares during Firing," *nterceram,* **47**[3] 155-63 (1998).

69. "Standard test methods for apparent porosity, water absorption, apparent specific gravity, and bulk density of burned refractory brick and shapes by boiling water." ASTM Designation: C 20-00. West Conshohocken, PA.

70. R. Zhou and J. Li, "The study of body, glaze and firing of ancient porcelain in Jingdezhen," *Silicate,* **2** (1960).

周仁，李家治，“景德镇历代瓷器胎、釉和烧成工艺研究”，硅酸盐，**2** (1960).

71. W. Nigel, *Some implication of recent analyses of Song Yingqing ware from Jingdezhen.* Science Press: Beijing, 1986.

72. M. G. N. C. Barry Carter, *Ceramic Materials: Science and Engineering,* Second ed. Springer Science+Business Media: New York, 2013.

73. C. e. Cao, "Fabrication of imitation greenish white glaze of Jingdezhen," *Journal of Ceramics,* **1** (2009).

曹春娥，“景德镇青白瓷釉的仿制”，陶瓷学报，**1** (2009).

74. Z. Hu, "The development of evolution of Jingdezhen ancient kilns"; M.S. Thesis. Jingdezhen Ceramic Insititute, Jingdezhen, 2013.

胡钟元，“景德镇古陶瓷窑炉的发展和演变”，理学硕士论文，景德镇陶瓷学院，景德镇，2013.

ADDENDUM

Model #2 was considered to be inapplicable for the shards due to difficulty in determining the primary mullite amount. It is proposed that the ratio of clay to feldspar can be obtained from chemical analysis. And that the ratio of clay: feldspar is equivalent to the ratio of primary : secondary mullite.

Al_2O_3 in a typical porcelain body can only originate from clay and feldspar. The amount of primary mullite in the shards can be calculated based on the subtraction of Al_2O_3 levels consumed in feldspars out of the overall Al_2O_3 levels via ICP, as described in Section 4.4.4. As demonstrated in Tables XVI and XVII, the ratio level can be used to obtain the feldspar and the residual Al_2O_3 assigned to kaolinite.

Table XVI. Simplified Chemistry of the Shards for Model #2 (Ignored Other Chemistry)

	R_2O (mol)		RO (mol)	R_2O_3 (mol)	RO_2 (mol)
	Na_2O	K_2O	CaO+MgO	Al_2O_3	SiO_2
WP#1	0.004	0.034	0.007	0.173	1.282
WP#2	0.002	0.027	0.006	0.163	1.313
WP#3	0.003	0.037	0.009	0.175	1.274
WP#4	0.008	0.034	0.007	0.172	1.268
WP#5	0.003	0.032	0.007	0.163	1.295
WP#6	0.002	0.027	0.013	0.170	1.296
WP#7	0.005	0.035	0.011	0.172	1.268
GWP#1	0.009	0.032	0.022	0.151	1.297
GWP#2	0.007	0.030	0.030	0.153	1.289
GWP#3	0.033	0.027	0.010	0.181	1.247
GWP#4	0.030	0.029	0.016	0.171	1.256
GWP#5	0.034	0.029	0.012	0.180	1.243
GWP#6	0.026	0.028	0.011	0.176	1.259
GWP#7	0.026	0.029	0.017	0.172	1.255
GWP#8	0.032	0.028	0.012	0.175	1.253
GWP#9	0.035	0.027	0.011	0.179	1.249
GWP#10	0.014	0.034	0.009	0.175	1.262
GWP#11	0.018	0.031	0.010	0.164	1.281

Table XVII. Calculation of Primary Mullite% from Chemical Analysis

	Feldspar (mol)			Overall Al_2O_3 in Feldspar (mol)	Overall Al_2O_3 in Feldspar (wt.%)	Clay (wt.%)	Primary mullite : Secondary mullite	Primary Mullite %
	Albite	Orthoclase	Anorthite					
WP#1	0.004	0.034	0.007	0.045	3.068	14.592	2.818	73.81
WP#2	0.002	0.027	0.006	0.035	2.380	14.250	3.607	78.30
WP#3	0.003	0.037	0.009	0.048	3.280	14.590	2.626	72.42
WP#4	0.008	0.034	0.007	0.049	3.345	14.165	2.502	71.45
WP#5	0.003	0.032	0.007	0.042	2.854	13.726	2.862	74.11
WP#6	0.002	0.027	0.013	0.042	2.818	14.522	3.062	75.38
WP#7	0.005	0.035	0.011	0.051	3.471	14.089	2.379	70.40
GWP#1	0.009	0.032	0.022	0.064	4.292	11.088	1.360	57.63
GWP#2	0.007	0.030	0.030	0.068	4.553	11.007	1.255	55.65
GWP#3	0.033	0.027	0.010	0.070	4.740	13.760	1.592	61.42
GWP#4	0.030	0.029	0.016	0.076	5.113	12.277	1.251	55.57
GWP#5	0.034	0.029	0.012	0.074	5.035	13.325	1.423	58.73
GWP#6	0.026	0.028	0.011	0.065	4.404	13.586	1.709	63.08
GWP#7	0.026	0.029	0.017	0.071	4.829	12.701	1.411	58.53
GWP#8	0.032	0.028	0.012	0.072	4.870	12.970	1.430	58.85
GWP#9	0.035	0.027	0.011	0.073	4.942	13.258	1.443	59.07
GWP#10	0.014	0.034	0.009	0.058	3.917	13.903	2.030	67.00
GWP#11	0.018	0.031	0.010	0.060	4.019	12.671	1.749	63.62

Based on this, the values of primary mullite% for the shards were calculated, as shown in Figure 37 . In WP specimens, the primary mullite was always greater than 65%. In the GWP specimens, the primary mullite level was typically close to 65% "cutoff". Therefore, the firing temperatures can be reasonably predicted from Model #2. The predicted temperatures are presented in Table XVIII. The difference of predicted temperatures for 3 and 4 days dwell times is only 10 K, which confirms that the contribution of dwell time is small.

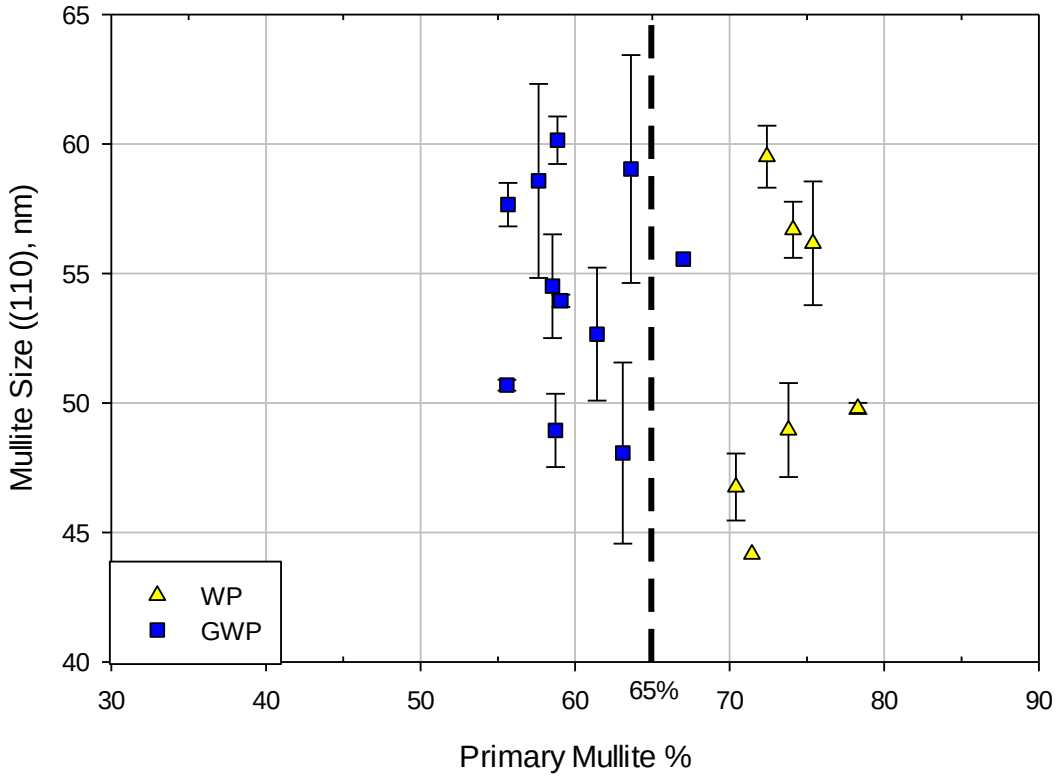

Figure 37. The values of primary mullite% of the shards.

Table XVIII. Predicted Firing Temperatures for Collected Shards (Model #2)

Body	Mullite Crystallite Size (nm)	Predicted Temp. for 72 hrs (°C)	Predicted Temp. for 96 hrs (°C)	ΔT of (72 and 96 hrs) (K)
WP#1	49.0	1210	1200	10
WP#2	49.8	1220	1210	10
WP#3	59.5	1300	1290	10
WP#4	44.2	1170	1160	10
WP#5	56.7	1280	1270	10
WP#6	56.2	1270	1260	10
WP#7	46.8	1190	1180	10
GWP#1	58.6	1290	1280	10
GWP#2	57.7	1280	1270	10
GWP#3	52.7	1240	1230	10
GWP#4	50.7	1220	1210	10
GWP#5	48.9	1210	1200	10
GWP#6	48.1	1200	1190	10
GWP#7	54.5	1260	1250	10
GWP#8	60.2	1310	1300	10
GWP#9	54.0	1250	1240	10
GWP#10	55.6	1270	1260	10
GWP#11	59.0	1300	1290	10

Figure 38 shows the comparison of predicted temperatures from both Model #2 and Model #3. The predicted temperatures incorporated with Model #2 are much higher than the results from Model #3 but much more consistent with the microstructural evidence (Figure 36).

Comparison of prepared bodies to Model #2 shows excellent correlation in Figure 39.

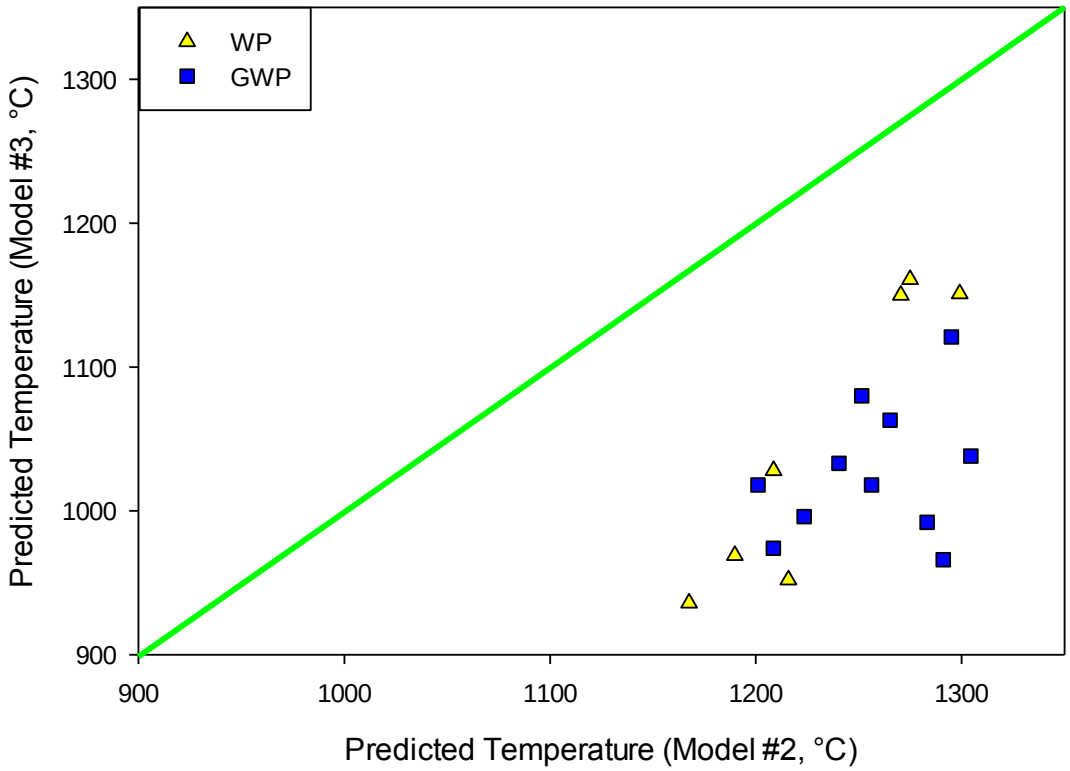

Figure 38. Comparison of predicted temperatures for Model#2 and Model #3.

Table XIX. The Checking of Model #2 with Known Firing Parameters

Body	Predicted Temp. for (1250°C, 3.2h) (°C)	Predicted Temp. for (1250°C, 32h) (°C)	10*Δt (K)	Predicted Temp. for (1300°C, 3.2h) (°C)	Predicted Temp. for (1300°C, 32h) (°C)	10*Δt (K)
C-VC	1240	1240	0	1290	1320	30
CC #1	1270	1240	30	1280	1330	50
CC #3	1250	1270	20	1300	1320	20
C-WL	1240	1250	10	1300	1280	20
CC #2	1260	1260	0	1290	1290	0
Average	1250	1250	12	1290	1300	24
Standard Deviation	13	11	13	10	21	18

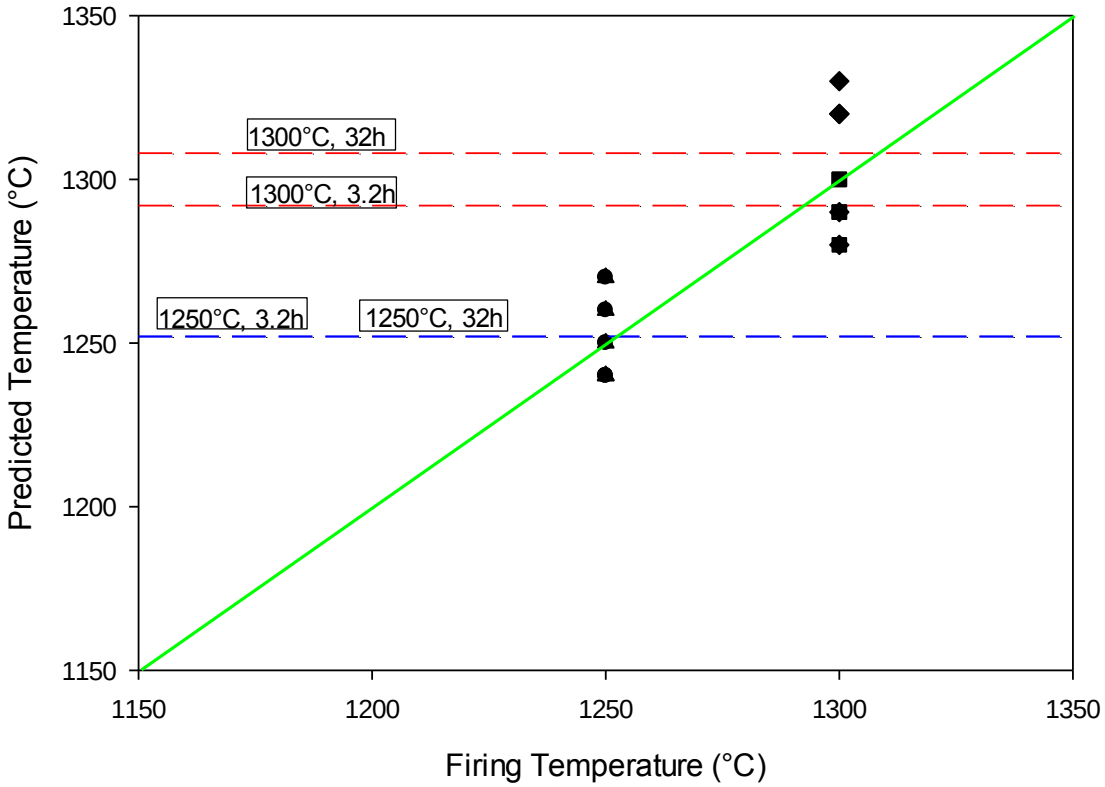

Figure 39.The examination of Model#2 with known firing conditions. The dashed lines are mean values of each predicted firing temperatures.

APPENDIX

	Front	Back	Cross section	Side
WP#1				
WP#2				
WP#3				

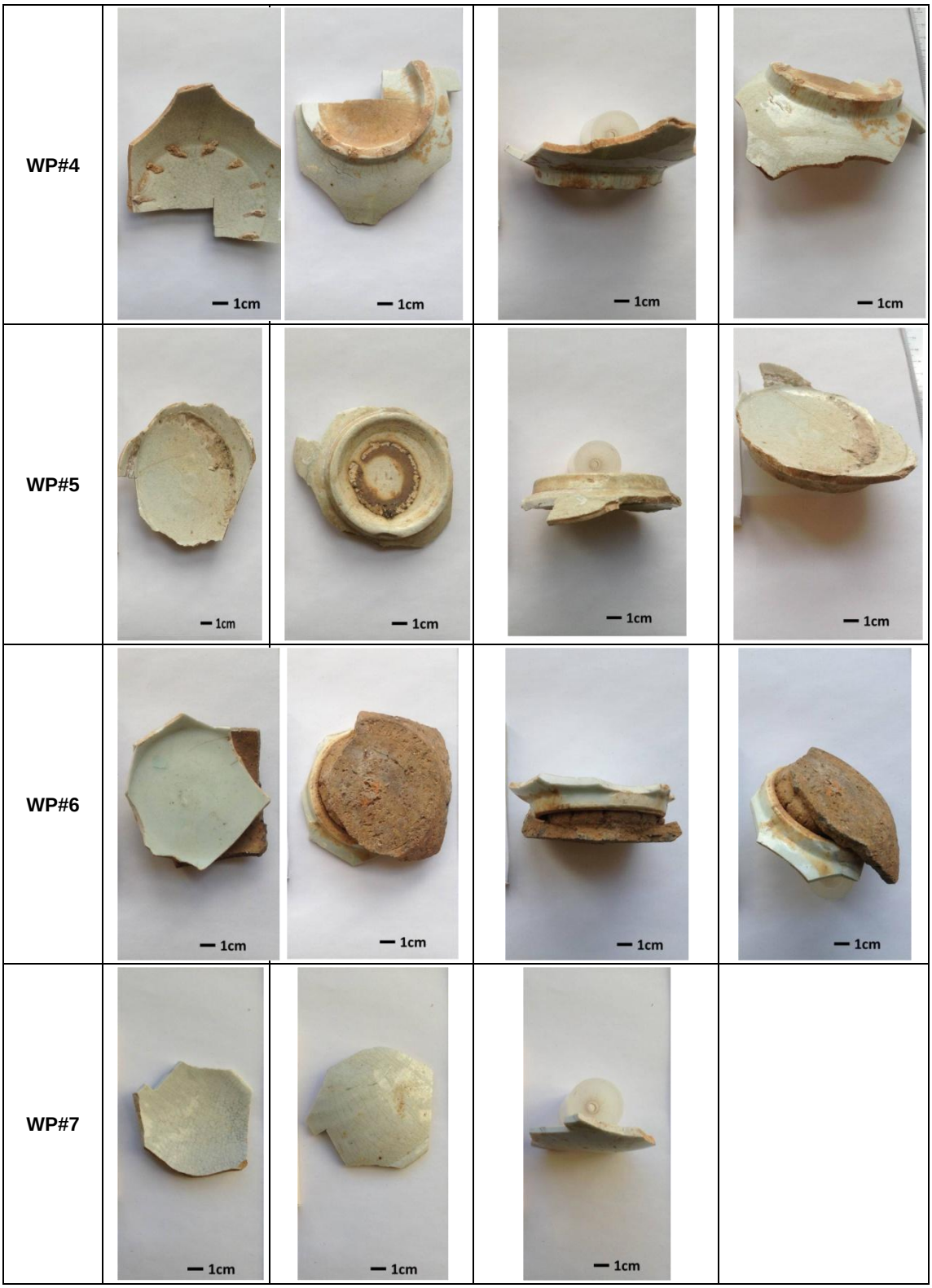

Figure 40. The photographs of white porcelain (WP) from Five Dynasties in Jingdezhen, China.

	Front	Back	Cross section	Side
GWP#1				
GWP#2				
GWP#3				
GWP#4				

GWP#5				
GWP#6				
GWP#7				
GWP#8				

GWP#9				
GWP#10				
GWP#11				

Figure 41. The photographs of greenish white porcelain (GWP) from Song Dynasty in Jingdezhen, China.

WP#1	
Ca	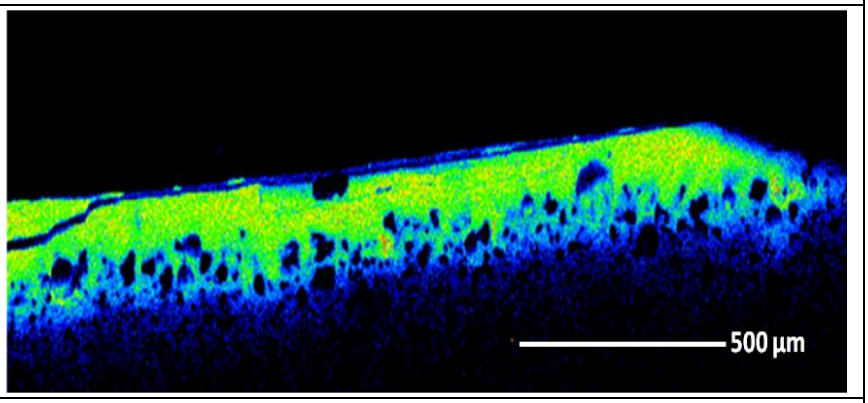
Si	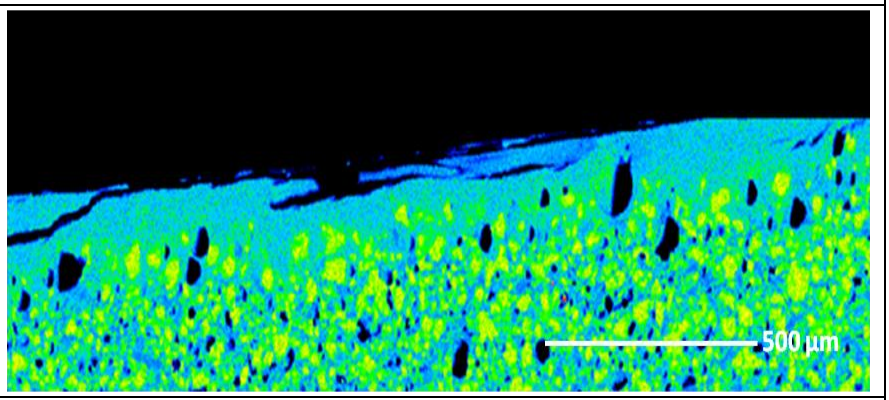
K	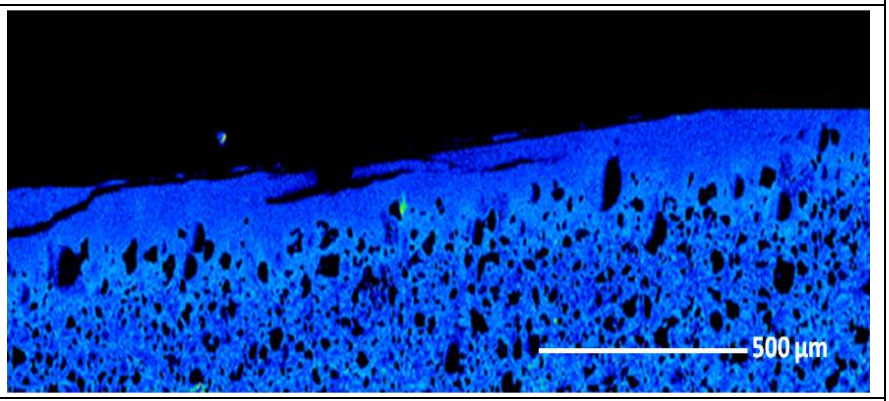
Al	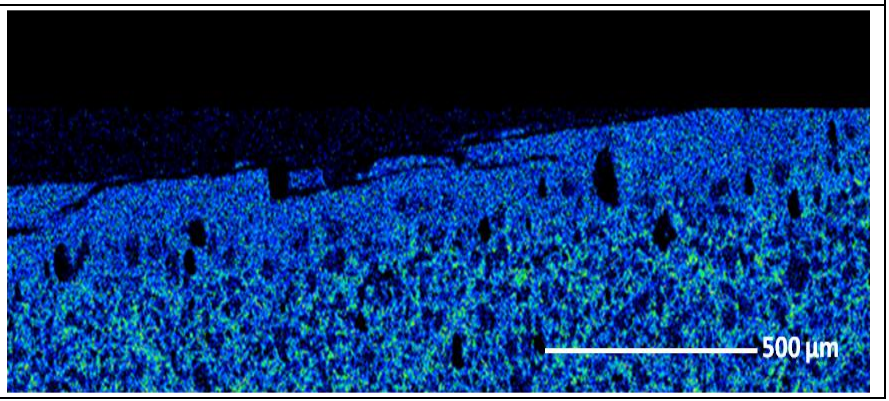

WP#2	
Ca	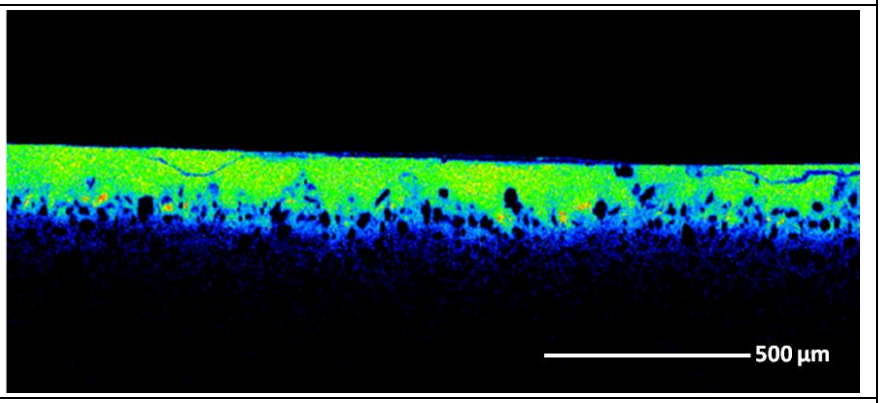
Si	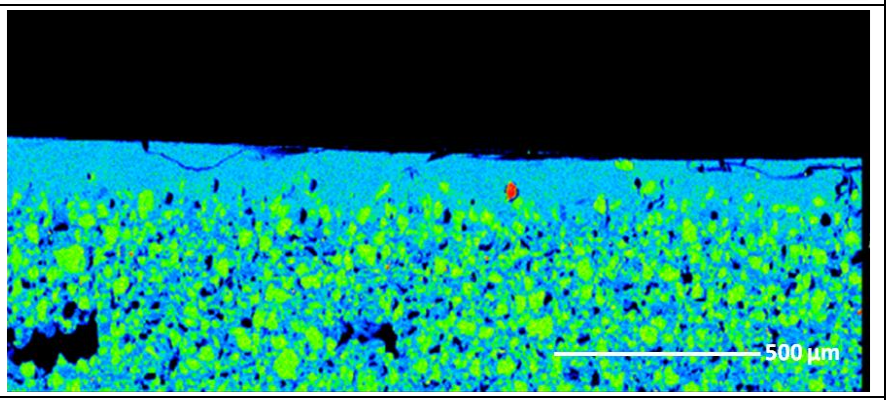
K	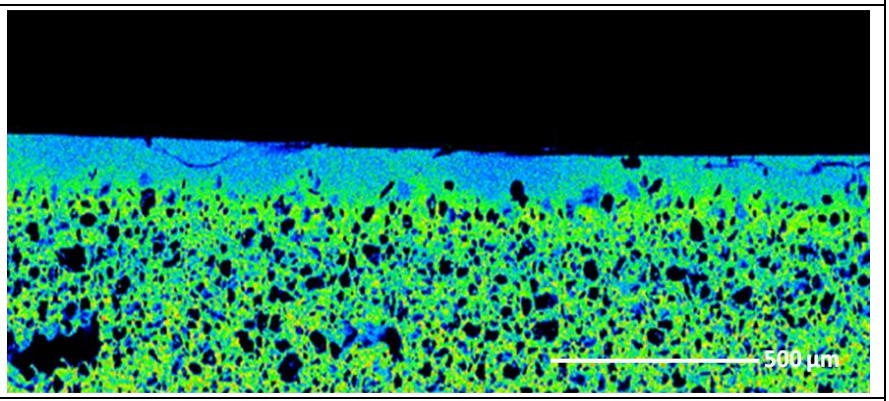
Al	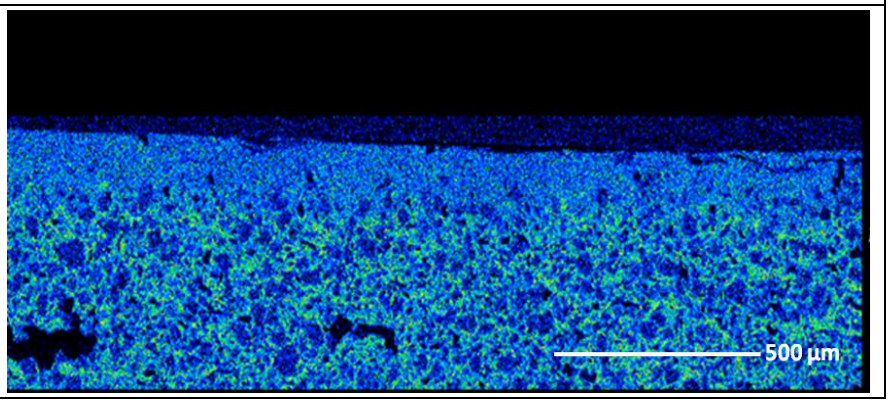

WP#3	
Ca	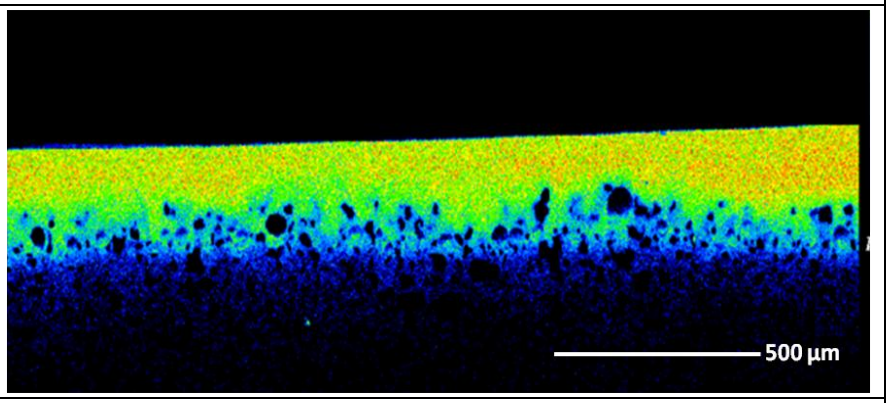
Si	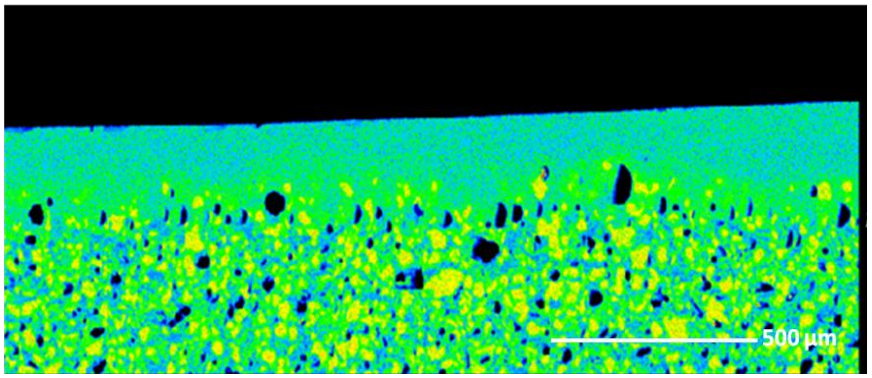
K	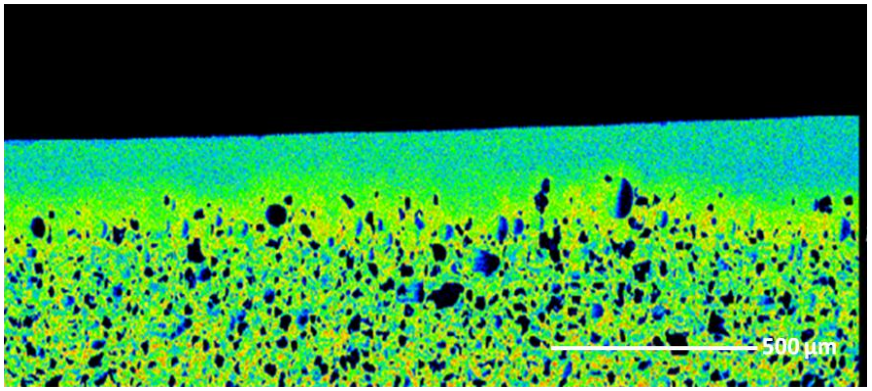
Al	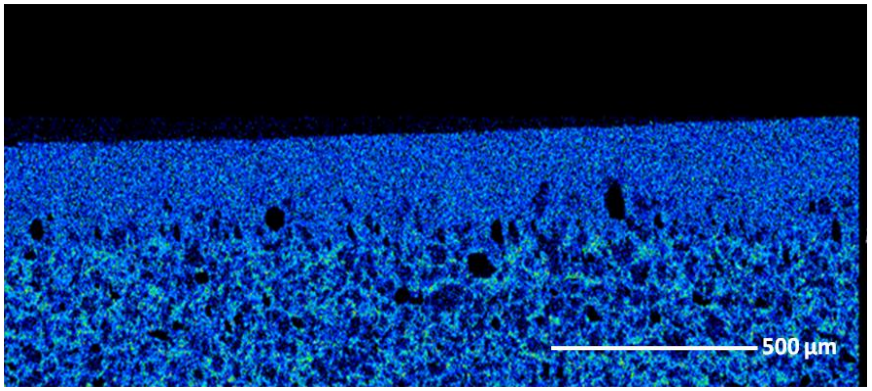

WP#4	
Ca	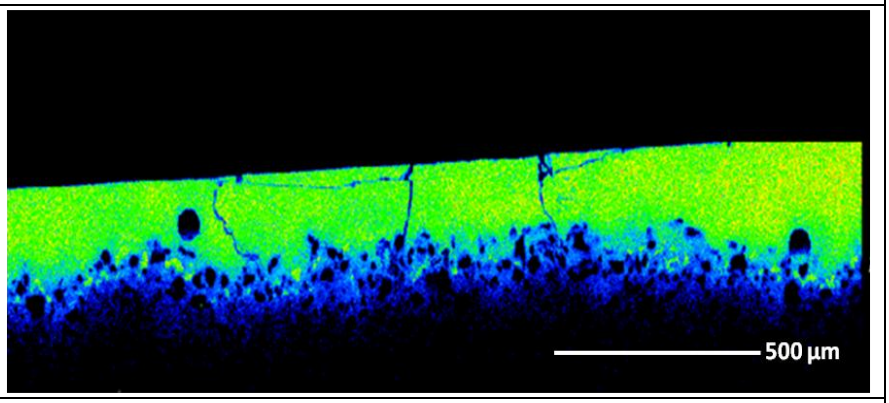
Si	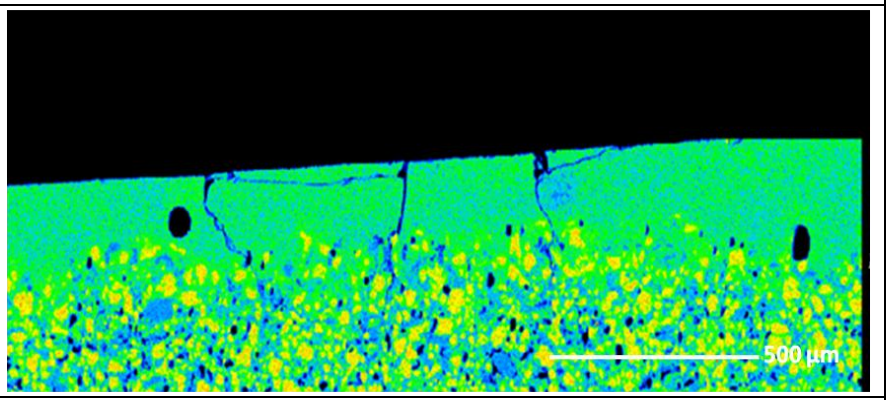
K	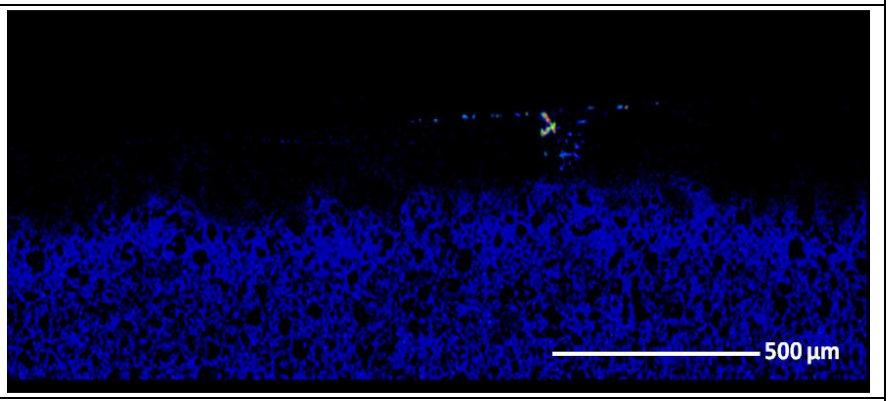
Al	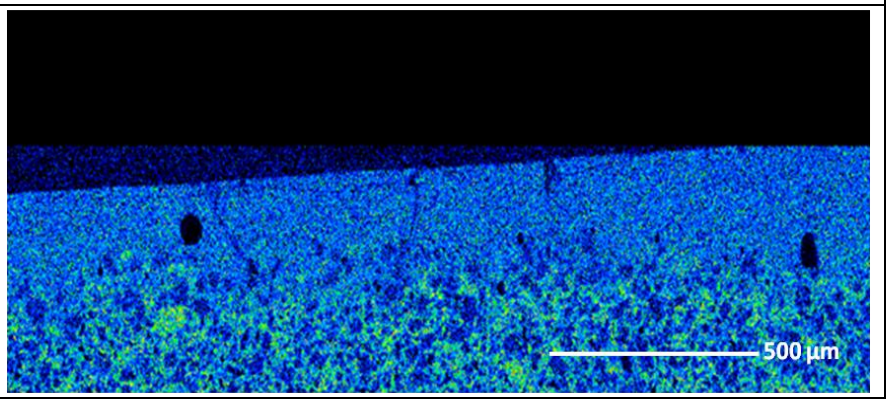

WP#5	
Ca	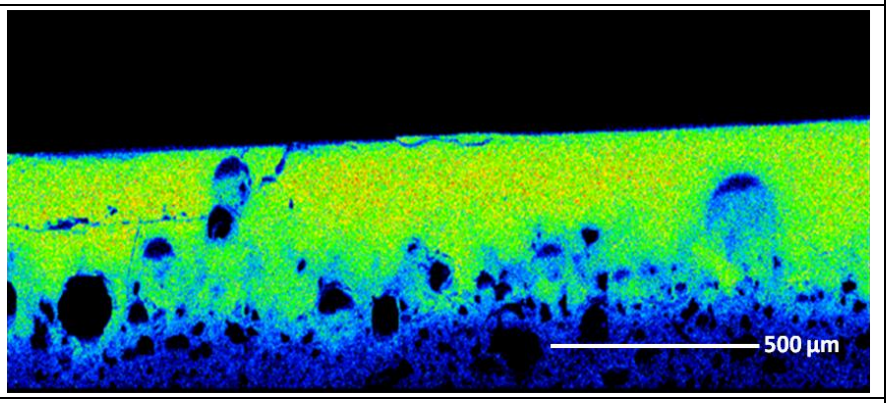
Si	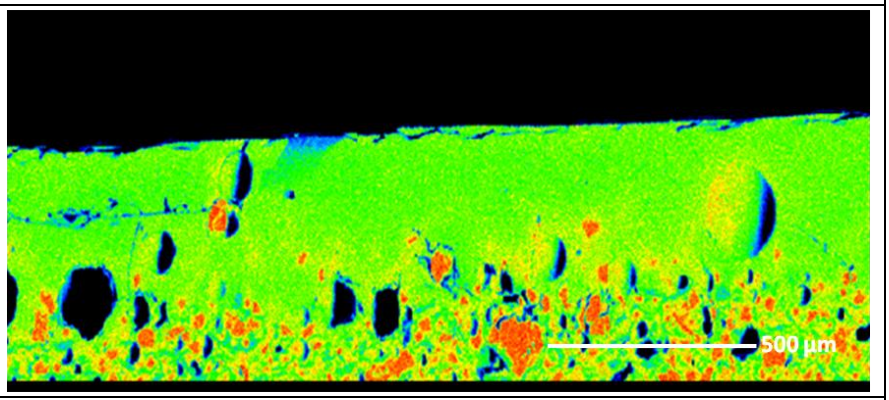
K	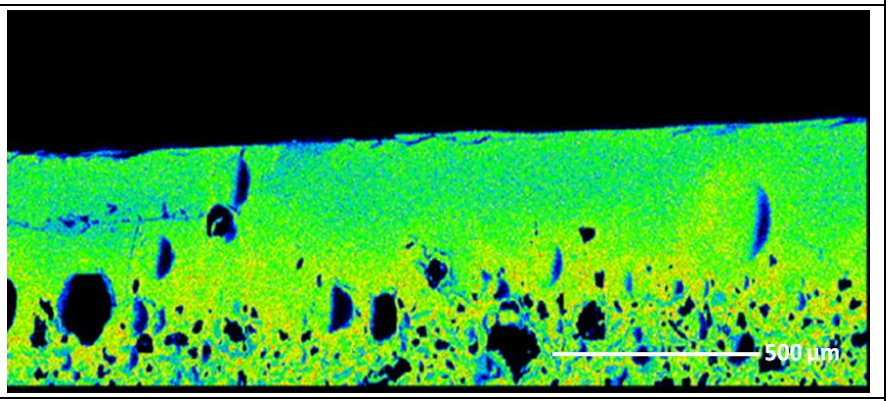
Al	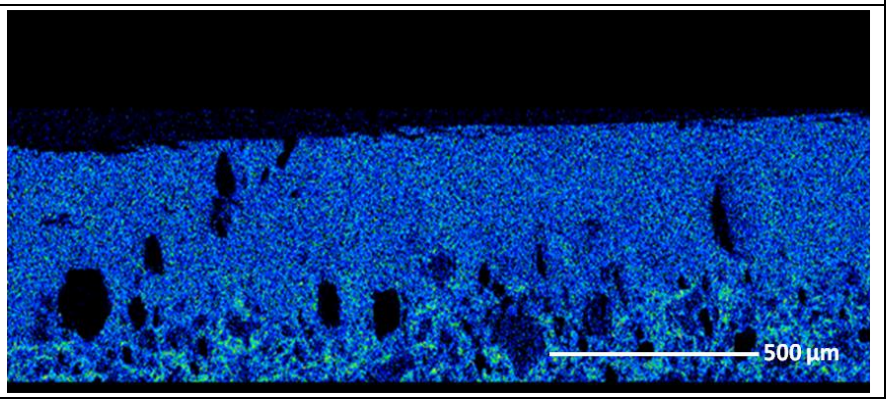

WP#6	
Ca	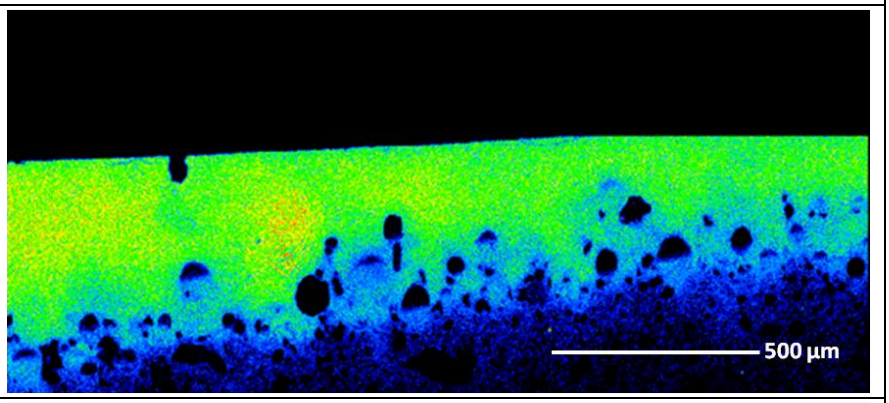
Si	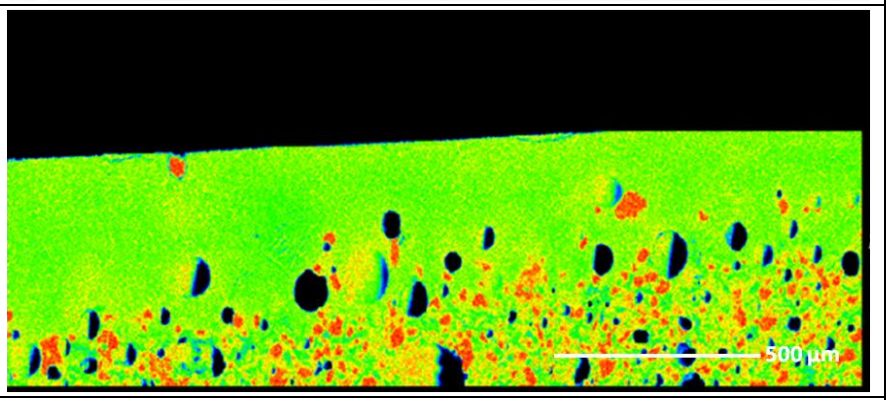
K	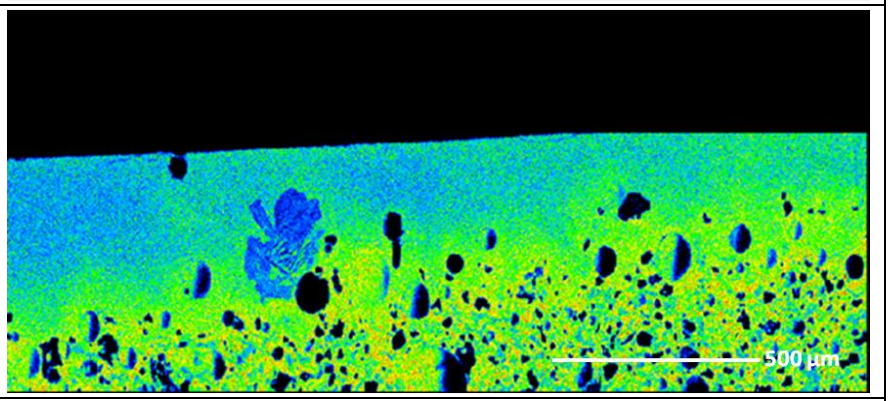
Al	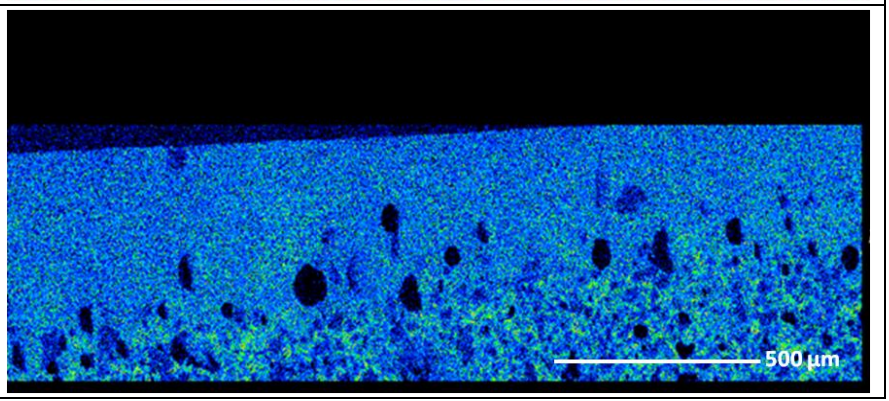

WP#7	
Ca	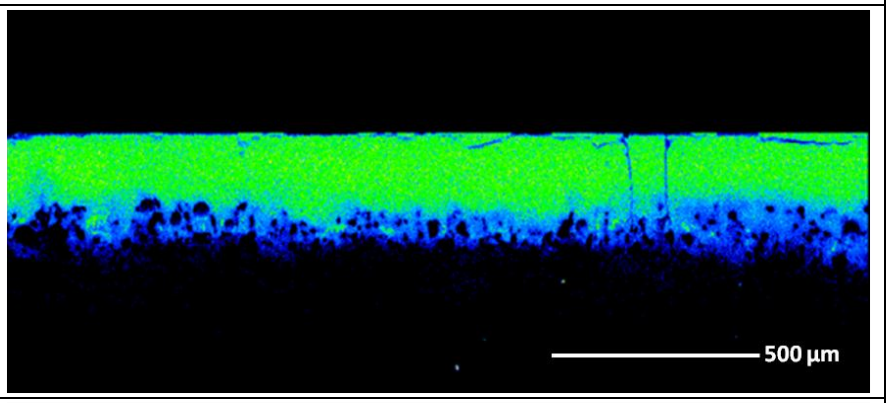
Si	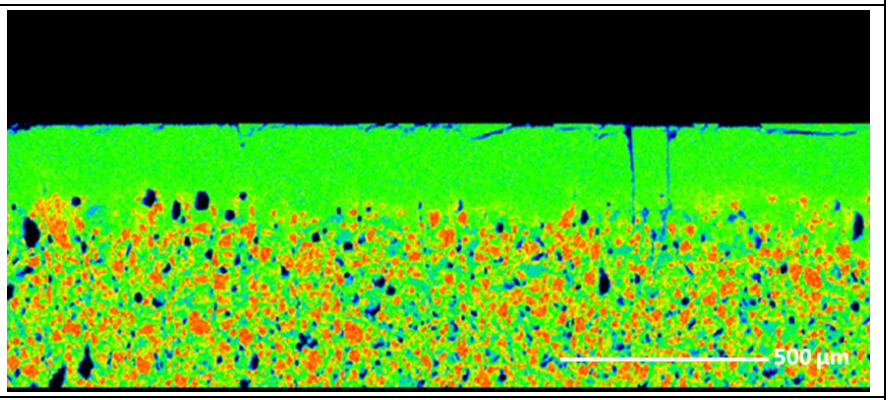
K	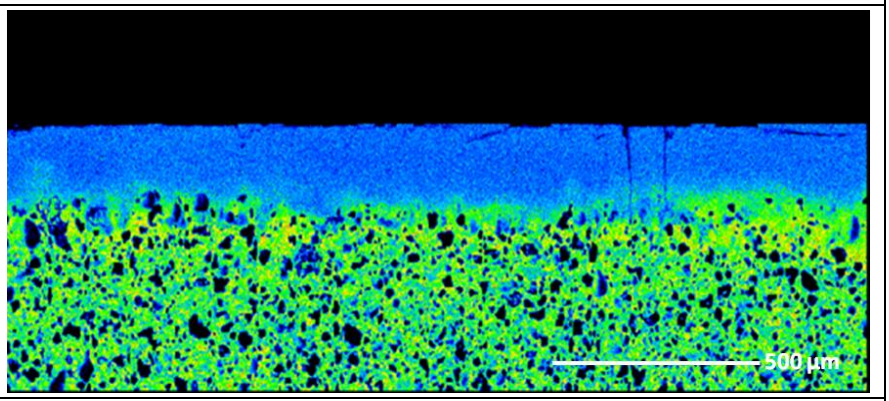
Al	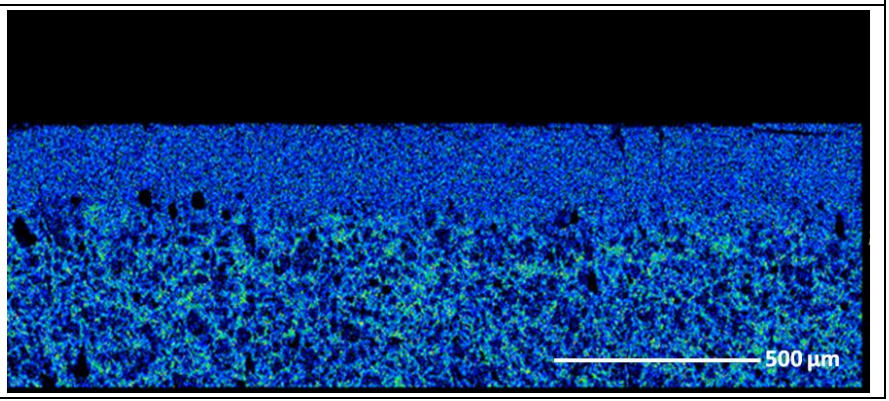

GWP#1	
Ca	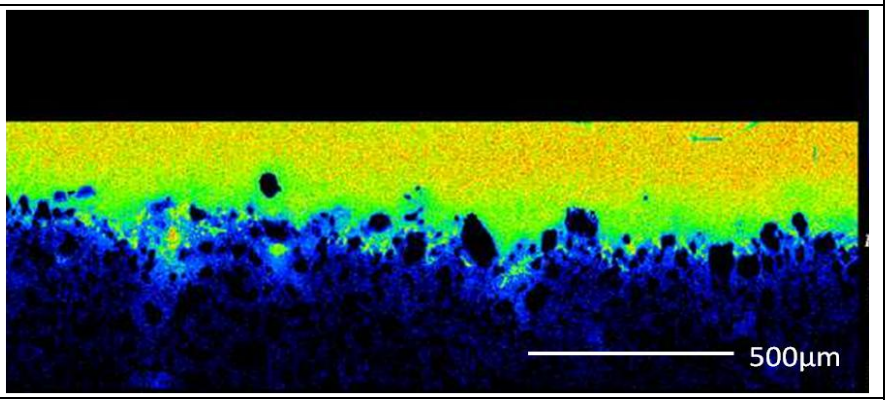
Si	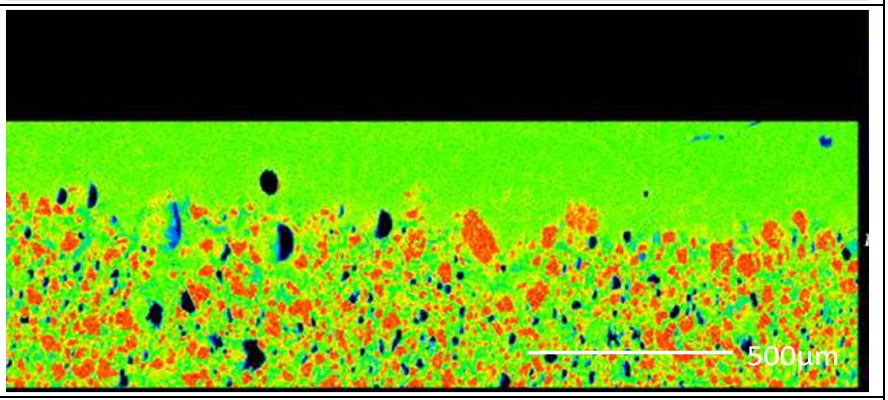
K	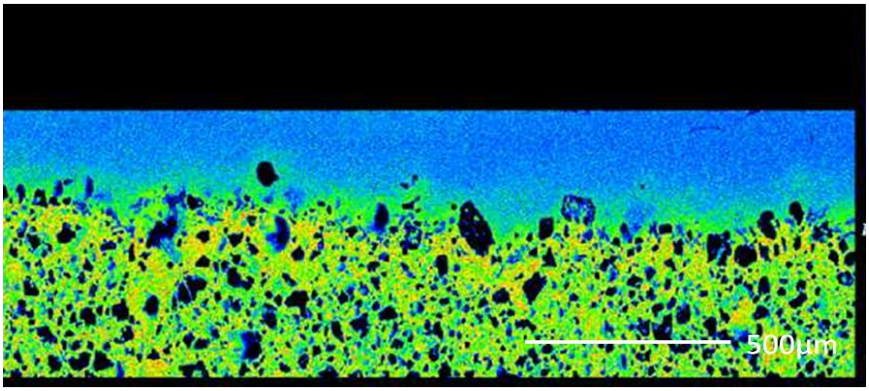
Al	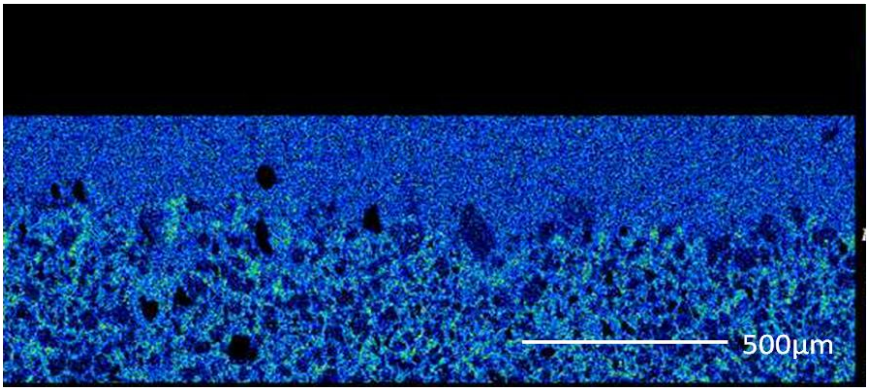

GWP#2	
Ca	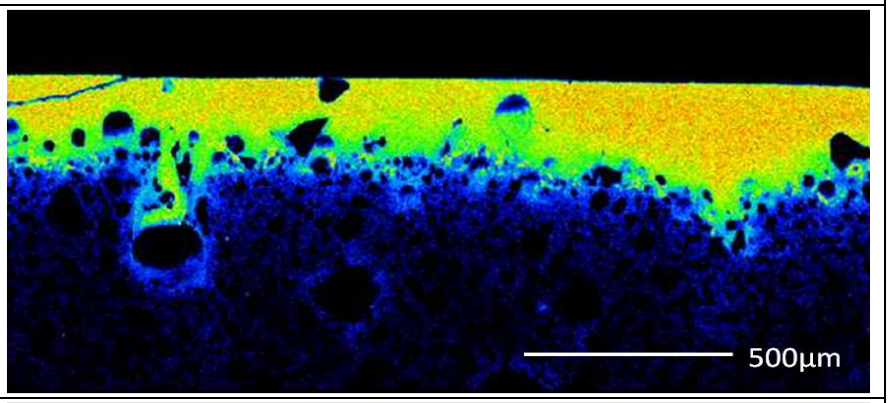
Si	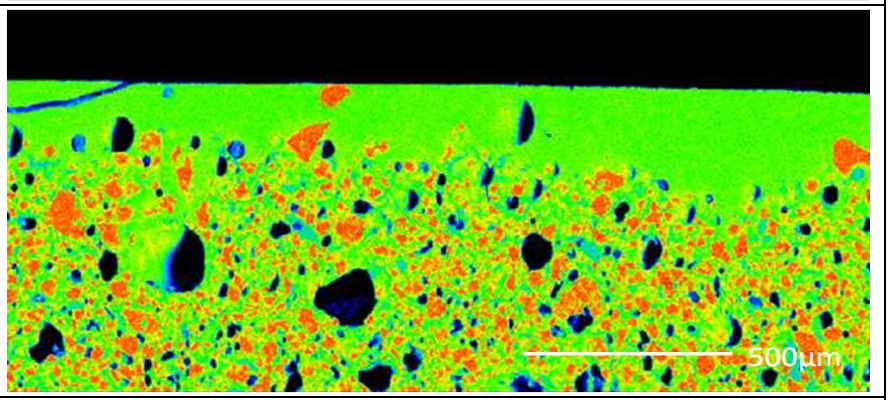
K	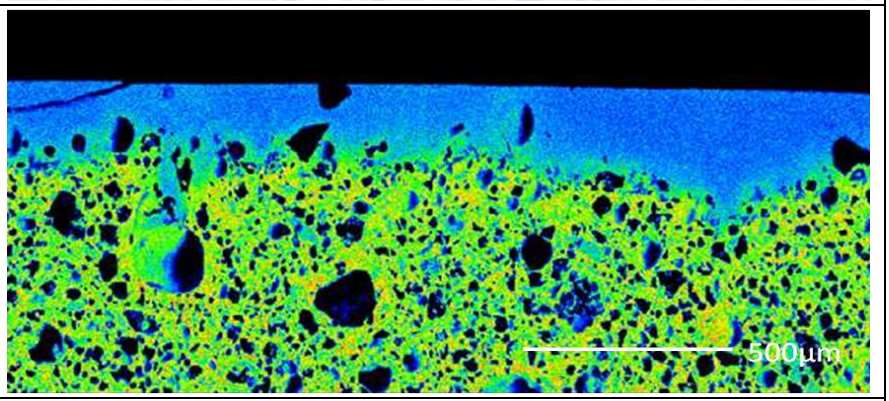
Al	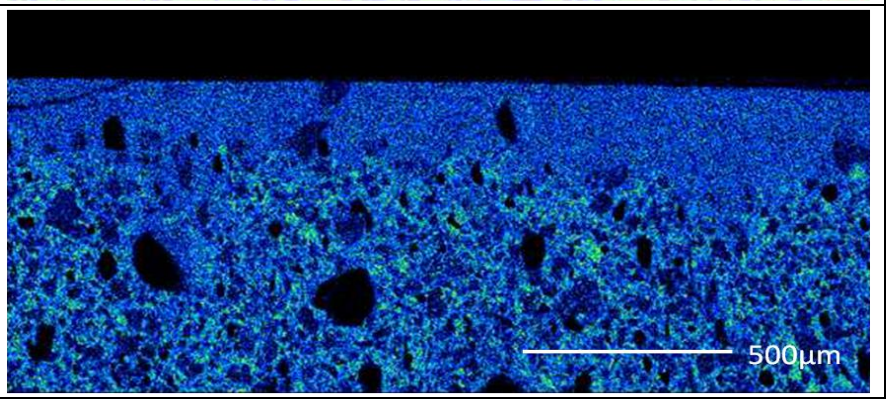

GWP#3	
Ca	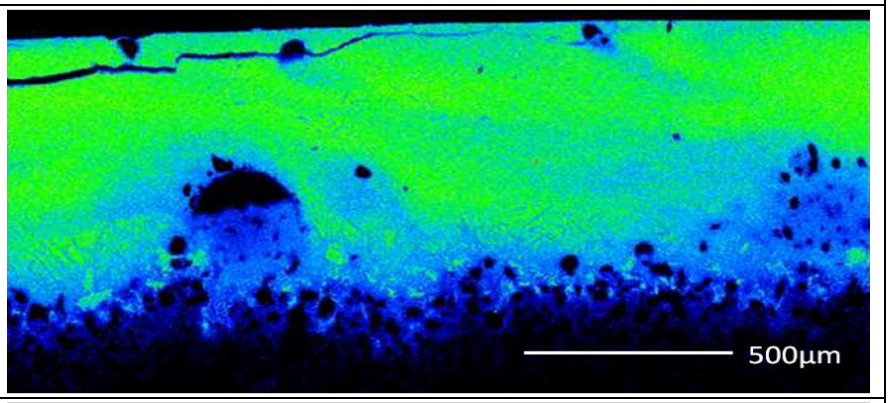
Si	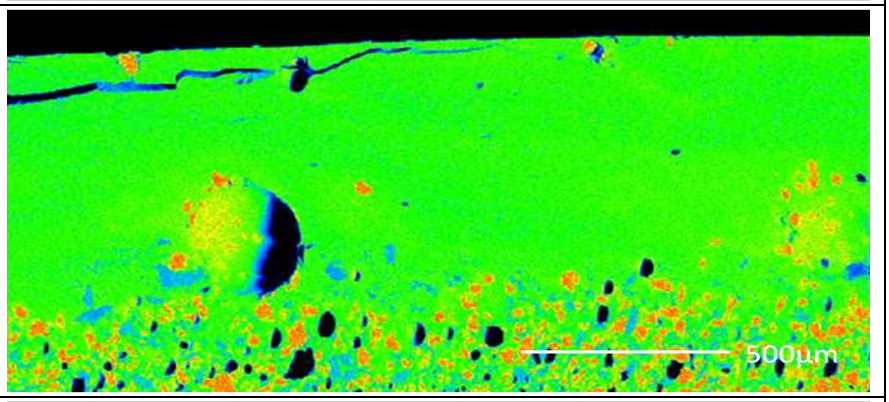
K	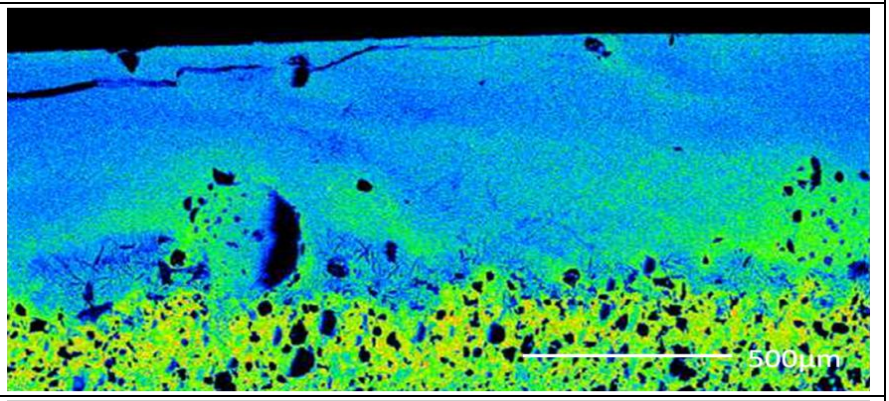
Al	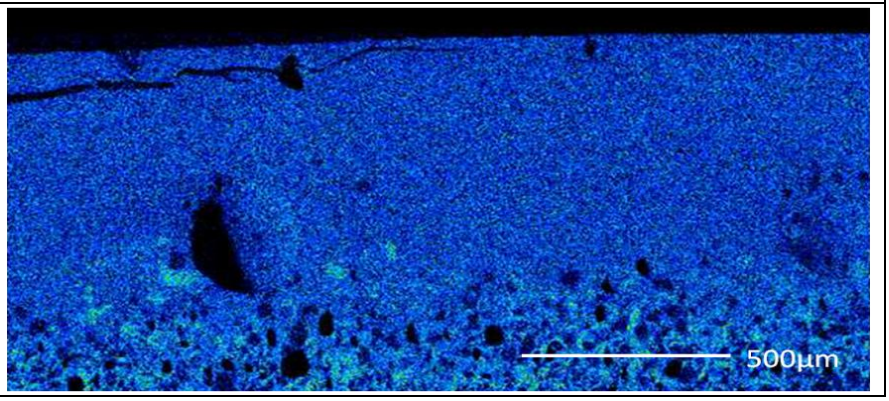

GWP#4	
Ca	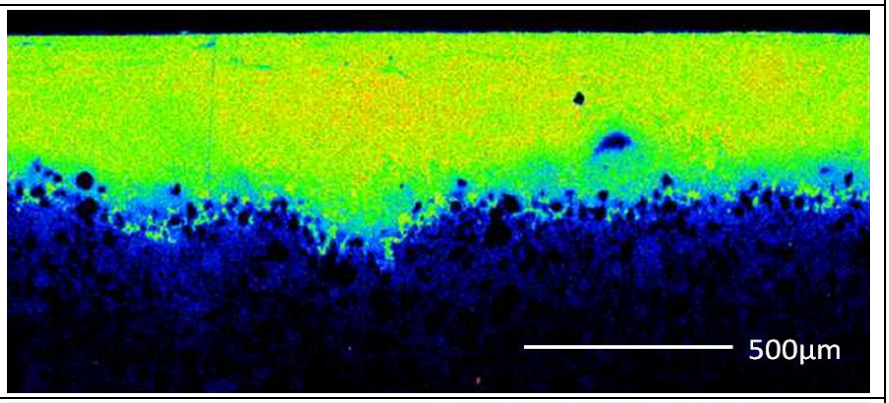
Si	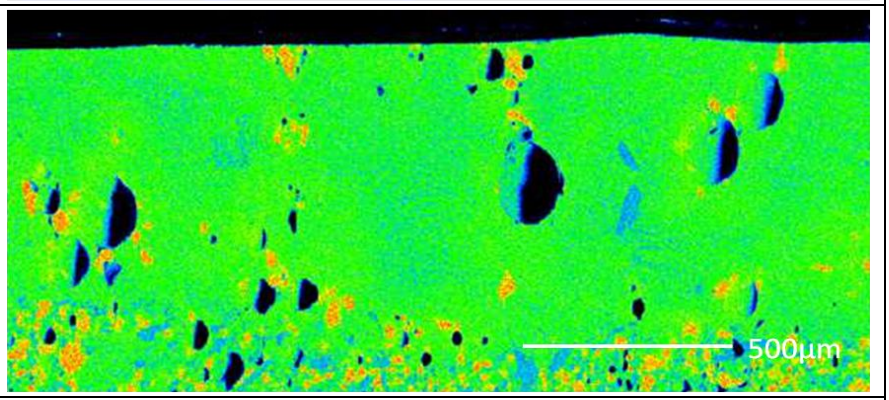
K	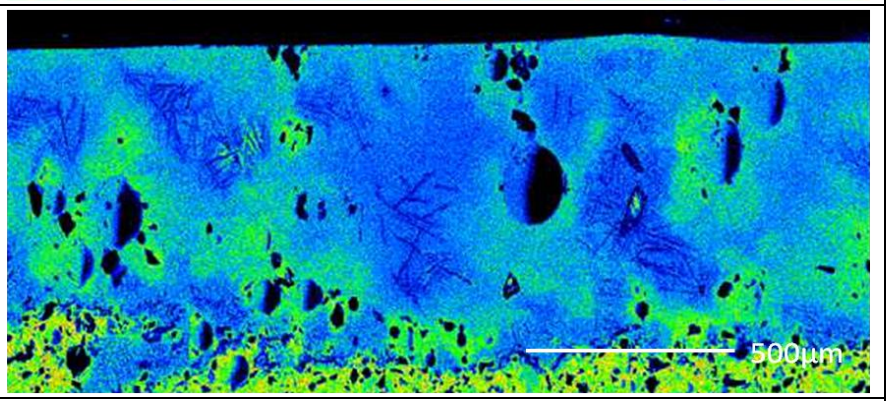
Al	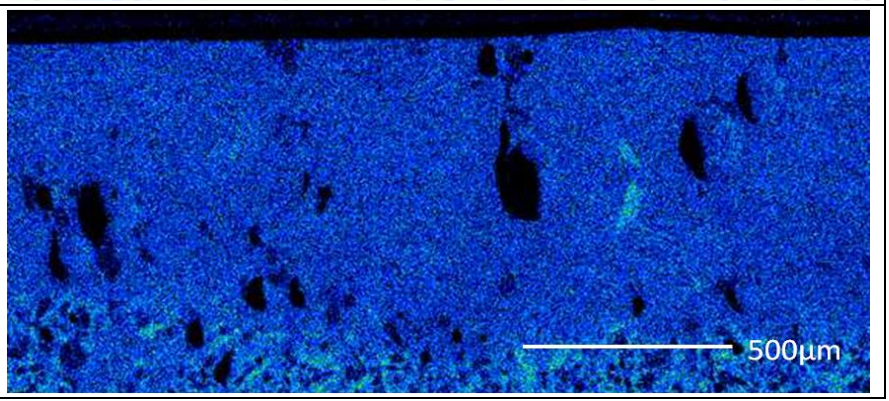

GWP#5	
Ca	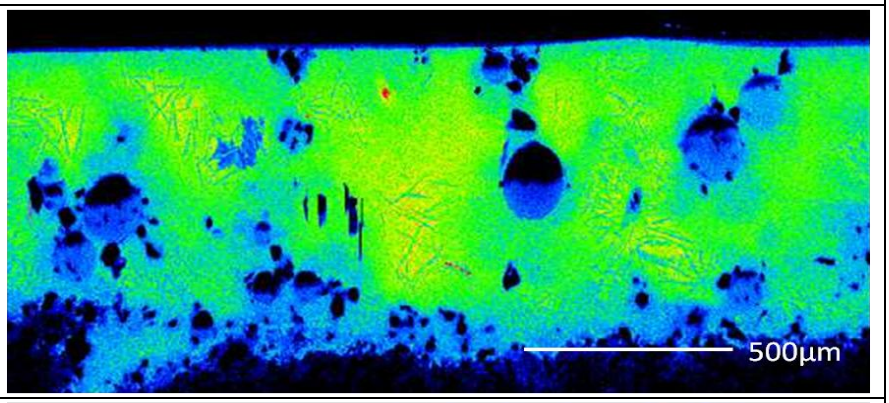
Si	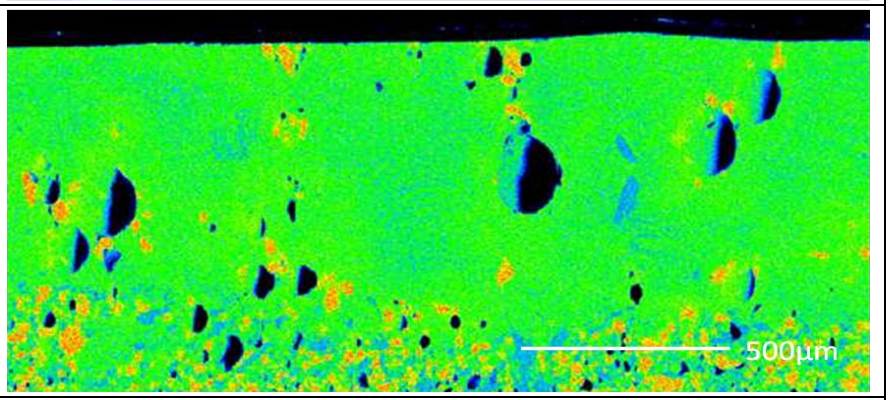
K	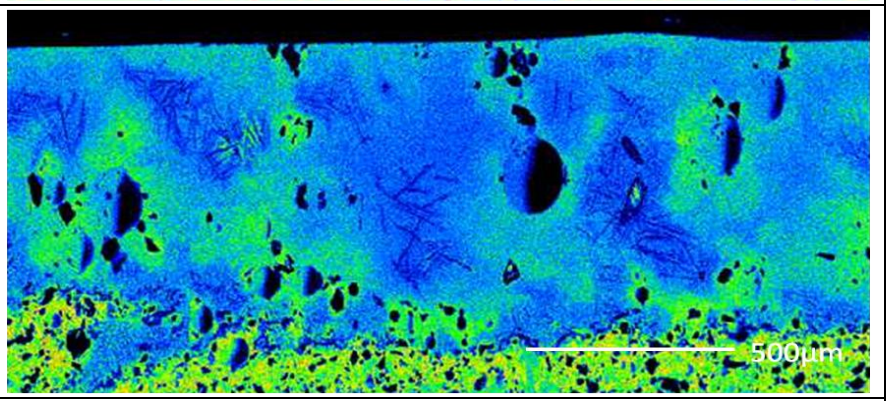
Al	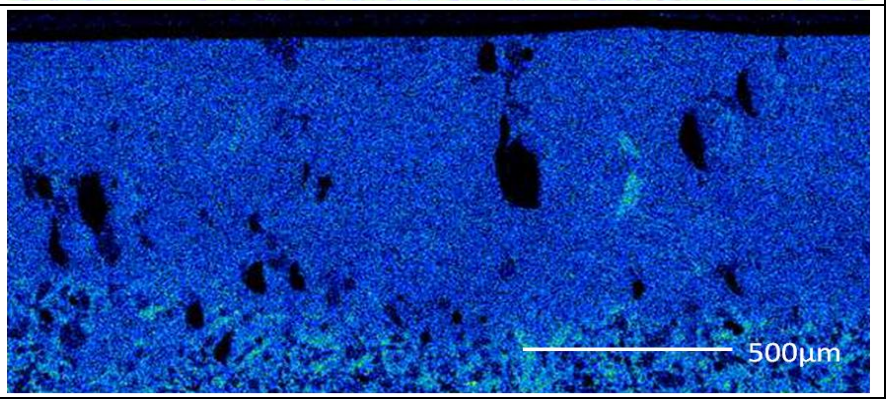

GWP#6	
Ca	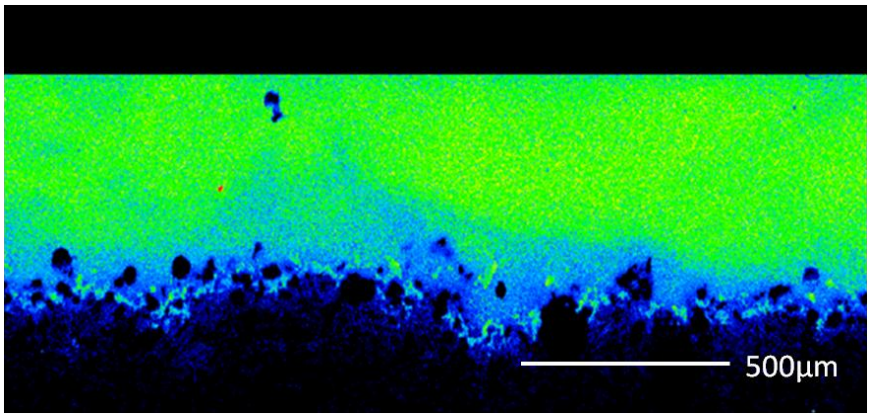
Si	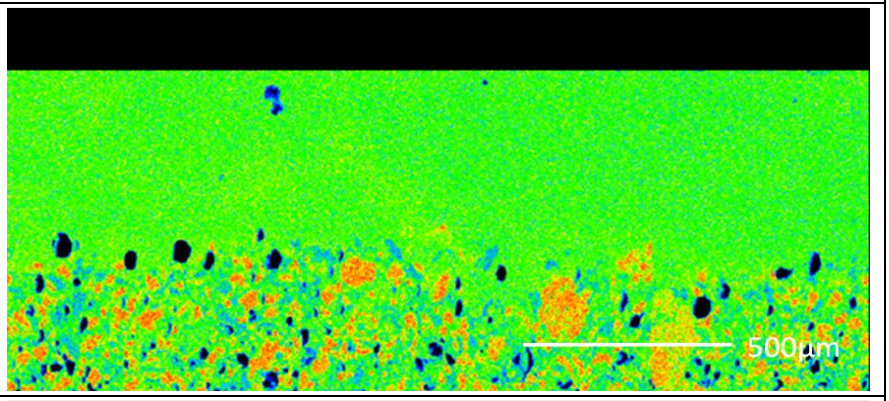
K	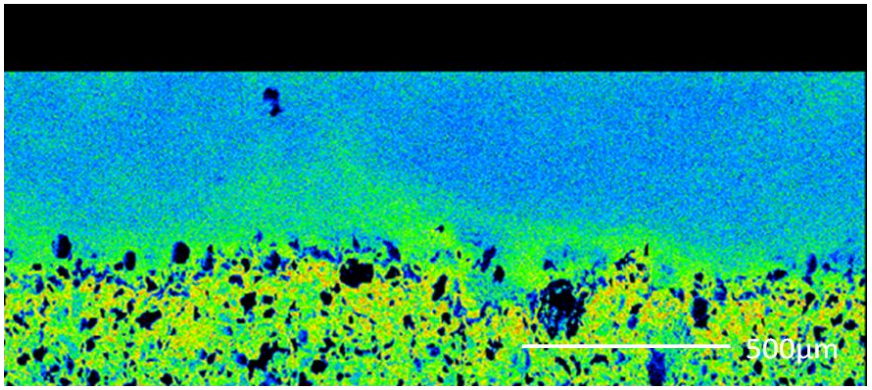
Al	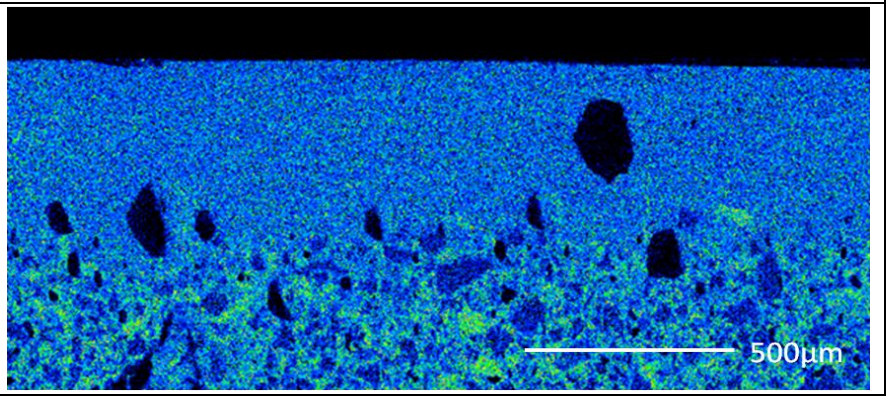

GWP#7	
Ca	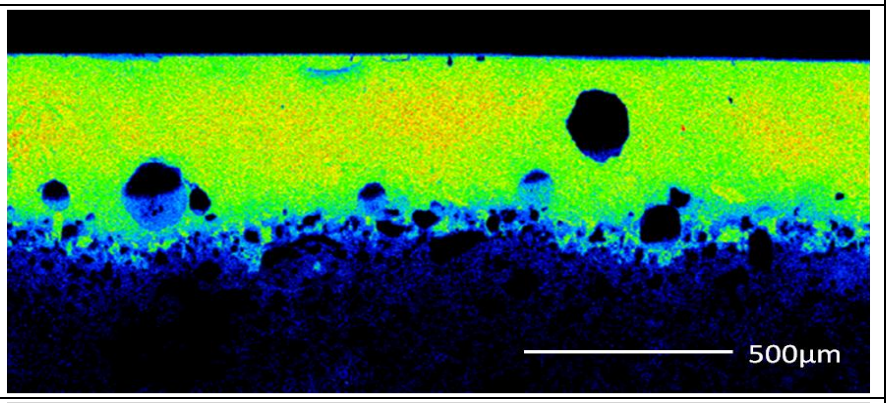
Si	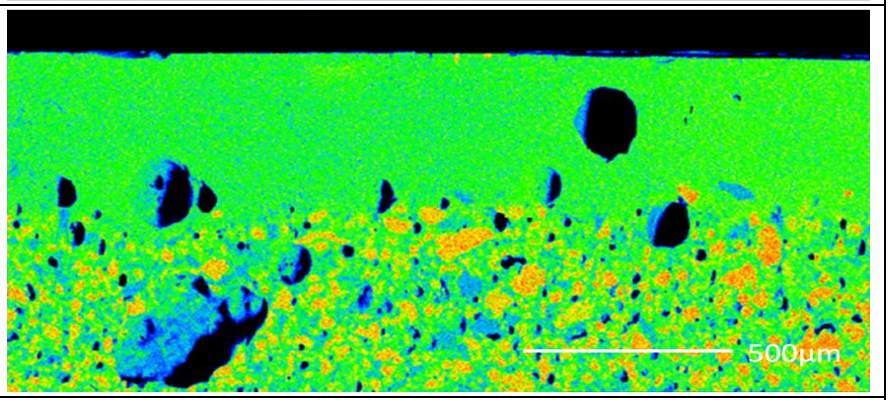
K	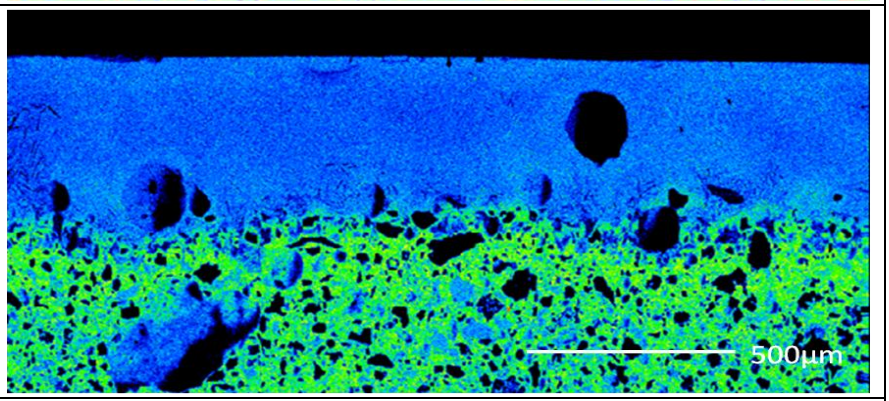
Al	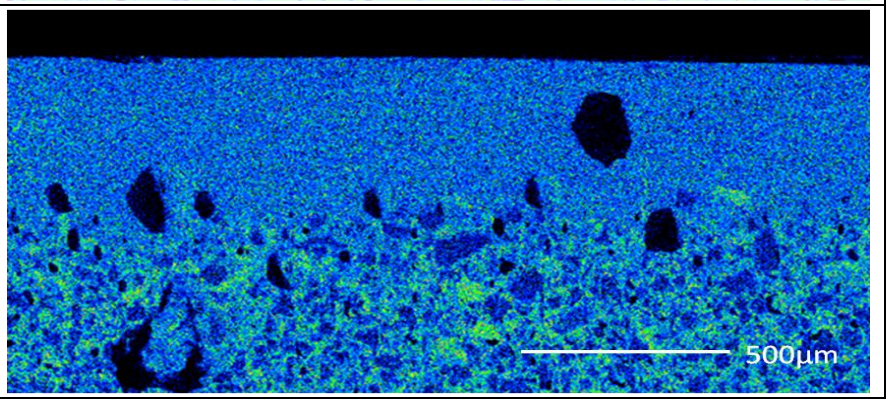

GWP#8	
Ca	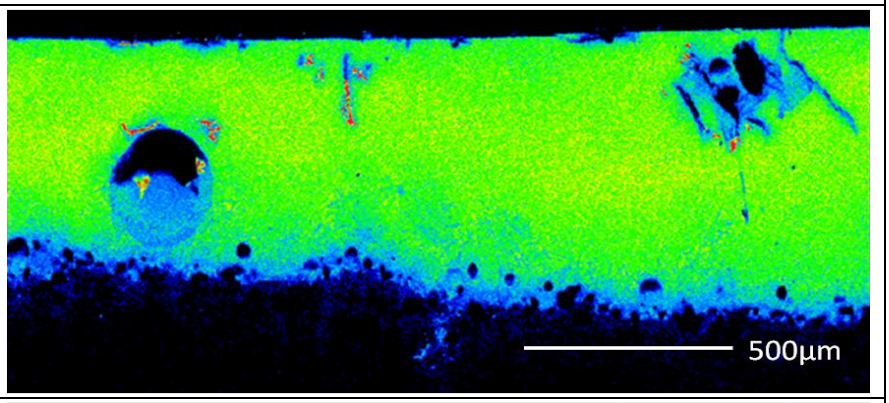
Si	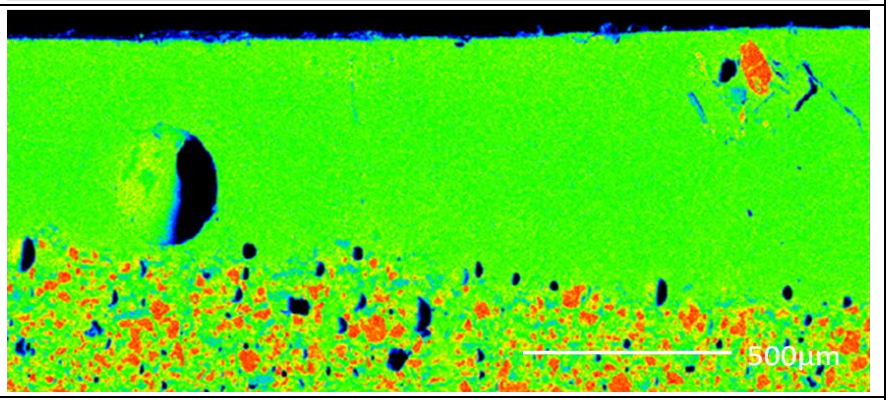
K	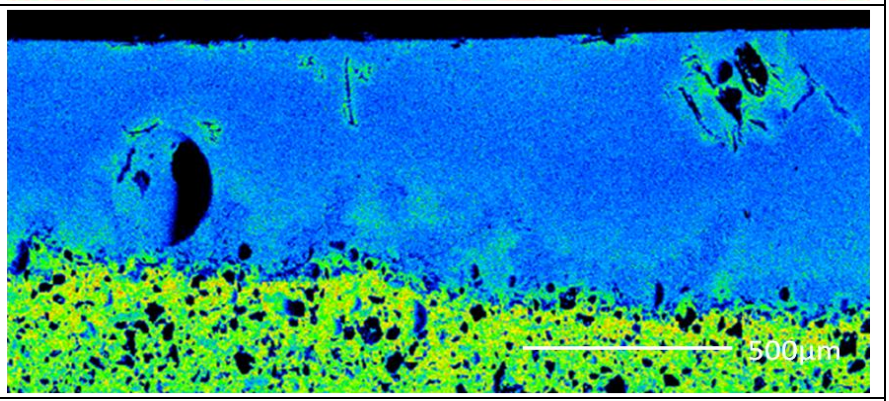
Al	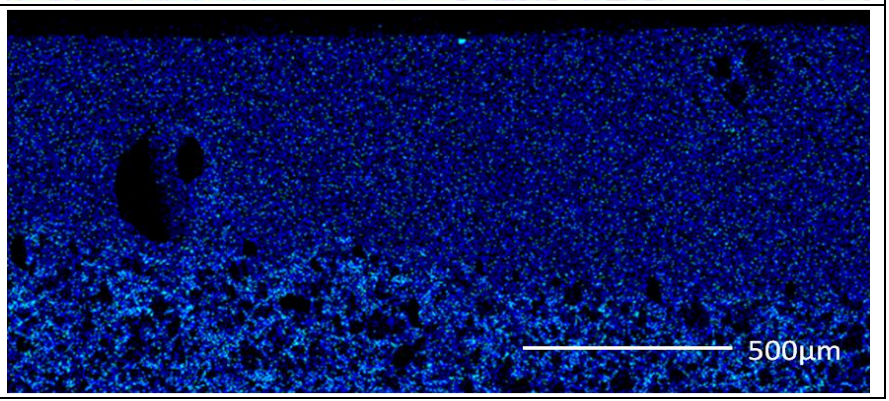

GWP#9	
Ca	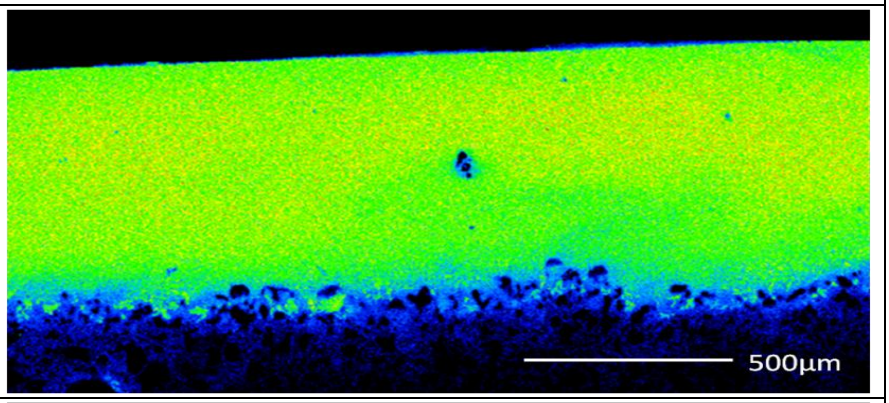
Si	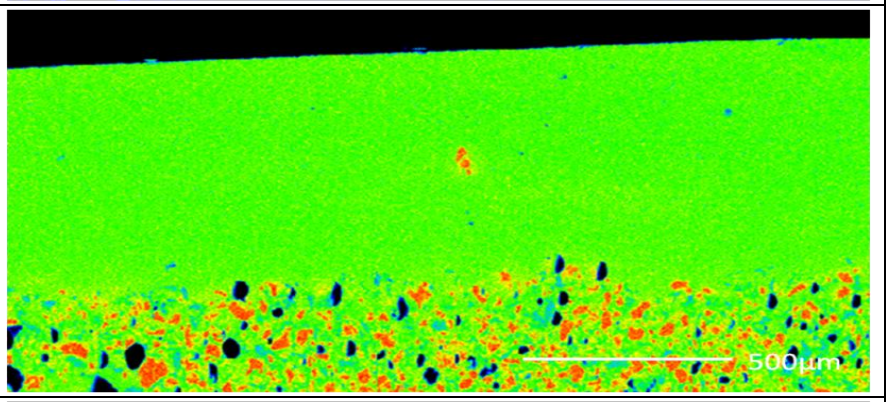
K	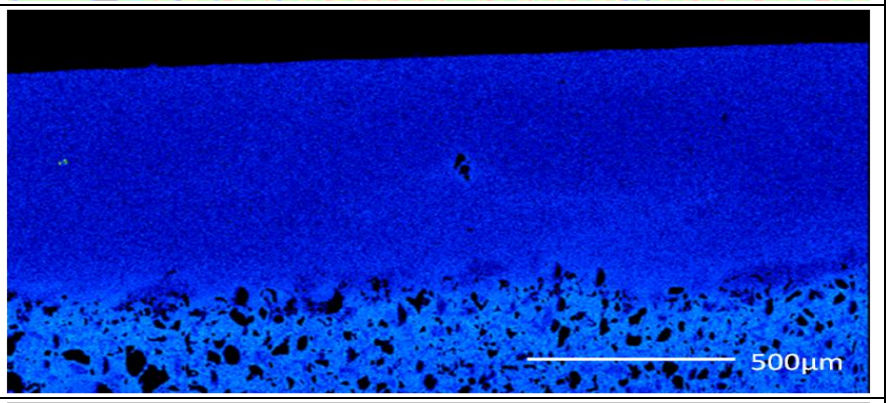
Al	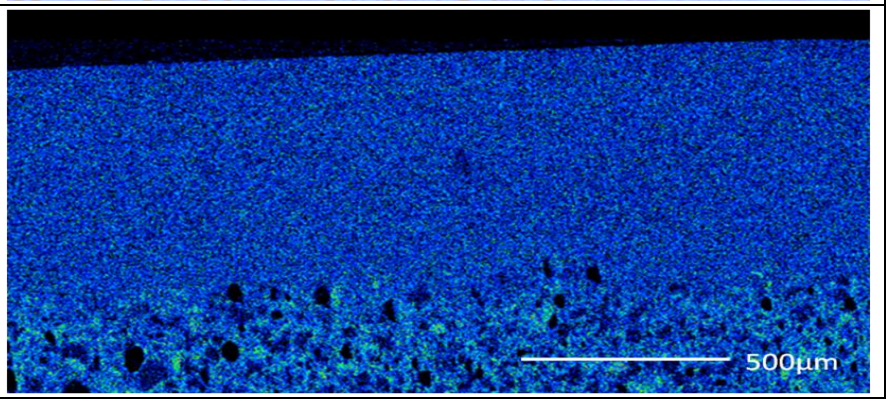

GWP#10	
Ca	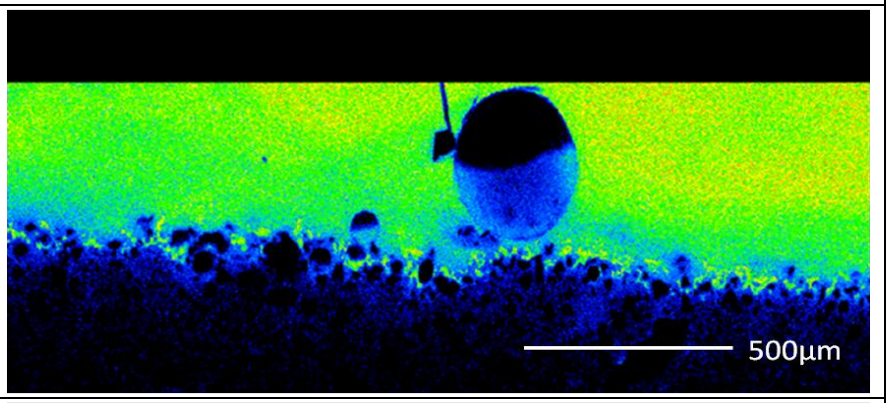
Si	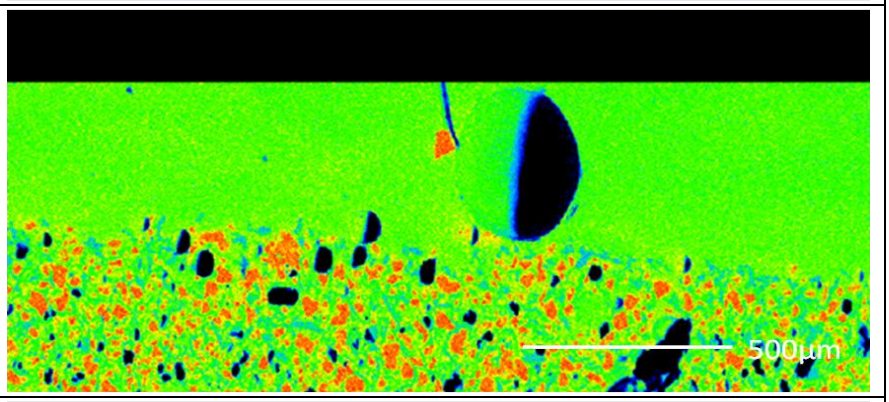
K	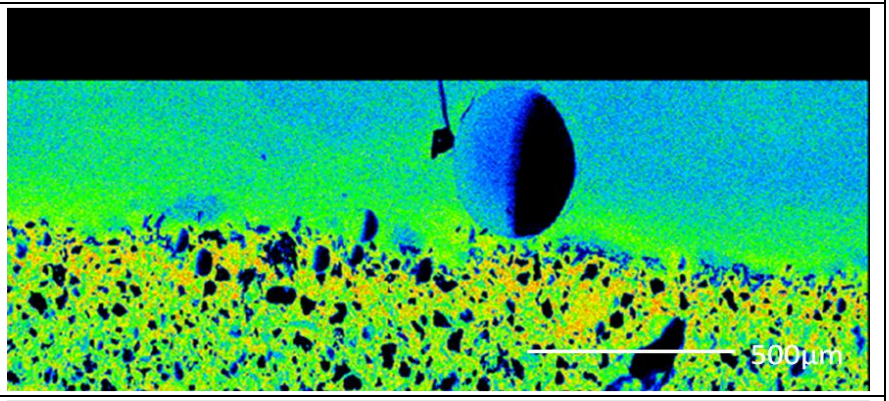
Al	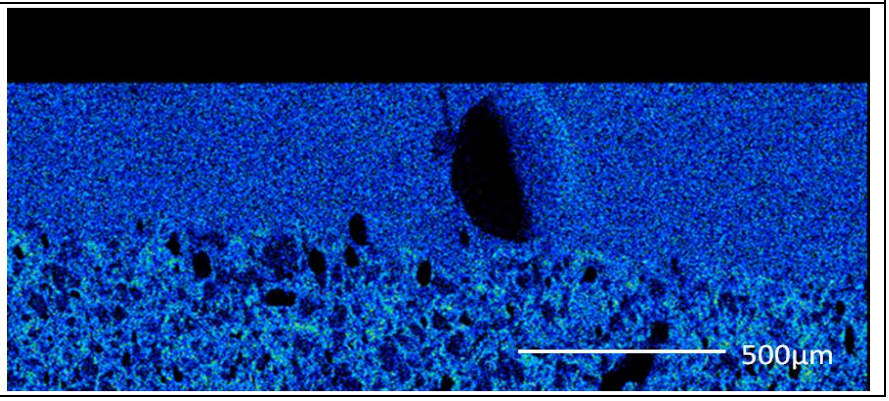

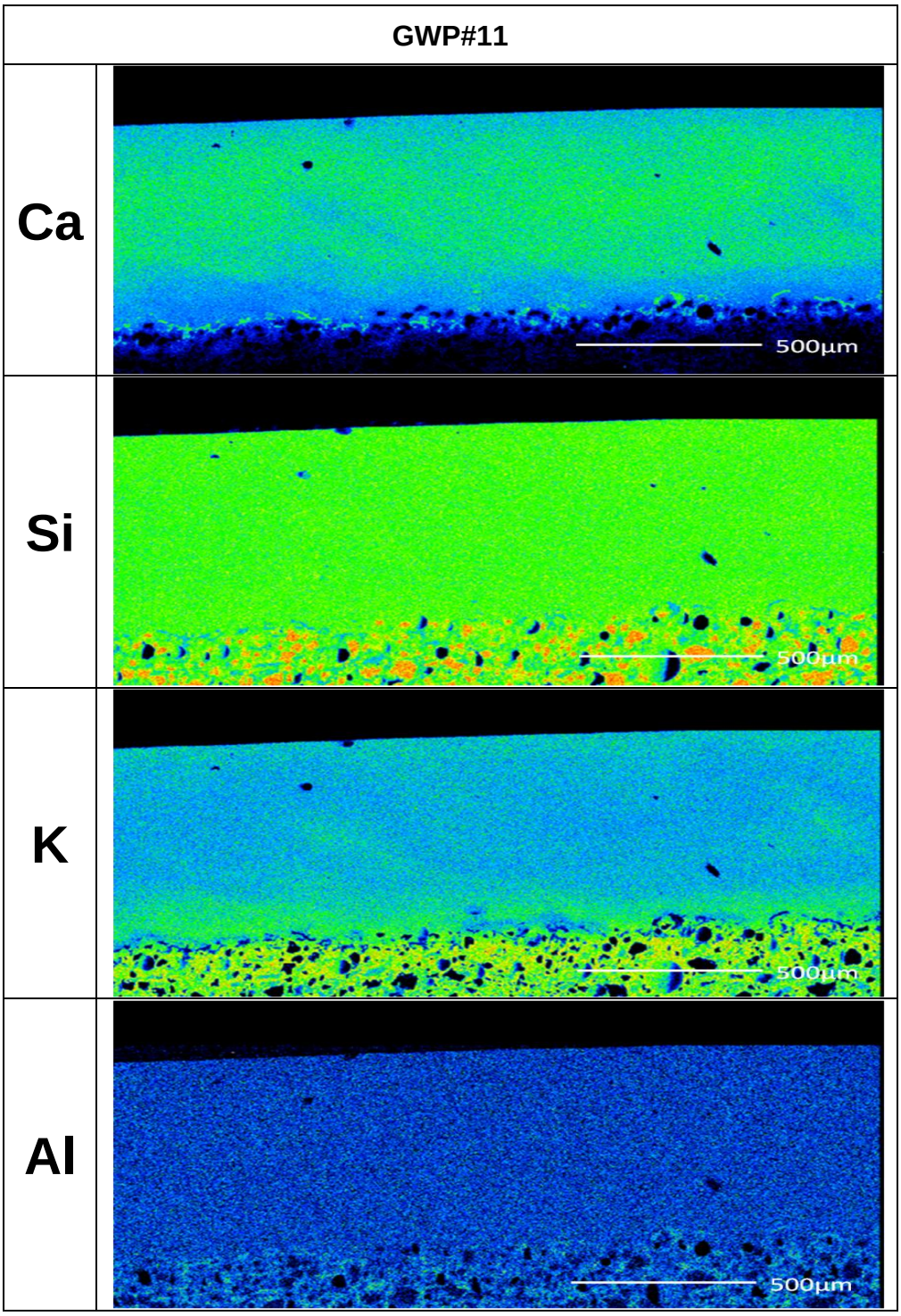

Figure 42. WDS maps of body-glaze interface for all collected ancient Chinese shards in this work: WP (#1~#7) and GWP (#1~#11).

Table XX. The Body Chemical Composition of White Porcelain (WP) in Jingdezhen from Five Dynasties to Song Dynasty by ICP

	SiO_2	Al_2O_3	Fe_2O_3	MgO	CaO	Na_2O	K_2O	TiO_2	P_2O_5	MnO	Cr_2O_3
WP#1	77.04	17.66	0.75	0.17	0.17	0.27	3.18	0.04	0.02	0.13	0.01
WP#2	78.89	16.63	0.56	0.17	0.11	0.14	2.54	0.04	0.04	0.09	<0.002
WP#3	76.54	17.87	0.60	0.20	0.21	0.18	3.46	0.03	0.03	0.10	<0.002
WP#4	76.21	17.51	0.64	0.19	0.14	0.50	3.18	0.03	<0.01	0.11	<0.002
WP#5	77.79	16.58	0.57	0.16	0.16	0.18	3.05	0.04	0.02	0.04	<0.002
WP#6	77.88	17.34	0.70	0.26	0.35	0.15	2.52	0.10	0.03	0.09	<0.002
WP#7	76.19	17.56	0.65	0.21	0.33	0.32	3.27	0.03	0.02	0.13	<0.002

Table XXI. The Body Chemical Composition of Greenish White Porcelain (GWP) in Jingdezhen from Five Dynasties to Song Dynasty by ICP

	SiO_2	Al_2O_3	Fe_2O_3	MgO	CaO	Na_2O	K_2O	TiO_2	P_2O_5	MnO	Cr_2O_3
GWP#1	77.91	15.38	0.88	0.20	0.98	0.57	3.04	0.04	0.02	0.06	<0.002
GWP#2	77.48	15.56	0.68	0.30	1.29	0.42	2.87	0.04	0.04	0.09	<0.002
GWP#3	74.93	18.50	0.93	0.16	0.36	2.03	2.53	0.05	0.02	0.06	<0.002
GWP#4	75.50	17.39	1.06	0.21	0.61	1.89	2.75	0.06	0.01	0.08	<0.002
GWP#5	74.71	18.36	0.94	0.17	0.43	2.08	2.72	0.05	0.01	0.06	<0.002
GWP#6	75.68	17.99	0.80	0.17	0.37	1.61	2.67	0.05	0.02	0.09	<0.002
GWP#7	75.39	17.53	0.93	0.18	0.69	1.59	2.72	0.06	0.01	0.09	<0.002
GWP#8	75.31	17.84	0.92	0.18	0.40	2.00	2.65	0.05	0.02	0.06	0.00
GWP#9	75.03	18.20	0.94	0.15	0.41	2.20	2.50	0.05	0.01	0.07	<0.002
GWP#10	75.86	17.82	0.87	0.15	0.31	0.87	3.24	0.04	0.01	0.06	<0.002
GWP#11	76.95	16.69	0.89	0.16	0.35	1.13	2.93	0.04	0.04	0.04	<0.002

Table XXII. The Glaze Chemical Composition of White Porcelain (WP) in Jingdezhen from Five Dynasties to Song Dynasty by EDXRF

	SiO_2	Al_2O_3	Fe_2O_3	MgO	CaO	Na_2O	K_2O	TiO_2	P_2O_5	MnO
WP#1	67.60	14.84	0.90	0.79	12.11	0.03	2.71	0.02	0.11	0.19
WP#2	73.58	14.58	0.71	0.76	6.29	0.19	2.87	0.03	0.10	0.23
WP#3	65.55	15.88	0.78	1.34	11.79	0.03	3.60	0.03	0.17	0.24
WP#4	69.02	12.72	0.71	0.77	13.29	0.21	2.26	0.03	0.13	0.15
WP#5	71.66	15.07	0.90	0.97	6.97	0.03	3.35	0.05	0.15	0.13
WP#6	71.21	14.30	0.91	0.98	9.52	0.03	2.02	0.05	0.26	0.13
WP#7	65.87	14.46	0.64	1.24	14.22	0.17	2.39	0.02	0.26	0.15

Table XXIII. The Glaze Chemical Composition of Greenish White Porcelain (GWP) in Jingdezhen from Five Dynasties to Song Dynasty by EDXRF

	SiO_2	Al_2O_3	Fe_2O_3	MgO	CaO	Na_2O	K_2O	TiO_2	P_2O_5	MnO
GWP#1	69.36	11.81	0.65	0.67	13.80	0.54	2.15	0.02	0.13	0.10
GWP#2	68.94	12.50	0.59	0.64	14.16	0.36	1.77	0.03	0.05	0.07
GWP#3	69.03	13.31	0.62	0.26	11.69	2.10	1.95	0.03	0.06	0.06
GWP#4	66.94	13.24	0.85	0.50	13.32	2.03	2.10	0.03	0.06	0.10
GWP#5	67.57	13.11	0.55	0.40	12.72	2.37	2.26	0.02	0.07	0.06
GWP#6	67.39	13.44	0.71	0.40	13.52	1.22	2.27	0.05	0.08	0.10
GWP#7	66.37	12.92	1.45	0.20	14.12	1.73	2.17	0.04	0.08	0.08
GWP#8	65.12	14.70	0.98	0.58	13.51	2.01	2.07	0.04	0.08	0.06
GWP#9	66.68	14.52	1.15	0.26	14.52	1.65	1.79	0.03	0.07	0.06
GWP#10	68.93	12.99	1.19	0.18	11.49	1.15	3.04	0.03	0.05	0.07

Table XXIV. The Measured Body Chemistry of "Spot Check" Group by ICP

	SiO_2	Al_2O_3	Fe_2O_3	MgO	CaO	Na_2O	K_2O	TiO_2	P_2O_5	MnO
S.C. #1	73.79	15.33	0.77	0.14	0.77	5.10	2.85	0.05	0.12	0.08
S.C. #2	74.01	18.21	0.80	0.30	0.68	0.78	3.67	0.06	0.04	0.13
S.C. #3	75.91	15.36	1.10	0.24	0.65	1.86	4.02	0.11	0.04	0.05
S.C. #4	75.30	15.38	0.78	0.20	0.51	3.49	2.81	0.04	0.10	0.05
S.C. #5	70.21	19.66	0.99	0.15	0.59	4.21	2.74	0.06	0.09	0.07
S.C. #6	73.46	20.04	1.08	0.28	0.54	0.62	2.96	0.08	0.04	0.11
S.C. #7	72.28	19.67	1.25	0.24	0.56	1.55	3.71	0.12	0.04	0.05
S.C. #8	71.87	20.21	1.07	0.20	0.45	2.81	2.64	0.07	0.08	0.05

Table XXV. The Measured Body Chemistry of "Comparative Experiment" Group by ICP

	SiO_2	Al_2O_3	Fe_2O_3	MgO	CaO	Na_2O	K_2O	TiO_2	P_2O_5	MnO
Previous model	68.67	25.15	0.72	0.42	0.24	0.44	2.46	0.45	-	-
Chin. ->Lerdprom's	67.37	26.36	1.34	0.26	0.40	0.44	2.61	0.10	0.02	0.08
Chin.->Colorado's	65.69	26.13	1.11	0.19	0.38	2.92	2.73	0.09	0.04	0.03
Chin. *Comm. #1	71.47	21.83	0.87	0.26	0.53	1.11	3.26	0.06	0.04	0.09
Chin. Comm. #2	71.71	22.24	1.47	0.19	0.26	0.34	2.93	0.10	0.03	0.05
Chin. Comm. #3	71.67	22.33	1.05	0.23	0.42	0.72	2.89	0.08	0.05	0.08

Table XXVI. Density Measurements and Calculations of Ancient Chinese Specimens from Jingdezhen in the Period of Five Dynasties to Song Dynasty

	Bulk Density (g/cm^3)	App. Porosity (%)	Water Absorption (%)	True Density (g/cm^3)	Calculated Glass Density (g/cm^3)	Std. Dev. of (Glass Density)
WP#1	2.24	0.81	0.36	2.4856	2.2278	0.0088
WP#2	2.17	5.36	2.47	2.4639	2.0826	0.0667
WP#3	2.13	2.26	1.06	2.4443	2.2408	0.0148
WP#4	2.18	4.86	2.23	2.4949	2.2372	0.0704
WP#5	2.11	3.15	1.49	2.5009	2.3325	0.0090
WP#6	2.14	2.27	1.06	2.5217	2.3663	0.0092
WP#7	2.16	5.30	2.45	2.5784	2.3980	0.0170
GWP#1	2.16	4.08	1.89	2.6211	2.5130	0.0019
GWP#2	2.01	4.11	2.05	2.5882	2.4699	0.0032
GWP#3	2.21	1.39	0.63	2.5436	2.3927	0.0060
GWP#4	2.13	3.85	1.81	2.5855	2.4743	0.0035
GWP#5	2.19	4.17	1.90	2.6576	2.5728	0.0047
GWP#6	2.16	3.27	1.52	2.5821	2.4415	0.0061
GWP#7	2.19	2.45	1.12	2.5697	2.4538	0.0029
GWP#8	2.24	1.83	0.82	2.5503	2.4182	0.0032
GWP#9	2.21	0.96	0.43	2.5369	2.4108	0.0009
GWP#10	2.26	2.86	1.27	2.6282	2.5222	0.0033
GWP#11	2.20	1.46	0.66	2.5847	2.4797	0.0012

Table XXVII. Mineralogy of Chinese Ancient Specimens from Jingdezhen in the Period of Five Dynasties to Song Dynasty

	1st		2nd		3rd		Silica in Glass (UMF)	Alumina in Glass (UMF)
	Undissolved Quartz (% Wt.)	Mullite (% Wt.)	Undissolved Quartz (% Wt.)	Mullite (% Wt.)	Undissolved Quartz (% Wt.)	Mullite (% Wt.)		
WP#1	29.49	18.49	29.73	17.43	30.57	16.82	15.17	0.94
WP#2	41.32	19.17	38.76	19.29	34.43	17.02	18.68	1.59
WP#3	16.12	19.06	18.40	19.23	16.65	19.12	18.16	1.21
WP#4	26.55	16.07	35.38	18.21	-	-	15.32	1.19
WP#5	19.34	16.51	19.77	16.79	18.54	15.68	21.68	1.25
WP#6	17.91	16.96	21.09	15.83	18.78	15.10	21.75	1.43
WP#7	31.46	16.59	32.67	17.12	30.94	15.00	13.39	1.31
GWP#1	28.70	13.17	27.89	12.80	31.75	12.70	11.09	0.98
GWP#2	27.18	12.86	26.65	12.60	29.14	11.65	11.08	1.04
GWP#3	23.28	15.29	23.28	15.29	24.38	13.86	11.07	1.16
GWP#4	23.73	12.94	24.24	12.67	25.89	11.59	10.10	1.02
GWP#5	28.06	13.70	26.88	13.12	27.05	12.83	9.80	1.08
GWP#6	25.33	15.58	25.02	15.39	26.58	14.09	11.53	1.19
GWP#7	23.17	12.55	22.75	12.31	25.55	12.31	10.83	1.20
GWP#8	23.70	13.35	23.51	13.24	23.75	12.73	11.07	1.16
GWP#9	19.55	13.40	19.44	13.32	21.01	13.01	11.44	1.14
GWP#10	22.39	14.84	21.65	14.35	24.67	14.92	13.53	1.17
GWP#11	21.41	12.75	20.89	12.44	20.87	13.10	14.64	1.20

Table XXVIII. Mineralogy of "Spot Check" Porcelain Specimens Fired under Different Conditions

	Temp. (ºC)	Dwell Time (hour)	Heating Rate (K/min)	Undisso. quartz (% Wt.)	Mullite (% Wt.)	Undisso. quartz (% Wt.)	Mullite (% Wt.)	Silica in Glass (UMF)	Alumina in Glass (UMF)
Sp. che.#2	1150	3.2	2.5	29.49	13.12	30.22	13.14	9.47	1.21
Sp. che.#2	1150	32	2.5	16.92	13.29	18.36	13.45	12.31	1.18
Sp. che.#2	1250	3.2	2.5	17.40	13.52	17.77	13.45	12.32	1.18
Sp. che.#2	1250	32	2.5	8.73	13.28	9.57	13.29	14.30	1.20
Sp. che.#3	1150	3.2	2.5	33.61	6.08	32.93	5.93	7.56	1.21
Sp. che.#3	1150	32	2.5	22.39	6.34	22.82	6.08	9.51	1.20
Sp. che.#3	1250	3.2	2.5	19.79	6.02	21.68	6.05	9.87	1.20
Sp. che.#3	1250	32	2.5	10.53	6.18	11.11	6.32	11.68	1.18
Sp. che.#4	1150	3.2	2.5	29.82	4.51	30.25	5.02	7.30	1.15
Sp. che.#4	1150	32	2.5	21.88	4.57	22.29	4.56	8.63	1.19
Sp. che.#4	1250	3.2	2.5	18.74	4.50	20.20	4.50	9.06	1.19
Sp. che.#4	1250	32	2.5	9.88	4.04	10.02	4.65	10.65	1.18
Sp. che.#6	1150	3.2	2.5	30.49	18.12	30.41	18.31	10.87	1.17
Sp. che.#6	1150	32	2.5	23.14	18.11	23.49	17.83	12.93	1.22
Sp. che.#6	1250	3.2	2.5	22.68	17.97	22.30	18.20	13.17	1.18
Sp. che.#6	1250	32	2.5	11.50	18.08	11.26	18.12	16.35	1.19
Sp. che.#7	1150	3.2	2.5	25.93	13.80	26.89	13.29	9.02	1.22
Sp. che.#7	1150	32	2.5	18.76	14.01	19.03	13.60	10.45	1.23
Sp. che.#7	1250	3.2	2.5	17.91	13.75	18.46	13.75	10.59	1.18
Sp. che.#7	1250	32	2.5	8.48	14.19	8.13	15.15	12.40	1.18
Sp. che.#8	1150	3.2	2.5	24.57	13.51	23.89	13.44	8.45	1.20

Sp. che.#8	1150	32	2.5	16.55	13.67	17.18	13.40	9.87	1.20
Sp. che.#8	1250	3.2	2.5	16.34	13.55	16.66	13.89	9.93	1.16
Sp. che.#8	1250	32	2.5	7.88	13.49	8.51	13.90	11.53	1.16

("Spot check #1 and #5" cannot be calculated due to high flux amount in the raw material (Sanbao Porcelain Stone), which leads to the entire dissolution of alumina into glass phase, and thus no precipitated mullite phases formulated.

Table XXIX. Mineralogy of "Comparative Experiment" Porcelain Specimens Fired under Different Conditions

	Temperature (ºC)	Dwell Time (hour)	Heating Rate (K/min)	Undissolved Quartz (% Wt.)	Mullite (% Wt.)	Silica in Glass (UMF)	Alumina in Glass (UMF)
Chin.->Lerdprom's	1250	3.2	2.5	19.44	27.56	13.81	1.33
Chin.->Lerdprom's	1300	3.2	2.5	13.94	30.12	15.45	0.96
Chin.->Lerdprom's	1250	32	2.5	10.48	28.90	16.76	1.14
Chin.->Lerdprom's	1300	32	2.5	5.96	28.39	18.36	1.21
Chin.->Colorado's	1250	3.2	2.5	12.40	23.91	8.84	1.00
Chin.->Colorado's	1300	3.2	2.5	8.58	21.96	9.67	1.16
Chin.->Colorado's	1250	32	2.5	6.60	22.42	10.13	1.12
Chin.->Colorado's	1300	32	2.5	4.82	22.11	10.38	1.15
Chin. Comm. #1	1250	3.2	2.5	20.62	18.91	11.07	1.18
Chin. Comm. #1	1300	3.2	2.5	15.05	20.14	12.34	1.06
Chin. Comm. #1	1250	32	2.5	13.16	17.95	12.95	1.28
Chin. Comm. #1	1300	32	2.5	9.37	19.83	13.74	1.09
Chin. Comm. #2	1250	3.2	2.5	25.11	23.83	14.45	1.10
Chin. Comm. #2	1300	3.2	2.5	16.81	24.70	17.36	0.96
Chin. Comm. #2	1250	32	2.5	14.28	22.48	18.51	1.30
Chin. Comm. #2	1300	32	2.5	8.08	23.22	20.68	1.19
Chin. Comm. #3	1250	3.2	2.5	22.64	24.87	12.60	0.79
Chin. Comm. #3	1300	3.2	2.5	16.28	22.13	14.74	1.14
Chin. Comm. #3	1250	32	2.5	15.02	22.77	15.06	1.06
Chin. Comm. #3	1300	32	2.5	8.13	21.19	17.26	1.06

Table XXX. Mullite Crystallite Size in (110) Direction of Chinese Ancient Specimens from Jingdezhen in the Period of Five Dynasties to Song Dynasty

Sample	2θ (°)	Θ (°)	Degree to Radian	Cos(θ)	FWHM (B)	0.94λ	2pi/360	B(rad)	Mullite Size(110) (nm)
WP#1	16.4150	8.2075	0.1432	0.989758	0.167	0.1449	0.0175	0.0029	50.24
WP#2	16.4150	8.2075	0.1432	0.989758	0.168	0.1449	0.0175	0.0029	49.94
WP#3	16.4150	8.2075	0.1432	0.989758	0.143	0.1449	0.0175	0.0025	58.67
WP#4	16.4150	8.2075	0.1432	0.989758	0.190	0.1449	0.0175	0.0033	44.16
WP#5	16.4150	8.2075	0.1432	0.989758	0.146	0.1449	0.0175	0.0025	57.46
WP#6	16.4150	8.2075	0.1432	0.989758	0.145	0.1449	0.0175	0.0025	57.86
WP#7	16.4150	8.2075	0.1432	0.989758	0.176	0.1449	0.0175	0.0031	47.67
GWP#1	16.4150	8.2075	0.1432	0.989758	0.150	0.1449	0.0175	0.0026	55.93
GWP#2	16.4150	8.2075	0.1432	0.989758	0.144	0.1449	0.0175	0.0025	58.26
GWP#3	16.4150	8.2075	0.1432	0.989758	0.154	0.1449	0.0175	0.0027	54.48
GWP#4	16.4150	8.2075	0.1432	0.989758	0.166	0.1449	0.0175	0.0029	50.54
GWP#5	16.4150	8.2075	0.1432	0.989758	0.168	0.1449	0.0175	0.0029	49.94
GWP#6	16.4150	8.2075	0.1432	0.989758	0.166	0.1449	0.0175	0.0029	50.54
GWP#7	16.4150	8.2075	0.1432	0.989758	0.158	0.1449	0.0175	0.0028	53.10
GWP#8	16.4150	8.2075	0.1432	0.989758	0.138	0.1449	0.0175	0.0024	60.80
GWP#9	16.4150	8.2075	0.1432	0.989758	0.156	0.1449	0.0175	0.0027	53.78
GWP#10	16.4150	8.2075	0.1432	0.989758	0.151	0.1449	0.0175	0.0026	55.56
GWP#11	16.4150	8.2075	0.1432	0.989758	0.150	0.1449	0.0175	0.0026	55.93

Table XXXI. Mullite Crystallite Size in (110) Direction for "Spot Check" Group under Different Firing Conditions

	Temperature (ºC)	Dwell Time (hour)	Heating Rate (K/min)	2θ (°)	Θ (°)	Degree to Radian	Cos(θ)	FWHM (B)	0.94λ	2pi/360	B(rad)	Mullite Size (110) (nm)
Sp. che.#2	1150	3.2	2.5	16.391	8.1955	0.1430	0.9897	0.176	0.1449	0.0175	0.0031	47.67
Sp. che.#2	1150	3.2	2.5	16.398	8.1990	0.1431	0.9897	0.161	0.1449	0.0175	0.0028	52.11
Sp. che.#2	1250	32	2.5	16.39	8.1950	0.1430	0.9897	0.1515	0.1449	0.0175	0.0026	55.38
Sp. che.#2	1250	32	2.5	16.392	8.1960	0.1430	0.9897	0.1425	0.1449	0.0175	0.0025	58.87
Sp. che.#3	1150	3.2	2.5	16.371	8.1858	0.1429	0.9898	0.2025	0.1449	0.0175	0.0035	41.43
Sp. che.#3	1150	3.2	2.5	16.373	8.1865	0.1429	0.9898	0.1865	0.1449	0.0175	0.0033	44.98
Sp. che.#3	1250	32	2.5	16.369	8.1848	0.1429	0.9898	0.148	0.1449	0.0175	0.0026	56.68
Sp. che.#3	1250	32	2.5	16.381	8.1908	0.1430	0.9897	0.126	0.1449	0.0175	0.0022	66.58
Sp. che.#4	1150	3.2	2.5	16.376	8.1883	0.1429	0.9898	0.148	0.1449	0.0175	0.0026	56.68
Sp. che.#4	1150	3.2	2.5	16.391	8.1958	0.1430	0.9897	0.1415	0.1449	0.0175	0.0025	59.29
Sp. che.#4	1250	32	2.5	16.377	8.1885	0.1429	0.9898	0.134	0.1449	0.0175	0.0023	62.61
Sp. che.#4	1250	32	2.5	16.39	8.1950	0.1430	0.9897	0.1205	0.1449	0.0175	0.0021	69.62
Sp. che.#6	1150	3.2	2.5	16.384	8.1920	0.1430	0.9897	0.2315	0.1449	0.0175	0.0040	36.24

Sp. che.#6	1150	3.2	2.5	16.399	8.1998	0.1431	0.9897	0.1905	0.1449	0.0175	0.0033	44.04
Sp. che.#6	1250	32	2.5	16.385	8.1928	0.1430	0.9897	0.183	0.1449	0.0175	0.0032	45.84
Sp. che.#6	1250	32	2.5	16.392	8.1960	0.1430	0.9897	0.159	0.1449	0.0175	0.0028	52.76
Sp. che.#7	1150	3.2	2.5	16.349	8.1748	0.1427	0.9898	0.232	0.1449	0.0175	0.0040	36.16
Sp. che.#7	1150	3.2	2.5	14.882	7.4410	0.1299	0.9915	0.194	0.1449	0.0175	0.0034	43.17
Sp. che.#7	1250	32	2.5	16.390	8.1950	0.1430	0.9897	0.176	0.1449	0.0175	0.0031	47.67
Sp. che.#7	1250	32	2.5	16.383	8.1915	0.1430	0.9897	0.1585	0.1449	0.0175	0.0028	52.93
Sp. che.#8	1150	3.2	2.5	16.375	8.1875	0.1429	0.9898	0.219	0.1449	0.0175	0.0038	38.31
Sp. che.#8	1150	3.2	2.5	16.386	8.1930	0.1430	0.9897	0.183	0.1449	0.0175	0.0032	45.84
Sp. che.#8	1250	32	2.5	16.397	8.1985	0.1431	0.9897	0.162	0.1449	0.0175	0.0028	51.79
Sp. che.#8	1250	32	2.5	16.426	8.2133	0.1433	0.9897	0.1505	0.1449	0.0175	0.0026	55.75

Table XXXII. Mullite Crystallite Size in (110) Direction for "Comparartive Experiment" Group under Different Firing Conditions

	Temperature (ºC)	Dwell Time (hour)	Heating Rate (K/min)	2θ (°)	Θ (°)	Degree to Radian	Cos(θ)	FWHM (B)	0.94λ	2pi/360	B(rad)	Mullite Size (110) (nm)
Chin.->Lerdprom's	1250	3.2	2.5	16.3850	8.1925	0.1430	0.989795	0.201	0.1449	0.0175	0.0035	41.74
Chin.->Lerdprom's	1300	3.2	2.5	16.4230	8.2115	0.1433	0.989748	0.173	0.1449	0.0175	0.0030	48.50
Chin.->Lerdprom's	1250	32	2.5	16.3930	8.1965	0.1431	0.989785	0.168	0.1449	0.0175	0.0029	49.94
Chin.->Lerdprom's	1300	32	2.5	16.3920	8.1960	0.1430	0.989786	0.141	0.1449	0.0175	0.0025	59.50
Chin.->Colorado's	1250	3.2	2.5	16.3930	8.1965	0.1431	0.989785	0.186	0.1449	0.0175	0.0032	45.11
Chin.->Colorado's	1300	3.2	2.5	16.3850	8.1925	0.1430	0.989795	0.180	0.1449	0.0175	0.0031	46.61
Chin.->Colorado's	1250	32	2.5	16.3640	8.1820	0.1428	0.989821	0.167	0.1449	0.0175	0.0029	50.23
Chin.->Colorado's	1300	32	2.5	16.3780	8.1890	0.1429	0.989804	0.140	0.1449	0.0175	0.0024	59.92
Chin. Comm. #1	1250	3.2	2.5	16.3980	8.1990	0.1431	0.989779	0.192	0.1449	0.0175	0.0034	43.70
Chin. Comm. #1	1300	3.2	2.5	16.3870	8.1935	0.1430	0.989792	0.171	0.1449	0.0175	0.0030	49.06
Chin. Comm. #1	1250	32	2.5	16.3920	8.1960	0.1430	0.989786	0.158	0.1449	0.0175	0.0028	53.10

Chin. Comm. #1	1300	32	2.5	16.4100	8.2050	0.1432	0.989764	0.143	0.1449	0.0175	0.0025	58.67
Chin. Comm. #2	1250	3.2	2.5	16.3780	8.1890	0.1429	0.989804	0.200	0.1449	0.0175	0.0035	41.95
Chin. Comm. #2	1300	3.2	2.5	16.3960	8.1980	0.1431	0.989781	0.170	0.1449	0.0175	0.0030	49.35
Chin. Comm. #2	1250	32	2.5	16.3780	8.1890	0.1429	0.989804	0.164	0.1449	0.0175	0.0029	51.15
Chin. Comm. #2	1300	32	2.5	16.3900	8.1950	0.1430	0.989789	0.153	0.1449	0.0175	0.0027	54.83
Chin. Comm. #3	1250	3.2	2.5	16.3930	8.1965	0.1431	0.989785	0.187	0.1449	0.0175	0.0033	44.86
Chin. Comm. #3	1300	3.2	2.5	16.3970	8.1985	0.1431	0.989780	0.178	0.1449	0.0175	0.0031	47.13
Chin. Comm. #3	1250	32	2.5	16.3900	8.1950	0.1430	0.989789	0.161	0.1449	0.0175	0.0028	52.11
Chin. Comm. #3	1300	32	2.5	16.4050	8.2025	0.1432	0.989770	0.152	0.1449	0.0175	0.0027	55.20